CHALMERS

Non-destructive evaluation of timber floors structure at Skansen Lejonet

Master's Thesis in the Master's Programme Structural Engineering and Building Technology

MAGNUS JOHANSSON

JOHAN SUIKKI

Department of Civil and Environmental Engineering
Division of Structural Engineering
Steel and Timber Structures
CHALMERS UNIVERSITY OF TECHNOLOGY
Göteborg, Sweden 2013

Master's Thesis 2013:40

MASTER'S THESIS 2013:40

Non-destructive evaluation of timber floors structure at Skansen Lejonet

Master's Thesis in the Master's Programme Structural Engineering and Building Technology

MAGNUS JOHANSSON

JOHAN SUIKKI

Department of Civil and Environmental Engineering
Division of Structural Engineering
Steel and Timber Structures
CHALMERS UNIVERSITY OF TECHNOLOGY

Göteborg, Sweden 2013

Non-destructive evaluation of timber floors structure at Skansen Lejonet

Master's Thesis in the Master's Programme Structural Engineering and Building Technology

MAGNUS JOHANSSON
JOHAN SUIKKI

Examensarbete 2013:40
Department of Civil and Environmental Engineering
Division of Structural Engineering
Steel and Timber Structures
Chalmers University of Technology
SE-412 96 Göteborg
Sweden
Telephone: + 46 (0)31-772 1000

Cover:
The picture shows the fortlet of Skansen Lejonet in Gothenburg. (Photo: Magnus Johansson, 2013)

Chalmers Reproservice
Göteborg, Sweden 2013

Non-destructive evaluation of timber floors structure at Skansen Lejonet

Master's Thesis in the Master's Programme Structural Engineering and Building Technology

MAGNUS JOHANSSON
JOHAN SUIKKI
Department of Civil and Environmental Engineering
Division of Structural Engineering
Steel and Timber Structures
Chalmers University of Technology

ABSTRACT

Continued use of existing structures is beneficial from a sustainability view point. In order to enable the continued use, an accurate assessment of the current and future structural capacity of old timber structures, it is necessary to develop non-destructive test methods. The aim of this thesis was to compare the influence of different non-destructive test methods with regard to assessment of existing timber structures. This was facilitated through a case study of two historic timber floor structures at the fortlet of Skansen Lejonet in Gothenburg. Each assessment process requires a well formulated approach to be successful. Therefore, in order to gain an understanding of current assessment procedures, three different standards published by ASCE, ISCARSAH and ISO were studied and used as a base for the chosen strategy.

The assessment process can be improved with a suitable combination of non-destructive test methods, depending on assessment objectives, actual structural condition and available information. The evaluated test methods were X-ray imaging, stress wave measurements and resistance drilling. These test methods acquire raw data by different measurements and provides varying types of outputs. X-ray imaging provides a two-dimensional projection of the member as well as the possibility to determine density which can be correlated to strength (and elasticity) properties/values. Stress wave testing provides the velocity of a wave within the member which may be used to determine the dynamic modulus of elasticity which can be further correlated to the static modulus of elasticity. Resistance drilling facilitates the detection of interior deterioration as well as the depth of surface deterioration.

It was found that damage of the joists had occurred but it was not an ongoing process, most likely from environmental conditions rather than due to large loads. The structure was evaluated for a load combination that imitated the original intended load as well as an Ultimate Limit State (ULS) load combination according to the existing standards, i.e. Eurocodes. It was concluded that requirements specified in Eurocodes were fulfilled for both the original intended load and the current load with the current condition of the joists.

Keywords: historic timber, NDT, non-destructive testing, radiography, resistance drilling, Skansen Lejonet, stress wave, structural assessment, X-ray

Contents

Preface

This case study was performed as a master thesis project, as a final work within our education in Civil Engineering. The thesis was written at the Division of Structural Engineering, Steel and timber structures at Chalmers University of Technology, Sweden. The study evaluated three non-destructive testing methods for timber, all of them applied on the timber floor structures inside the fortlet of Skansen Lejonet in Gothenburg, Sweden. The intention of the project from the very beginning was that it should provide some valuable information about how these test methods could be applied in an optimized manner in-situ, either solely or combined with each other. In order to be able to reach this target, we wish to thank a number of people who have helped us.

First of all we would like to thank Erik Pehrsson at Götiska Förbundet, for his nice collaboration in making the fortlet accessible for us during testings and inspections. Also Bengt Gustafsson and other companions of Götiska Förbundet have been very helpful to us. Thanks to Statens Fastighetsverk and Mikael Nädele at GAJD Arkitekter for enabling this case study at Skansen Lejonet. We would like to specially thank Assistant Professor Tomasz Nowak at Wroclaw University of Technology, for providing FAKOPP and resistance drilling equipments and for his large contribution during the in-situ testing. Furthermore, we are thankful to COST for enabling this collaboration through the FP1101 action. Also our supervisor Lars Bengtsson and some of his colleagues at ELU have been very helpful during the structural analysis of the timber floor structure. Finally, at Chalmers, we would like to gratefully thank our examiner Professor Robert Kliger for all his professional support in the project, as well as our supervising PhD-student Thomas Lechner who continuously and enthusiastically helped us during all phases of the project.

Gothenburg, June 2013

Magnus Johansson and Johan Suikki

1 Introduction

1.1 Background

Current assessment procedures for structural timber are somewhat arbitrary and often based on the performer's experience. Hence there are possibilities for improving these kinds of assessment with the use of non-destructive testing (NDT) methods, which provide parameters that can be used to determine timber properties. There are different NDTs available, with varying degrees of damage that can be applied. However, it is important to keep in mind that the damages only concern the aesthetics and not the structural performance. For instance the method of resistance drilling leaves tiny visible holes, but the influence of these holes on the overall performance is negligible. It would be beneficial knowing which type of method or combination of methods that is suitable for different purposes.

Some of these NDT's can be seen as refinements of traditional qualitative and subjective methods for assessing timber quality. With these refinements it has become possible to determine the quality more accurately. Stress wave measurements can be compared to traditional sounding techniques while manual resistance drilling has become digitalized and more accurate which enables reliable recording of data. Furthermore, large X-ray devices, used primarily for medical and industrial purposes, have been developed into portable X-ray devices.

The development of NDT allows for careful investigation of heritage timber structures without major alterations to the original appearance and function of it. This advantage is not reserved for historical timber structures, but these methods can also be applied to new timber structures for continuous maintenance inspections. Therefore it is possible to substantially extend the service life for both types of structure, e.g. NDT's give the opportunity to reuse older buildings for new purposes, providing a decrease of the environmental footprint. However, heritage structures often require a holistic approach in the assessment. This interdisciplinary approach enables architectural and historical values to be accurately interpreted and considered, resulting in minimum interventions.

In order to investigate this topic a case study, regarding two pine timber floor structures at the fortlet of Skansen Lejonet were performed. Skansen Lejonet was built in the late 17th century to provide defence against past enemies. It is one of few remaining traces of the original defence structures that made Gothenburg the heaviest fortified city in the country at that time. Relevant to this thesis is the interior timber floor structures that may have suffered some damage and offer opportunity to apply and compare different non-destructive test methods.

1.2 Aim of the thesis

The aim was to evaluate and to assess the structural performance of two timber floor structures from the 17th century at Skansen Lejonet by applying an appropriate assessment strategy and combining non-destructive testing methods. The influence of each test method applied in-situ was investigated, as well as the important aspects of how to combine and consider these methods.

In order to fulfil the aim, the following objectives for the work were formulated:

- Perform a well prepared in-situ inspection and testing by applying the three NDT methods at interesting and critical locations in the floor
- Obtain material properties by analyzing the test data
- Establish structural models representing the current structural behaviour, but with material data from different combinations of NDT methods
- Calculating utilization ratios for critical sections in the different models.

1.3 Scope and method

A case study of the fortlet of Skansen Lejonet was performed, using X-ray imaging, resistance drilling and stress wave testing. From the measurements, a number of structural models were established considering different combinations of methods. The structural analysis indicated the influence of the used methods by comparing the different structural models established.

1.4 Limitations

This thesis comprehends the evaluation of the different models, and therefore the NDT methods, by means of calculating utilization ratios for bending moment, shear force and buckling of columns. The effect of mechano-sorptive creep was not accounted for in the structural analysis. Furthermore, the thesis did not suggest any measures for potential problems that may be revealed. During the in-situ investigations, the function of the floor structures was not affected and no noticeable changes to the general appearance were made.

2 Properties of timber

In this case study it is preferable to briefly present some timber properties that may affect the measurements with the non-destructive test methods used. The structure of timber and moisture content are the main topics regarding properties that should be considered in order to correctly evaluate the timber joists at Skansen Lejonet.

2.1 Structure of timber

Timber is an anisotropic material, which means that the same property parameter in general varies in each three-dimensional direction. Therefore it is not straightforward to apply different design and analysis calculations equally whichever behaviour that is studied in a timber structure. While looking upon the interior of wood at a macroscopic level, three important directions can be distinguished (see Figure 2.1); radial, tangential and longitudinal direction (Dinwoodie, 2000). In order to correctly consider the differences in properties due to anisotropy, it is essential to have a certain understanding of the structure of timber. The structure of timber is briefly presented below at both macroscopic and microscopic level. For a more detailed discussion of these topics, please refer to Dinwoodie (2000).

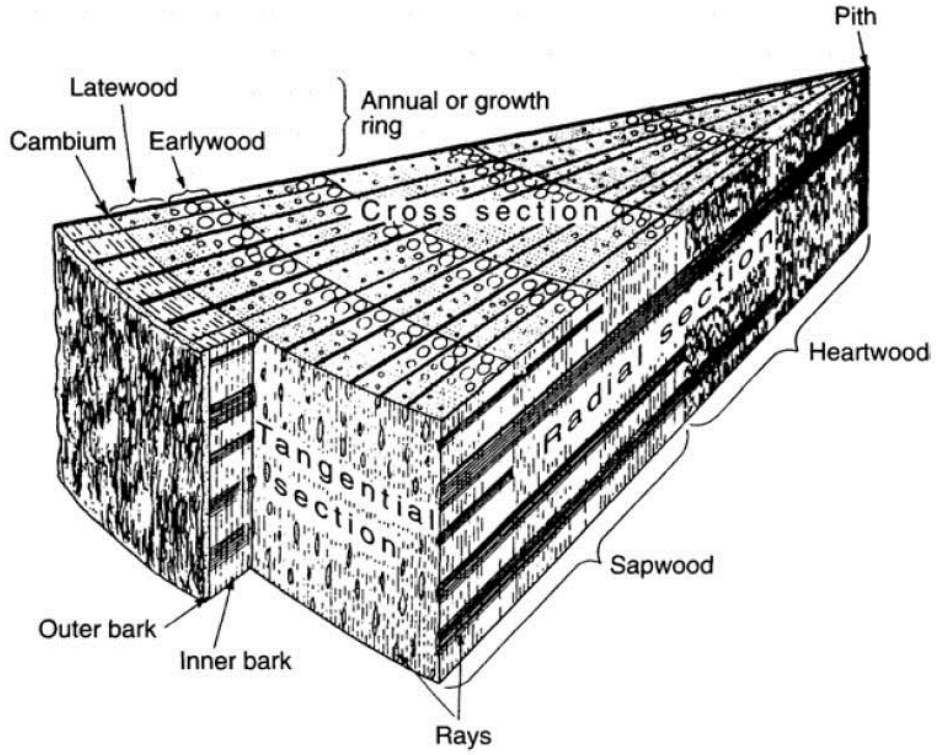

Figure 2.1 *Illustration of the three important directions in coniferous wood to consider in engineering purposes. (Dinwoodie, 2000)*

2.1.1 Timber at macroscopic level

The cross-section of the tree trunk reveals the annual growth rings which are formed by the growing of the tree, i.e. each ring indicates one experienced growing season and a dormant season for the tree. In Figure 2.2 below the growing seasons are

indicated by the light rings while the dark rings indicate the dormant seasons. However, the composition of the organic material of timber varies between different regions in the tree. From this fact it is suitable to consider the wood consisting of sapwood and heartwood (see Figure 2.2). The former undergoes frequent development in its chemical composition as the tree grows in size (probably a consequence of the survival of the fittest theory) in order to fight for the sunlight, which is a necessary ingredient in the photosynthesis (Dinwoodie, 2000).

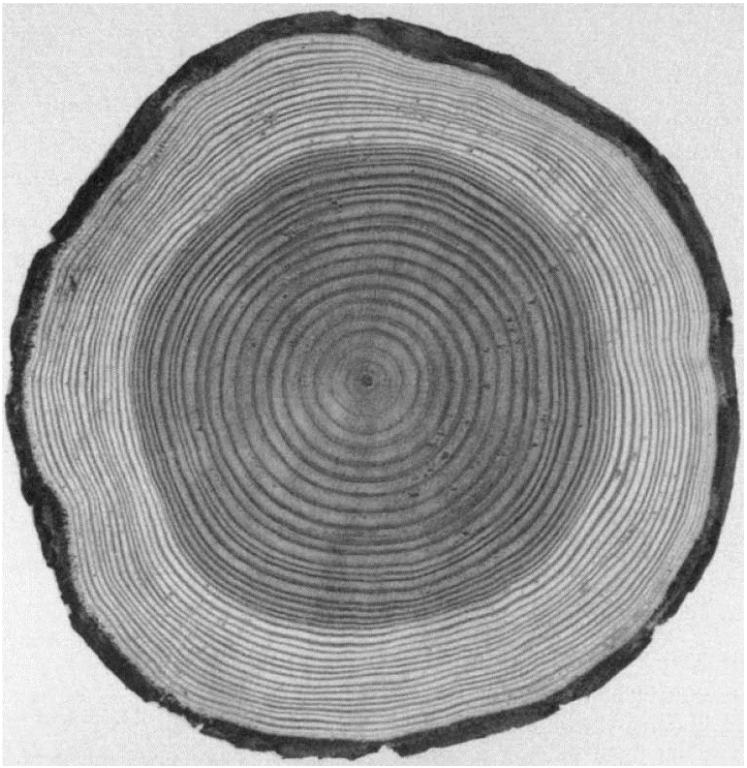

Figure 2.2 *Cross-section of a trunk of Douglas fir tree, indicating the growing season rings (light) and the dormant season rings (dark). One light and one dark ring represent an annual growth ring. Further, the dark area consists of heartwood while the light area consists of sapwood. Note that the outermost narrow region is the bark of the tree. (Dinwoodie, 2000)*

When the crown diameter and height grows, so does the trunk in order to maintain adequate support for the crown. The sapwood characterizes the growth of the trunk and is located in the outer regions of the trunk since the growth occurs there. Meanwhile, enveloped by the sapwood layer another separate composition of the wood exists, namely the heartwood. As the sapwood represents the region aligned for development and consequently the region for storage of minerals, the heartwood consists of former sapwood cells. This transformation of sapwood cells to heartwood cells is mainly a result of chemical changes. Like most parameters in timber engineering the width of the sapwood varies much between different species of timber, rate of growth and age of the tree. A common range is that the width of the sapwood region is 20% to 50% of the radius of the trunk (Dinwoodie, 2000).

2.1.2 Timber at microscopic level

The possibility to explain the anisotropy of timber emerges when studying the structure of timber at the microscopic level. The difference in performance between different directions in the timber is related to the layout of the cells. In softwoods (coniferous) cells are aligned in the vertical/longitudinal axis to the extent of 90%, while the corresponding value for hardwoods (broadleaved) differ between 85% and 95%. The rest of the cells are designated to the other two principal axes (Dinwoodie, 2000).

The growth of timber is recognized by the division of cambium, producing wood cells that are not living. However, the cambium zone is a circumferential layer of living cells between the bark and the wooden material in the trunk. The cambium hibernates during the winter, but with the debut of the spring this layer awakes due to the climate which is characterized by the increase of the thickness of the layer from, in general, one cell to approximately ten cells. The focus of wood created during this early phase of the season,kNown as earlywood, is on developing the conduction property of the tree. Each dividing cell produces a vertical wall (called the primary wall) and the subsequent division helps producing daughter cells. Following division creates the inner secondary wall for each cell, which thickness depends on the function of the cell. Depending on the location of a daughter cell, this can remain as a cambial cell within the cambial layer, develop into bark outside or wood inside the cambial layer. Since the activity of producing new cells decreases in the autumn, the focus in the later stages of the growing season is to transform the remaining living cells into bark or wood, prioritizing the development of support for the tree. This phase of the season is characterized as latewood. After this the activity vanishes completely and consequently one cycle or season has elapsed (Dinwoodie, 2000).

As the diameter of the tree increases, the cambial zone increases as well by periodic tangential division of cambial cells. Studying Figure 2.1 and Figure 2.2 it can be understood that this results in a larger circumference of the cambial layer. Parallel to the formation of the secondary wall, the daughter cells experience the process of differentiation, this results in transformation of the daughter cells into one of four possible basic cell types. Softwoods have two basic cell types while hardwoods have four. The cell types of hardwoods is to a greater extent more tailored to its purpose compared to the cell types of softwoods, i.e. hardwoods possess more or less one distinct cell type for each function; storage, support and conduction (Dinwoodie, 2000).

The density of timber varies significantly between species but the density of the cell wall material is the same for all timber species, with a value of approximately 1500kg/m^3. However, it has been explored that timber density correlates well with some timber strength properties (Dinwoodie, 2000). This implies that it is the distribution of different cell types within the microstructure that determines the characteristic density of species. It has also been shown that the density is determined by the ratio between cell wall thickness and cell diameter; the higher ratio the higher density. As the microstructure can deviate within the tree, different locations in the tree can possess different densities. Knowing the density is appropriate when determining the timber strength and one common relationship found in literatures is:

$$f = k \cdot g^n$$

where f is any arbitrary strength parameter, g is the specific gravity (ratio between density and reference density, usually water), k is a proportionality constant depending on which strength parameter that is studied, and n determines the type of curve established. However, both within species and between species a linear relationship between density and the strength parameter can be assumed. But, this assumption is not valid for shear and cleavage (Dinwoodie, 2000).

2.2 Moisture in timber

Timber is likely to experience dimensional changes even without being subjected to external stress. In such cases the changes may instead arise from variations in the moisture content or temperature or both, within the timber. Considering the magnitude of the dimensional changes though, the variation of moisture content is far more decisive than the temperature. The primary reason to this behaviour is that timber is a hygroscopic material that either emits or absorbs moisture. This means that timber strives for a moisture content that is in equilibrium with the relative humidity of the surrounding atmosphere. The definition of moisture content μ [%] in timber is:

$$\mu = \frac{m_{init} - m_{od}}{m_{od}} \cdot 100$$

where m_{init} is the initial mass of a considered sample and m_{od} is the mass of the same sample after that it has been oven-dried at 105°C (Dinwoodie, 2000). There are sorption isotherms available illustrating what moisture content that matches different atmospheric conditions, i.e. different relative humidity in the ambient air. Since the surrounding conditions vary during the season the moisture content in timber also will. Although the season of the year affects the moisture variation within the green tree, the structure of the tree causes greater differences through the cross-section. For example sapwood may contain more moisture than the heartwood, this phenomenon or difference is more pronounced for softwoods than for hardwoods (Dinwoodie, 2000).

2.2.1 Effect on strength and elasticity properties

One important feature of moisture in wood is that decreasing moisture content, e.g. as a result of drying, increases the timber strength. This relation is valid when the moisture content is below 27-30%. This moisture content corresponds to the fibre saturation point, which is the state in timber with maximum chemically bound water (water content in the cell walls) and no excess water in the cavities (Dinwoodie, 2000). This finding implies that only the chemically bound water affects properties for strength and elasticity of timber. Figure 2.3 shows the relationship between longitudinal compressive strength and moisture content in timber together with the relationship between modulus of elasticity (MOE) in the longitudinal-radial plane and moisture content for Sitka spruce.

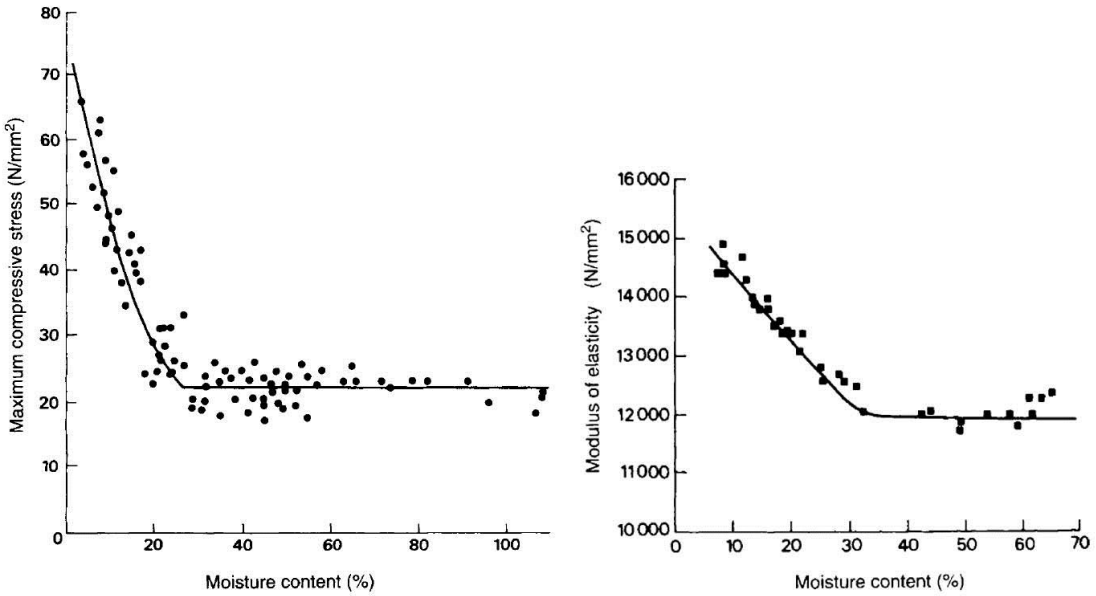

Figure 2.3 *Relationship between longitudinal compressive strength and moisture content in timber (Left), relationship between MOE in the longitudinal-radial plane and moisture content for Sitka spruce (Right) (Dinwoodie, 2000).*

Once the moisture content in timber has been reduced to the fibre saturation point, further drying will reduce the amount of water in the cell walls. At a microscopic level this reduction is a result of extended drying of the water-reactive matrix between the microfibrils. Upon this, adjacent microfibrils become able to approach each other. This results in a proportional increase in interfibrillar bonding and simultaneously in a decrease in overall dimensions. These changes are reversible to a great extent. It has also been discovered that the moisture content affects MOE in a similar manner, however not to the same extent as for strength (Dinwoodie, 2000).

Regarding deformations in timber subjected to loads, moisture may also lead to substantial creep effects. When unsteady moisture conditions are prevailing, i.e. moisture is alternately absorbed to timber and desorbed from timber in several cycles, the phenomenon of mechano-sorptive creep takes place. This creep is far more excessive than ordinary elastic creep. Research has shown that the mechano-sorptive creep deflection, of a timber specimen subjected to 3/8 of its ultimate load, can be 25 times the initial deflection at the time of failure. Simultaneously, the elastic creep deflection of an identical specimen subjected to the same load for the same duration, but with constant relative humidity, is just twice the initial deflection. This difference between steady and unsteady state may vary. However, greater moisture gradients in each cycle lead to greater mechano-sorptive creep deflections (Dinwoodie, 2000).

In a doctoral thesis regarding creep, a portion of the test specimens (pine) were 360 year old and had been used in trusses. Tests showed the MOE to be around 10.5GPa and MOR to be 70-90 MPa for clear wood specimens. Furthermore, the samples of historic timber (both clear wood and larger members) showed less total deformation, including creep effects than contemporary timber which had less initial deformation due to a higher MOE (Mohager, 1987).

2.2.2 Moisture damages

A major factor for decay in timber structures is moisture. However, timber can be deteriorated either by physical processes or biological processes. The later ones are often represented by fungal and insect attacks, which impair the wood more rapidly than a third possible biological decay mechanism, bacteria. Fungi in wood comprise mildew, stain and decay fungi. Among these fungi, just the last type decays wood with time, as the name implies. Decay fungi may in turn be divided into three different types, namely brown rot, white rot and dry rot. However, distinguishing these when inspection of timber structures is carried out is not necessary. Instead the location and extent of corresponding deterioration should be determined. Deterioration has the worst impact on the structural integrity of timber if the heartwood is being attacked. This can be the case when water is absorbed through end grains or minor disturbances such as checks and holes. Although, due to the presence of extractives (amount varying between species) in the heartwood, this inner region of the trunk is more resistant against fungi decay than the sapwood is. The reason to this is that the extractives are toxic to the fungi (Anthony, 2007).

A common thing between the biological attacks is that these types of damage can be avoided, provided that structural timber is not subjected to any wetting. If this is the case, timber as a construction material has a great resistance to most biological attacks and hence is very durable for use in structures. Fungal attacks require oxygen, food and water, but as long as a building is kept dry and is sufficiently ventilated the necessary levels of water will not be present. Therefore, in such a building, fungi attacks will not occur. This corresponds to keep the moisture content in the timber below 20-22% (Williams, 2009).

Deterioration due to moisture can be detected at a visual inspection. There are typical signs of decay for each type of deterioration. Fungal attacks can be detected if fruiting bodies are present. Decay can either be indicated by sunken faces as a result of decay voids near surface of the member or by staining, discolouration (see Figure 2.4) or rust stains which all indicate that the member has been subjected to a moist climate. For the same reason plant or moss growth may be found in cracks. Finally holes, frass and powder posting can indicate insect attacks, which in turn can indicate decay (Ross et al., 2006).

Figure 2.4 *Example of discolouration in Skansen Lejonet on a primary beam (to the right).*

2.3 Characteristics of historic timber

Literature shows that methods for choosing and producing construction timber were well developed in the 19th century and were presumably at a similar level before that time. Since there was no extensive harvesting or plantation of new trees, older trees were readily available for use contrary to the currently available timber. Trees grown in oligotrophic soil were preferred since the slow growth causes a dense annular ring structure and subsequently a strong trunk (see Figure 2.5). Additionally it should have grown in group with others to further slow the growth as well as reduce the number of knots and the impact of wind. Furthermore the appearance of bark and twigs were used as indicators for a slow grown tree and if it was a mature tree, i.e. had stopped growing. In addition to the growing conditions a log should be straight and hitting the log should not produce a dull and muffled sound. Trees were felled during winter to reduce the moisture and sap content. The bark was left on the log until spring in order to reduce the drying speed and minimize cracking, after that it was wholly or partially removed to reduce the risk for rot or insect attack, due to trapped moisture between wood and bark. If possible only the heartwood was used since the sapwood was considered to be sensitive to moisture, although dimensions were a limiting factor (Grödinger et al., 1982).

Figure 2.5 *Cross-section of a removed timber part from Skansen Lejonet showing dense annular rings (Left), cross-section of a young tree with fast growth (Right).*

A traditional method of protecting timber from deterioration is charring. The timber is subjected to fire until the outer 3-13mm has turned into a char-layer which is not susceptible to fungal attack. Additionally the heat may produce products within the timber that can be toxic to fungi. The drawback is that the structural strength is lost in the treated parts (Weiss, 1915).

3 Non-destructive test methods

Investigations of existing heritage structures must be conducted carefully, otherwise culturally valuable structures or members might be destroyed. Therefore any intervention on a heritage structure should always be weighed against the loss of culturally valuable material (Lourenço, 2005). With the use of non-destructive test (NDT) methods the interference with the structure can be minimized by reducing the damage from assessment. Further, subsequent repair work can be efficiently designed with accurate information. The principle of reusing buildings rather than constructing new ones becomes more and more common, why the need for NDTs increases (Ross & Pellerin, 1994). The NDT methods assigned for this master thesis are X-ray, stress wave and resistance drilling. While the technology of these methods progresses continuously, a state of the art of these are presented in this chapter to serve as a background to the in-situ testing.

3.1 X-ray

X-ray technology has been used since the 1960s for in-situ inspections of timber structures. The previous techniques emitted rays with high energy levels through a member of interest and a film just behind this member depicted the interior of it (Anthony, 2003). X-rays are created from the impact of high-speed electrons hitting a matter, usually made of tungsten (Kasal et al., 2010a). This impact results in energy loss of the electrons, whereas much of this energy yields heat while little energy is reserved to the formation of short wavelength radiation, known as X-ray. The relationship between the energy of an X-ray beam E and its corresponding wavelength λ is:

$$E = \frac{hc}{\lambda} = \frac{1{,}24}{\lambda}$$

where h is Planck's constant and c is the speed of light. Shorter wavelengths can therefore penetrate any medium more than longer wavelengths, since higher energy enables more penetration.

Since the 1960s huge steps has been taken in improving the user interface and the safety of operation of the technology, the latter one in terms of decreasing the energy level of the rays. Also the portability of some available X-ray devices is a huge advantage, which is a development from previous large X-ray devices, used primarily for medical and industrial purposes. Among the user interface improvements the most crucial one is probably the ability to record images which enables post-processing (Anthony, 2003), i.e. image enhancement which is illustrated in Figure 3.1. This post-processing provides the opportunity to accurately investigate the images in order to make proper conclusions of the investigations in-situ. These improvements are said to have generated both safer and cheaper X-ray techniques to be applied in-situ.

The ability to penetrate wood with lower-level energy X-rays and to record images with adequate quality, was evaluated in 1996 and further evaluations identified technical and logistical issues (Anthony, 2003). For the time being there are different X-ray equipment available and portable units have shown to be promising, both with regard to quality and feasibility (Lechner et al., 2011).

The concept of X-ray is to determine to what extent X-ray bursts are attenuated, i.e. loss in intensity or the extent of absorption, through the thickness of a member. By means of intensity it is then possible to determine the density of the member, according to the following equation:

$$I_X = I_0 \cdot e^{-\mu \cdot t}$$

where I_X is the residual intensity of the ray after passage through the member, I_0 is the initial intensity of the ray, t is the thickness of the member and μ is the linear absorption coefficient per unit thickness.

The coefficient of μ is dependent on material and its density. Hence the density for the member emerges from the coefficient of μ and from this discovery it is possible to conclude whether there are any decayed regions or not, since timber density is linked with decay in timber (Kasal et al., 2010a). As commonly stated, timber density also correlates well with other significant parameters such as MOE and bending strength (modulus of rupture, MOR), why X-ray imaging also provides indirect information about these properties. In order to obtain correct data the X-ray equipment must be calibrated and an example of this is presented by Lechner et al. (2011). In the same study it is proved that the method is satisfactory to use for in-situ assessments, since high coefficients of determination (R^2) are obtained between the density and the mean greyscale value for different test configurations.

Figure 3.1 *Example of X-ray device in-situ pointed at a primary timber beam, middle) radiograph showing the interior of a secondary timber beam at the end support (Left), image enhancement of the radiograph (using the software ImageJ) that reveals the wood grain (Right).*

An in-situ investigation with a portable X-ray device needs three units. Firstly an X-ray source must be placed at a certain distance from the member (see Figure 3.*1*) and secondly an imager placed on the opposite side of the member. Also a laptop computer is necessary as a control unit, enabling real-time view of the interior of interest. In order to obtain good quality of the images, the placement of the emitter (X-ray source) and imager is dependent on the exiting angle of the X-rays. Good quality refers to images with high contrast and sharpness in order to ease inspection and interpretation of radiographs. This is explained by the geometric unsharpness U_g below:

$$U_g = S\left(\frac{b}{a}\right)$$

where S is the size of the focal spot within an X-ray tube, a is the distance between the X-ray source and the member and b is the distance between the member and the imager. For instance it is preferable to mount the imager directly on the opposite face

of the member in order to minimize b and hence also U_g. Although it is sometimes desirable to magnify some small details by increasing b, it is important to simultaneously consider the eventual decrease in sharpness due to this (Kasal et al., 2010a).

One drawback with this X-ray technique is that the three-dimensional interior of the member is reproduced as a two-dimensional image, where the intensity of greyscale (presented by means of the RGB colour model) in each pixel in the image relates to the average attenuation or density through the thickness of the member. This means that if a significant change in attenuation can be identified in a region, it is difficult to localize the depth from the wooden surface where this change occurs, i.e. where the timber may be damaged. Also the projection slightly distort the sizes of the object, but this can be overcome by taking multiple pictures (radiographs) or by studying the geometry of the equipment configuration (distances a and b above) (Anthony, 2007). Further, any possible defects that are oriented perpendicular to the path of the X-rays, will be difficult to reveal. Due to these drawbacks that may cause some significant damages being missed out, it is recommended to adapt the X-ray testing in such a manner that members are radiated from different angles and on different faces. Improved image enhancement of radiographs is being researched in order to further overcome these quandaries (Kasal et al., 2010a).

When conducting X-ray measurements it is important to be aware of natural variations in density; all variations in density may be interpreted as natural ones, but here natural variations concern such due to early-, late-, heart- and sapwood. By considering this, correct interpretations of wood status can be done in order to identify eventual decay. Regarding sound wood, a well-defined wood structure will be recognized and annular rings will be visible on radiographs. If any partial decay has taken place this will show a certain loss of timber and the appearance of annular rings will be diffuse. If any partial decay has developed to a decayed area, the wood structure will be illustrated by a vague mass in the radiograph. The more the decay is progressing, the more severe and distinguished these signs become (Kasal et al., 2010a). It is also important to consider thickness of and moisture content within the member due to the calibration (see Section 7.4.2).

3.2 Stress wave

Timber can be assessed by measuring the behaviour of a stress wave through the specimen. The method can be divided into two types, sonic stress waves and ultrasonic stress waves. The former are often produced by hammers while the latter are produced by special equipment (Kasal et al., 2010b). Ultrasonic stress waves have frequencies of 20-500 kHz, i.e. above what can be perceived by human ear while the sonic stress waves are in the audible spectrum. The higher frequency of ultrasonic stress waves makes it possible to detect smaller defects than with sonic stress waves. However, a drawback is that attenuation, loss of energy due to reflection and absorption, increases for higher frequencies and is greater in the transverse direction than in the longitudinal direction (Bucur & Böhnke, 1994). This might be limiting for the maximum size of the specimen.

There are different types of measurements that can be made to evaluate the specimen, one type of test is the time of flight measurement. Such a test is conducted by placing a signal source and receiver at a known distance from each other and measuring the

time needed for the wave to travel that distance. Since the time and distance are known, the velocity of the wave can be calculated and used to determine the dynamic modulus of elasticity E_d with the following formula:

$$E_d = v^2 \cdot \rho$$

where v is the velocity and ρ is the density of the specimen. This is a one-dimensional simplification that disregards the anisotropic behaviour of wood, although research has found it to be an adequate approximation (Ross & Pellerin, 1994). There is a strong relationship between the dynamic and static modulus of elasticity, the static modulus is approximately 90% of the dynamic modulus. Values for the static modulus of elasticity E_s are usually acquired through a linear equation (Feio, 2006):

$$E_s = a \cdot E_d + b$$

where a and b are constants depending on the material. The propagation velocity is affected by many factors, primarily by the testing direction (see Figure 3.2). Transverse tests have lower velocities than longitudinal tests due to lower stiffness (FPL, 2001). Similarly, ring orientation affects the velocity and can therefore result in differences in measurements over a larger specimen, even if there is no deterioration. Radial measurements produce higher velocities than tangential measurements, the lowest velocities occur when the wave travels both tangentially and at 45° inclination from radial direction (Ross et al., 2004).

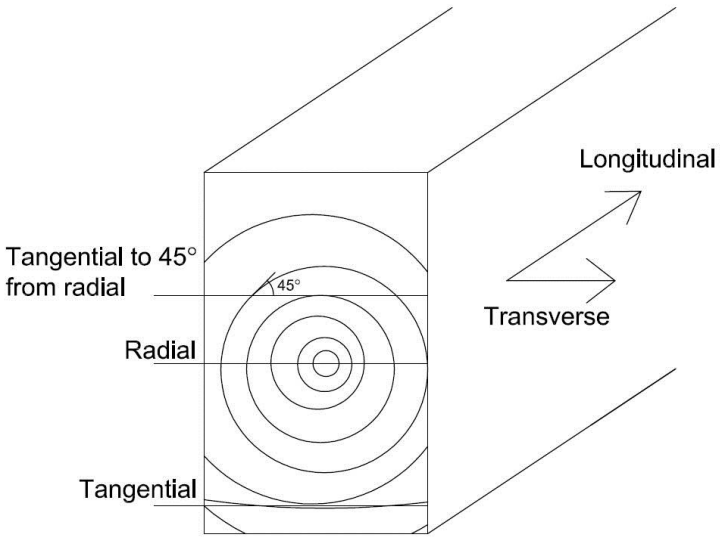

Figure 3.2 Definition of directions for stress waves (adapted from Ross et al. (2004)).

There are different methods to protect timber from fire and rot. One of these methods, that affect stress wave measurements by decreasing the velocity, is the use of oil-based products. Another phenomenon that affects the velocity is moisture content which reduces the stiffness. An increase in moisture content until the fibre saturation point will give a lower velocity and continued increase of the moisture content will decrease the velocity further although at a lower rate (Ross et al., 2006). Natural defects such as drying checks can give a false appearance as a deteriorated area since these cause the wave to travel a longer distance (Feio, 2006). Similarly, internal voids due to deterioration will not transmit the wave (Ross & Pellerin, 1994). This is illustrated in Figure 3.3.

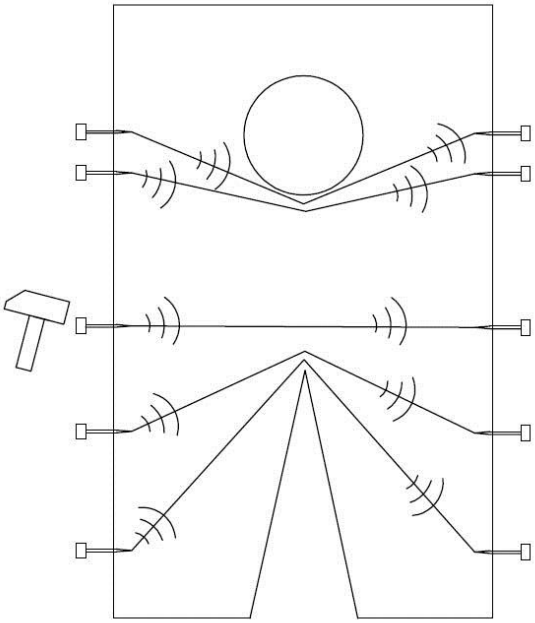

Figure 3.3 Deterioration (circle) and cracks cause the waves to travel a longer distance.

A longitudinal test gives an average value along the tested distance and less information regarding deteriorated regions since the fastest transmission time is measured. A transverse test gives a local value at the tested point, multiple tests at an area suspected to have deterioration can map the extent and location of the damage (Kasal et al., 2010b).

In addition to the time of flight test, attenuation and frequency analysis can be utilized to assess the specimen. In a specimen without defects the amplitude of the wave will be decreasing exponentially while deterioration will cause an irregular behaviour of the wave (Ross et al., 1997). The natural frequency of timber is related to the mass and stiffness of the specimen, properties that are affected by deterioration and aging. A decrease of the frequency will therefore correspond to a loss of one or both properties. Measurements can be made locally at a surface (Kasal et al., 2010b) or for the whole structure which requires knowledge of the boundary conditions, since these affect the fundamental natural frequency (Soltis et al., 2002).

3.3 Resistance drilling

The development of modern resistance drilling started in the 1980s, although manual resistance drilling has been used since the 1920s. Early models consisted of a scratch pin and spring to record the resistance. There were attempts to reduce the resonance phenomena of the spring by adding additional springs, although this introduced thresholds leading to inaccurate resistance profiles. Further development during the late 1980s showed that electronic regulation and recording of the motors energy consumption is necessary for reliable results (Rinn, 2012).

When using a resistance drill, the torque required for the drill bit to be rotated with constant speed while being driven forward with constant speed is recorded. The torque is related to the resistance of the timber, producing a graph with the relative resistance of the specimen (see Figure 3.4). From this graph, the location and extent of interior decay can be determined since the affected areas offer lower resistance. Other defects such as knots and cracks can also be identified due to their respective increase or lack of resistance (Lear et al., 2010).

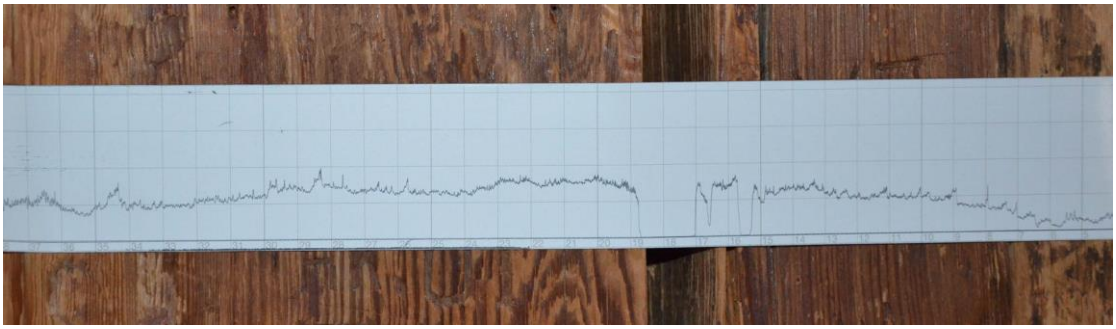

Figure 3.4 *Graph from resistance drilling superimposed over the drilled member in order to illustrate the varying resistance through the cross-section and the lack of resistance at the crack.*

The results from resistance drilling are local and multiple tests have to be performed to map the decay in an area. Resistance drilling can be considered as a non-destructive method since its effect on the structural performance is negligible, but the hole from the drill may limit its use due to aesthetics (Lear et al., 2010). The head of the drill bit is wider (2-3mm) than the shaft (1-1.5mm) in order to eliminate friction from the shaft and therefore only records the resistance at the top of the drill (Feio, 2006). A side effect of the small diameter is the low stiffness of the shaft, due to this the drill may deviate during the drilling process which leads to additional friction along the shaft anyway (Lear et al., 2010).

There have been attempts to relate the resistance to the density with R^2-values ranging from 0.21 to 0.85 (Lear, 2005), requiring further development before being used for in-situ evaluation (Kasal & Anthony, 2004). Although a close correlation to the gross density from X-ray testing has been found (Feio, 2006). Use of a modern, electrical, resistance drill is crucial for density measurements. Knowledge of the type of wood and annual ring orientation is required to make a proper interpretation of the produced graph. For example softwoods tend to have a lower density at the centre, which can falsely be interpreted as decay. The drilling should be performed radially to provide the most information regarding annual rings and simplify the identification of decay. (Rinn, 2012)

4 Current assessment strategies

In order to assess timber structures there are some standards and recommendations that can be adopted. Here documents published by the International Organization for Standardization (ISO), International Council on Monuments and Sites (ICOMOS) and The American Society of Civil Engineers (ASCE) are presented. The purpose of this chapter is to give an overview of available standards that can be completely or partially adopted for this case study. Some parts of the standards will be selected to be part of the adopted strategy (see Chapter 5). These standards share a common sequential methodology of anamnesis, diagnosis, therapy and control. These are medical terms, used by ICOMOS, referring to different stages of treatment. Anamnesis is a term referring to the gathering of information about the original structure and changes to it (e.g. damages, repairs, change of purpose etc.). Diagnosis is the investigation and analysis of the status of the structure to determine its current capacity. Therapy refers to interventions such as replacement or repairs of members. Control is the qualified estimation of future behaviour, residual service life and how it subsequently should be monitored. (ISCARSAH, 2003) Although the documents follow the same work sequence, they put emphasis on different parts (Magnus, 2008).

4.1 International standard ISO13822

According to ISO13822 (*Bases for design of structures – Assessment of existing structures*) the procedure of the assessment should account for the assessment objectives, specific circumstances and actual conditions. Furthermore, the standard may be applied on susceptible heritage structures, as long as eventual preservations of the historical appearance and materials are considered carefully. However, this standard emphasizes the anamnesis and diagnosis, which is in line with this thesis. The procedure in ISO13822, which is specified below and further explained thereafter, is strongly dependent of the actual assessment objectives:

a) Specification of the assessment objectives

b) Scenarios

c) Preliminary assessment:

    1) study of documents and other evidence

    2) preliminary inspection

    3) preliminary checks

    4) decisions on immediate actions

    5) recommendation for detailed assessment

d) Detailed assessment:

    1) detailed documentary search and review

    2) detailed inspection and material testing

    3) determination of actions

    4) determination of properties of the structure

5) structural analysis

6) verification

e) Results of assessment:

1) report

2) conceptual design of construction interventions

3) control of risk

f) Repeat the sequence if necessary

The very first step in the procedure is that concerned persons together should specify the assessment objectives. This specification forms the basis for the subsequent assessment approach. After this initiation it is crucial to identify different scenarios that may affect the structure in different ways and from here determine critical situations.

The following preliminary assessment is of a qualitative nature and aims at gathering relevant information about the structure by means of document studies and preliminary inspection (also in a non-destructive manner), in order to obtain understanding about the condition of the structure and its behaviour. In order to prepare future assessment of the structure, preliminary checks can be performed to map things like poor details. Such eventual details may jeopardize the future safety and serviceability, why the preparation of the future assessments should highlight these deficiencies. Sometimes the preliminary inspections and/or checks indicate critical issues that need either immediate actions or immediate further assessment with eventual subsequent actions. However, sometimes issues are not that critical, why further detailed inspection is appropriate before conclusions about the structural condition are drawn. In case of issues are absent, the following detailed inspection, is superfluous.

The detailed assessment phase in ISO13822 is of a quantitative nature and is a deepening of the preliminary inspection, now searching for and studying detailed documents such as drawings, specifications, structural calculations, inspection and maintenance records, details of modifications etc. If these documents are insufficient for identification of details and dimensions of the structure and determination of material properties, a detailed inspection including material testing is recommended. This conduct should generate that information, which is of great importance in the subsequent structural analysis. The previous gathered information will serve as a basis for the detailed inspection and material testing. After this sub-phase it is stated that particularly environmental actions on the structure should be determined by analysis as in ISO2394 (*General principles on reliability for structures*). In cases where detailed structural analysis or inspection solely lacks in illustrating adequate structural reliability of the structure, it is possible to determine the properties of the whole structure as a complement to the material properties. At this point it is possible to conduct the structural analysis. This should be in accordance with ISO2394 where possible deterioration should be considered. The structure should either be verified by lasting and reliable codes or satisfactory historical performance.

Regardless of the results of the performed assessment, these results should be reported. This report shall serve as a basis for a conceptual design of construction

interventions whenever the structure turns out to possess insufficient safety and/or serviceability. Alternatively, control of risk can be initiated by restricting imposed actions, changing the use of the structure or installing a monitor system in-situ.

4.2 Publications from ICOMOS

ICOMOS has published several recommendations and guidelines regarding historic structures and other heritage values. Due to the mission and intent of ICOMOS, the organization focuses on the restoration and preservation parts of assessment procedure (ICOMOS, 2013). In 1999 ICOMOS adopted the *Principles for the preservation of historic timber structures* which is a brief guideline for how interventions should be performed, in cases that interventions are deemed necessary. The quality of the preceding assessment steps is required to be thorough and accurate. It describes how refurbishment should be carried out so that the original characteristics and function remain intact. This guideline is not of greater significance for this thesis, since it emphasizes the methods of interventions, which is beyond the scope of this thesis (ICOMOS, 1999).

Recommendations for the analysis, conservation and structural restoration of architectural heritage is a document published by International Scientific Committee for Analysis and Restoration of Structures of Architectural Heritage (ISCARSAH), part of ICOMOS. Its focus lies on the assessment of the structural condition rather than the following interventions. These recommendations favour an interdisciplinary approach that combines different interests and knowledge (ISCARSAH, 2003).

The document is divided into two parts, where the first presents basic principles for the assessment and repair (ISCARSAH, 2003). These principles can be summarized into that interventions should be minimal and only be made after a thorough understanding of the damage and its causes has been reached. The second part further expands on the principles resulting in guidelines regarding how the assessment should be performed. The structure of the document does not offer a structured approach to follow although the arrangement of the chapters appears to suggest the following work order by chapters and subchapters:

- Acquisition of data: Information and Investigation
  - historical, structural and architectural investigation
  - survey of the structure
  - field research and laboratory testing
  - monitoring
- The structural behaviour
  - the structural scheme and damage
  - material characteristics and decay processes
  - actions on the structure and the materials
- Diagnosis and safety evaluation

The acquisition of data chapter is divided into four different parts. The first specifies that changes to the structure, as well as the traditional methods used to construct it, should be researched. Although it should be kept in mind that those documents likely were not produced for structural engineering purposes. Survey of the structure refers to visiting the building in order to identify and map any visible damage, as well as possible causes. Additionally a suggestion for the actual structural behaviour should be established. Field research and laboratory testing refers to both tests to acquire

material properties as the identification of discontinuities, stresses and deformations of the structure. The last subchapter suggests that if deemed necessary the behaviour over time for the structure should be monitored, reasons for this could be if there is active deterioration of the structure (ISCARSAH, 2003).

The structural behaviour chapter offers advice for different effects that should be considered in the structural analysis. The first subchapter discusses the choice of structural scheme and how the intended scheme might have been changed due to alterations to the building. The second subchapter consists only of a brief mention that material properties may change over time, but the subject is further expanded upon in the subchapter about actions on the structure and the materials. In addition to changes in materials, that chapter discusses different types of loads that typically can occur (ISCARSAH, 2003).

Diagnosis and safety evaluation is a chapter that discusses the validity of the safety evaluation. The advantages and drawbacks of different evaluation methods (historic, qualitative and analytical) are discussed. Due to the qualitative nature of the assessment process the document calls for an "Explanatory Report" in which choices made, and resulting inaccuracies, during the assessment process are explained. The final chapter, not featured in the list above, contains a brief explanation of common problems for different building materials, providing help to identify areas of interest (ISCARSAH, 2003).

4.3 ASCE standard 11-99

The American Society of Civil Engineers has published a standard (*Guideline for Structural Condition Assessment of Existing Buildings*) relevant to the thesis, like the ISO13822 standard it follows a layout of preliminary and detailed assessment. The purpose of the preliminary assessment is to evaluate the need for a detailed analysis and what that analysis should focus on, while the detailed analysis should verify if the structure satisfies the performance criteria and suggest suitable interventions if it fails to. According to the standard the preliminary assessment may be omitted if it has been determined beforehand that a detailed assessment is necessary (ASCE, 2000).

The preliminary assessment consists of inspection, document review, and preliminary analysis. During inspection the structural system and critical members should be identified for the subsequent analysis and as a basis for eventual detailed assessment. If the documentation lacks information regarding the materials used for construction, the standard suggests that in-situ testing may be justified if the material properties have a significant impact on the behaviour of the structures. Otherwise, approximations should be made according to common values at the time of design and construction. The preliminary analysis should be focused on critical members and connections. Results from this analysis should be compared to the current condition of the structure in order to determine the need for a detailed assessment (ASCE, 2000).

In the detailed assessment the entire structural system should be considered rather than being treated as separate members and connections. The same steps as in the preliminary assessment are performed in the detailed assessment, although more comprehensively. If the structure fails to pass the performance criteria the assessment may be further refined, i.e. a more detailed analysis and testing, before being deemed as insufficient. The result of the detailed assessment should be presented along with

recommendations for actions if the structure failed to pass the assessment (ASCE, 2000).

Included in the standard is also a summary of state of the art of different test methods, both non-destructive and destructive ones as well as in-situ and in laboratories at the time the standard was written (ASCE, 2000).

4.4 Comparison between documents

The earlier presented publications are hereafter referred to by the publishing organisation names rather than the document names. A major difference between the documents is that ISO and ASCE are standards while ICOMOS is a set of recommendations when assessing heritage structures. Upon comparison of these documents it is revealed that ISO and ASCE are primarily written with regard to newer structures where current or recent design codes have been applied in the design and comprehensive documentation can be used as an information source. In ICOMOS the literature study is instead focused on determining the historical value of the structure.

ISO states that it may be applied to heritage structures as well, by carefully considering the preservation techniques and by restricting the use of the newer codes in the assessment. However, ICOMOS provides a more focused assessment procedure for these types of structure.

In ASCE the results of the preliminary structural analysis should be integrated with the actual conditions to draw a conclusion, but for a detailed analysis the performance criteria must be reached. A similar point in ISO is that differences between results of the structural analysis and actual condition of the structure should be explained. Both ISO and ICOMOS offer the possibility to use the structures past performance to determine the structure as safe and serviceable. Additionally ICOMOS suggests comparing the structure to similar structures already deemed safe, although ICOMOS points out that both these qualitative analyses as well as a quantitative analysis has uncertainties and advocates a combination of both type of analyses.

Included in ASCE and ICOMOS are recommendations regarding features in the structure that should be investigated, mainly connections and the behaviour of the structure as a whole. Similar tips are not included in ISO, although it can be argued that the structural engineer involved should have sufficient experience to identify these features.

Both ASCE and ISO divide the assessment into a preliminary and detailed phase. In ASCE these phases differ in the sense that the preliminary analysis considers critical members and connections while the detailed analysis considers the whole structure working as a system. ISO lacks a clear division between the preliminary and detailed assessment, suggesting that the division should be made from experience.

5 Adapted assessment strategy

Each building requires a unique assessment strategy. In this case study, the standard of ISO13822 was modified to match the nature of Skansen Lejonet and the aim of the thesis. Assigned technologies for this case study were X-ray imaging, stress wave testing and resistance drilling (all described in Chapter 3). These can provide information of the timber properties which cannot be measured by traditional methods, such as visual inspection. The strategy for the detailed assessment needed to be well formulated in order to achieve accurate and reliable results in-situ. The adapted assessment strategy is as follows and explained afterwards in this chapter:

a) Specification of the assessment objectives

b) Scenarios

c) Preliminary assessment:

    1) study of documents and other evidence

    2) preliminary inspection

d) Detailed assessment:

    1) detailed inspection

    2) material testing

    3) structural analysis

    4) verification

e) Results of assessment

This explicit assessment strategy for Skansen Lejonet was fundamentally based on ISO13822, with some sub-phases removed or altered from the original list that was presented in Section 4.1, due to the nature of this assessment. However, the methodology of an initial qualitative survey followed by a quantitative survey and analysis was retained. The explanation of this adaptation, utilizing the aforementioned NDT methods, is presented as follows, in accordance to the list above.

5.1 Specification of the assessment objectives

The assessment objectives for this case study were chosen accordingly to the objectives stated for the thesis in Section 1.3. Briefly recalled here, the aim of evaluating different combinations of NDTs was reached by four main objectives. By performing in-situ inspection together with NDT testing, material properties can be obtained. This test data together with geometrical information were used as input data for several structural models that reflect the current behaviour of the floor structures. Finally, relevant utilization ratios (see Section 5.4.4) were calculated and compared between the models.

5.2 Scenarios of the two load cases

Two scenarios were considered, the current use for ceremonial events which corresponds to load category C2 (4.0 kN/m^2) in Eurocode 1 (SIS, 2002) and the original intended use as artillery battery floors. The latter one was represented by load category A (2.0 kN/m^2) in Eurocode 1 together with point loads from cannons at varying positions. Furthermore, the removal of primary beams in the upper floor was considered for the original intended use. These scenarios were treated as two different load cases in the detailed assessment.

5.3 Preliminary assessment

The preliminary assessment was not decisive for this strategy due to the aim of the thesis; the detailed assessment will be performed regardless of the results of the preliminary assessment. Also some sub-phases in the preliminary assessment are superfluous and therefore not explicitly performed or presented. However, the preliminary assessment is still essential, since it facilitates the preparation of the detailed assessment (ISO13822, 2001), i.e. identifying points with suspected damage where NDT should be performed.

5.3.1 Study of documents and other evidence

Regarding the history of the building, literature study was focused on finding relevant events (e.g. fire, repairs, change of use) which may have affected the behaviour of the structure (ISCARSAH, 2003). These events were then further studied in the following detailed assessment.

5.3.2 Preliminary inspection

The first course of action should be an initial visit to the site to identify the general condition of the building (ISO13822, 2001). To obtain a proper basis for the detailed assessment the qualitative preliminary assessment should be focused on comprehending connections, geometry, moisture conditions, deterioration and other visible phenomena based on a simple inspection (ISCARSAH, 2003). As mentioned in Section 2.2 the presence of moisture in timber has a certain relationship to deterioration in timber. Therefore, signs of moisture damages may motivate for further material testing with NDTs at affected locations. In order to facilitate proceeding documentation and in-situ communication, preparation was made by organising the members in a methodical way. Preferably this nomenclature is established in a manner that gives each connection a unique designation.

5.4 Detailed assessment

The detailed assessment phase was divided into two major parts; the initial quantifying survey including NDT executions and then the following quantitative analysis of the structure. For a successful assessment the sequence of applied NDT methods may be of significant importance, the sequence should therefore consider the assessment purpose and output from each method.

5.4.1 Detailed inspection

In the detailed inspection events discovered in the preliminary assessment were studied in detail in order to quantify the corresponding actions on the structure. Also the geometries and conditions were mapped for both floors, according to the prepared nomenclature from the preliminary inspection. Data sheets for each member should be prepared in advance allowing for a standardized assessment (Palaia, 2007). The established data sheets for this case study can be seen in Appendix A.

5.4.2 Material testing

The aim of the quantifying survey was to determine the relevant properties of both damaged and sound timber members, as well as determining which members that were damaged and to what extent. Since measurements of each member were not always possible due to accessibility, it is preferable to test a few members along the entire lengths rather than spreading the test points between many different members (Williams, 2009). In this case study of Skansen Lejonet the untested members were therefore assigned properties based on similarities to tested members. The sought properties were:

- Timber density ρ
- Static modulus of elasticity E_s and
- Second moment of area I

The second moment of area I is obtained from the cross-section geometry of the beams measured during the detailed inspection. The product of I and E_s gives the stiffness of a beam. With this data it was then possible to establish the structural models for the timber floor structures and perform the structural analyses.

It is discussable in which sequence the different NDT methods should be applied, in order to optimize the efforts for the assessment. As presented in Chapter 3, the different NDT methods have different characteristics and hence also different suitability depending on the type of structure being assessed. A preferable sequence for execution of relevant NDT methods is:

1. Stress wave
2. X-ray
3. Resistance drilling

When points suspected to damage have been identified, it is preferable to continue the detailed investigation with the test method associated with the least effort to quickly confirm deteriorated sections (Kasal & Anthony, 2004). Therefore one should start with the stress wave testing since this can be conducted quickly and systematically by surrounding a suspected area and then re-surround it in order to approach and map the location and extent of the damage (see Figure 5.1).

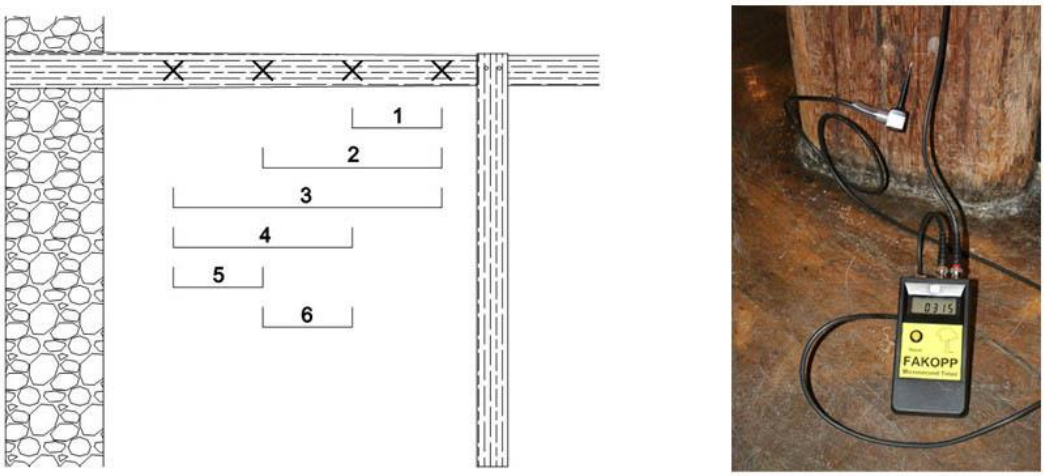

Figure 5.1 *Approach for tracking eventual deterioration or different quality of wood in a member (Left), setup of stress wave measurement (Right).*

Since the stress wave testing only maps the condition of the tested member in terms of velocities, this measurement of the condition must be complemented with information about the density in order to determine the dynamic and static modulus of elasticity (see Section 3.2). Reasonable velocities for sound wood are approximately 1000 m/s and 4000-5500 m/s for transverse and longitudinal testing respectively (Ross et al., 2004). The density information may be obtained either by X-ray or resistance drilling, but in this case X-ray is preferable. Resistance drilling has one major drawback; it requires several drillings to get reliable results leaving many residual holes (therefore sometimes considered as a semi-destructive test) (Feio, 2006). In contrast X-ray provides data over a larger region with one successful exposure as well as a comprehensive view of the interior. Although, due to the elaborate placement of the equipment, X-ray imaging requires more effort than the stress wave testing and resistance drilling.

In this case study, the testing sequence was altered slightly, initial X-ray imaging was followed by stress wave testing and finally resistance drilling, due to availability of equipments. This alteration was not ideal, but the impact could be minimized by first performing X-ray imaging to determine the density based on visual inspection. The following stress wave testing could then indicate eventual further need for X-ray imaging. Resistance drilling may be used for measuring the depth of charring and surface deterioration. With these results it was possible to calculate the effective cross-section at certain locations. The sought material properties (timber density and static modulus of elasticity) were obtained via the respective approach for each NDT method. However, the determination of density via X-ray was done by analyzing the greyscale of radiographs in the software ImageJ. These approaches or functions are here recalled from Chapter 3 and summarized in Table 5.1.

Table 5.1 *Associated approaches or functions for determination of material properties for each NDT method used.*

NDT method	Associated approach or function(s)
X-ray	Greyscale analysis of radiographs
Stress wave	$E_d = V^2 \cdot \rho \quad , \quad E_s = a \cdot E_d + b$
Resistance drilling	Qualitative interpretation of data

5.4.3 Structural analysis

The structural analysis for each floor structure was carried out in terms of establishing several digital structural models based on the detailed inspection and material testing. The outputs of bending moment and shear force values served as inputs for the structural verification.

5.4.4 Verification

The structural capacity was verified by applying Eurocode 5 (SIS, 2004) and determining the Ultimate Limit State (ULS) capacity and utilization ratios for:

- Bending moment
- Shear force
- Buckling of columns

These calculations excluded any partial safety factors since actual material properties are estimated through testing. Further, any bending moments and shear forces were not reduced due to geometrical configurations.

5.5 Results of assessment

The results of the assessment are presented within the thesis, corresponding to some of the reports requested by the standard, although not in the suggested format. Instead the results of the study of existing documents will be presented in Chapter 6 (Case study of Skansen Lejonet), while the preliminary and detailed in-situ inspection as well as material testing is presented in Chapter 7 (In-situ assessment of timber properties). The models for the structural analysis are presented in Chapter 8 (Structural analysis of floor structures) together with results and verification. The standard also requests design of interventions and control of risks associated with the interventions. This was not performed due to the aim and limitations of the thesis.

6 Case study of Skansen Lejonet

Skansen Lejonet was built in the years 1687-1693, designed by Swedish count, military and architect Erik Dahlbergh, as part of the defence of Gothenburg, besides Skansen Kronan that was built at the same time. As a fortlet, Skansen Lejonet required a certain structural strength in order to withstand possible attacks from enemies. The outer masonry wall is at some spots approximately 4 meters thick, providing armour against cannon attacks. The interior core is separated into two major vertical cells by a circumferential masonry arch with the upper cell further divided by timber floors (see Figure 6.1). Although Skansen Lejonet has never been attacked by artillery, it has been exposed to some environmental attacks during its lifetime.

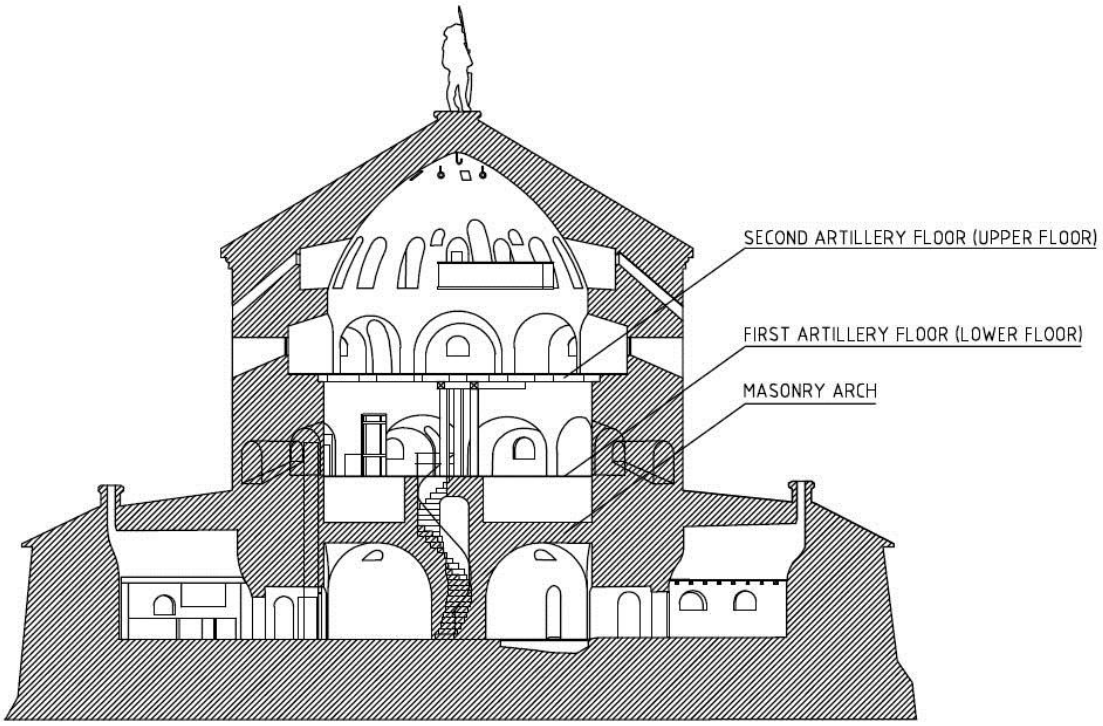

Figure 6.1 *Cross-section of Skansen Lejonet as it is today (modified with text). (Andersson, 2011)*

6.1 Important historical events and load history

In this section, some events that may be critical regarding environmental damaging during the lifetime of Skansen Lejonet are presented briefly:

1687 Beginning of construction

1693 Completion of Skansen Lejonet

1755 Reconstruction of the roof with a new lead cover and replacement of deteriorated timber members

1806 Due to Napoleon's Berlin Decree the fortlet was armed

1822 Used as storage for nearby ammunition factory

1891 Fire in both the lower roof structure and in the top of the tower, ignited by sparks travelled by wind from nearby warehouse

1893 Refurbishment of the fire damages completed

1895 Ammunition factory moved to Kviberg, resulting in Skansen Lejonet was left without purpose

1908 Remodelling to a facility for storage for the third-class infantry, removal of the two uppermost floor structures (excluded in Figure 6.1) and installation of windows in all openings in the tower

1942 The end of storage for third-class infantry, resulting in Skansen Lejonet being deserted and subsequently vandalized, e.g. entrance floor was partially burnt down and some windows were broken

1973 Flooding of the well on entrance level and a comprehensive refurbishment of the interior; new flooring at all levels and installation of heat and ventilation systems

1987 Replacement of timber joists in two of the outworks

2010 Roof structure of the tower was replaced and concrete mortar in façade was replaced

During the first half of the 20th century there were several requests for repairs and some of them were performed. These efforts concerned the roof structure, windows and masonry with no mention of the timber. Since 1973 Götiska Förbundet operates in the building as well as leasing for weddings and dinners for up to 130 people. These events often occur in both artillery floors.

6.2 Structural description of Skansen Lejonet

Skansen Lejonet is founded directly on bedrock, eliminating risks for uneven settlements. The outworks and the wall of the circular tower were made with lime mortar and blocks of diabase, granite and gneiss, probably from local bedrock. The thickness of the wall is varying between approximately three and four meters and has openings for infantry as well as artillery. The roof cover is supported by a plastered masonry vault, created by curling the walls inwards at the top of the tower.

The entrance level originally had timber flooring above the now dry well and earthen flooring for the remaining parts. During refurbishments the earthen floor has been replaced by slate and the timber floor structure has been rebuilt with supplementary flooring from the upper levels. There is a masonry staircase covered with plaster in the middle of the floor which is connected to the outer wall by the circumferential masonry vault. The vault is either made from rocks or bricks and the bottom surface is covered with plaster while the top is covered with aggregate.

Between the entrance floor and the first artillery floor is the so called hidden floor which is accessible through a hatch in the first artillery floor. The hidden floor was not present in early drawings and was believed to have been added to adjust the height of the first artillery floor with regard to firing angles for cannons. The floor has traditionally been used for storage and continues to do so. It has also provided ventilation for the upper levels. Heated air was released into the hidden floor and seeped up to the first artillery floor through gaps between the flooring and outer wall. The floor originally consisted of the brick masonry staircase in the middle of the room and the outer wall of which neither are covered with plaster. During the refurbishment in the 1970s ventilation equipment was installed and the staircase masonry was

reinforced with additional masonry. The flooring consists of the aggregate which cover the vault of the entrance floor.

The staircase from the entrance floor emerges in the middle of the first artillery floor which is now used as a dining area. In addition to the staircase there are four timber columns, which support the second artillery floor, placed in the centre of the floor. The original flooring was used in the 1970s refurbishment of the entrance and second artillery floor, and was replaced by parquet. One of the embrasures has been covered and now contains a kitchen elevator and air intake for earlier ventilation system. The outer wall is covered with plaster and contains a staircase leading up to the second artillery floor.

The second artillery floor is currently the top floor of the building and used for ceremonies and meetings. Originally there was an infantry floor as well as additional floors in case an attic was needed. However, the timber floors were removed and the infantry floor was remodelled into a balcony in 1908. Drawings from 1807 reveal that there were columns continuing up to the eventual attic, these were placed on top of the columns in the first artillery floor. Furthermore, these drawings show an opening in the floor between the primary beams for the second artillery floor. Additionally a second, larger, opening in the floor was made at a later stage to the side of the primary beams. Currently the openings are covered but traces can be seen in the secondary beams which are replaced below the first opening and missing a portion beneath the second. However, the source for the timber used for this replacement was uncertain. It was also difficult to verify whether the other members are original or not, but there are no signs of any replacements of these. The original flooring was repaired with flooring from the first artillery floor and has been covered with parquet. Due to the removal of the infantry floor the ceiling consists of the plastered walls merging together to form a vault.

6.3 Description of floor structures

Both investigated floor structures consist of two primary beams which support a large number of secondary beams. Pine timber was used for the construction. Despite being referred to as secondary, the beams have large cross-sections, sometimes of the same size the primary beams. Each beam differs in cross-section from each other but the general cross-section is about 30x30cm, the beams have a close spacing of approximately 60-70cm and the longest members are 12-13m long. The primary beams are supported at the middle of each room by the staircase masonry and columns, respectively. There is no ceiling in either floor, so the timber floors are fully visible and accessible, except for a portion of the first artillery floor which is obscured by a recently built archive and the staircase masonry. Although the height in the second artillery floor, approximately 4m, is a limiting factor regarding accessibility, while the height in the first artillery floor is approximately 1.8m. Both timber floor structures are illustrated in Figure 6.2.

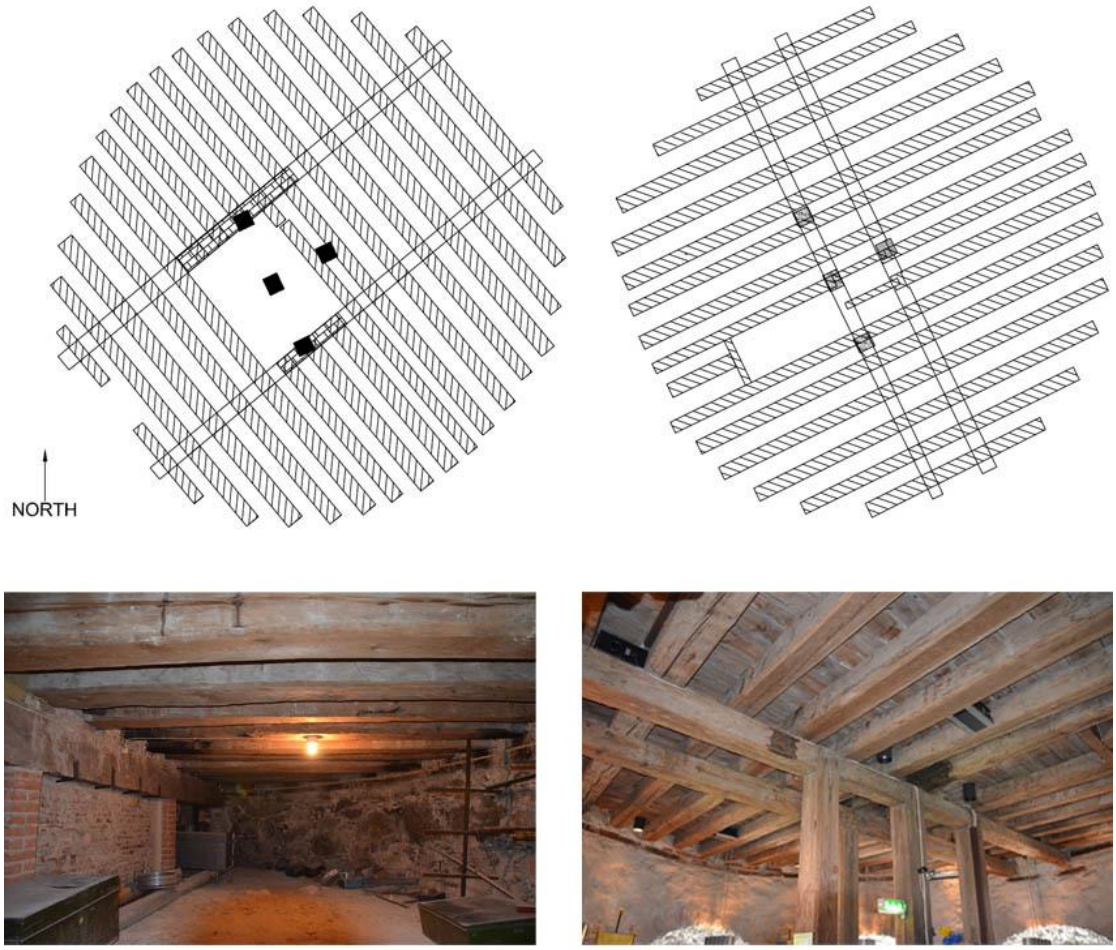

Figure 6.2 *Illustration of both floor structures showing the general appearances. First artillery floor (Left) and second artillery floor (Right).*

6.4 Load history during service life

The original armament on both artillery floors of Skansen Lejonet consisted of one 12-pound cannon and twelve 6-pound cannons, although documents do not specify the placement (Bernung & Bengtsson, 1993). A 12-pound cannon weighed 1632-1700kg and a 6-pound cannon 850-913kg, depending on if the cannon was made out of cast iron or an alloy (usually bronze or brass). An example of contemporary cannon is shown in Figure 6.3. In addition to the cannons an average of 100 cannonballs were kept per cannon; a cannonball weighs 3kg (6 pounds) or 6kg (12 pounds) depending on cannon (Grenander, 1993). Details regarding the armament in 1806 was not available, but developments in the design of cannons had led to reduced weights (Granefelt et al., 2011), why the original armament was deemed to be the critical load situation.

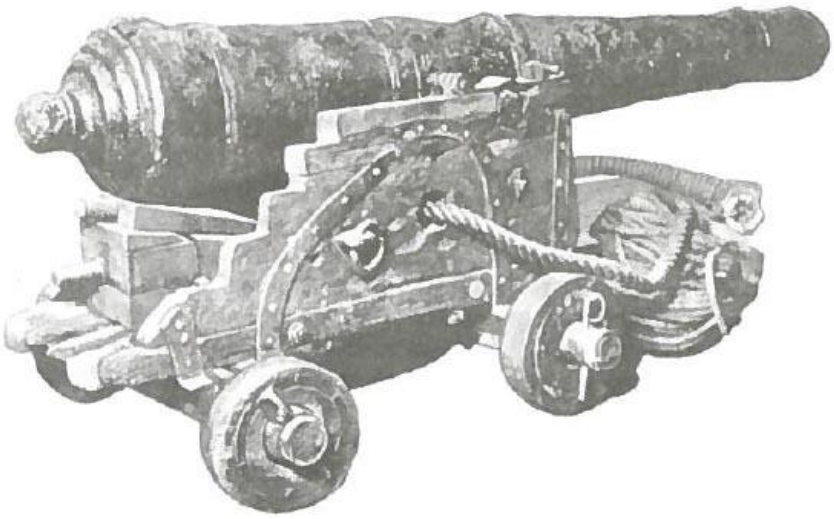

Figure 6.3 *Example of the appearance of the cannons. The figure shows a contemporary 8-pound cannon used in ship (Grenander, 1993).*

Besides the imposed loads from infantry and cannons, there have been environmental loads acting on the floor structure due to moisture. In 1822, the building started to be used as a storage facility for ammunition until 1895 when it was left empty for 13 years. Then in 1908 windows were installed and the building was used for storage until 1942 when it once again was left empty. Considering the dimensions of the floor structures, these have not been subjected to large loads, why any damage (and deflections) would rather have been caused by the lack of maintenance and climate control. Regarding the inner climate, this may be considered as poor until the installation of windows in 1908. Before this installation it is reasonable that the timber floor structures have been exposed to mechano-sorptive creep due to seasonal weather variations. For about 30 years, between 1940s and 1970s, the building was empty and not in use leading to vandalism, poor inner climate and bird droppings. These factors may have degraded the timber floor structure to some extent, since maintenance during those years was minimal (Bernung & Bengtsson, 1993).

7 In-situ assessment of timber properties

The in-situ assessment of Skansen Lejonet was a direct implementation of the adapted assessment strategy developed in Chapter 5. It consisted of the preliminary and detailed inspection as well as material testing using the aforementioned NDT methods.

7.1 Preliminary inspection

At the initial visit, the general function of the floor structure and any obvious deterioration were identified. It was discovered that both floors had similar structures consisting of several secondary beams supported on two primary beams. These were mapped, in terms of member names, by numbering the primary beams and columns with numbers and the secondary beams with letters. This was subsequently complemented with member cross-sections, spans and spacing (edge-to-edge distances), in the detailed inspection.

During the preliminary inspection the search for signs of deterioration was emphasized on the lower floor due to accessibility and the absence of conditioning of this floor structure. In the upper floor, the beams appeared to have been conditioned during the refurbishment, i.e. eventual signs of deterioration were removed to some extent. Charring of varying extent was visible at several secondary beam supports, as well as char-like stains in the spans of the lower floor. Further inspection of a stain revealed it to be char residue on the surface and assumed to only be superficial with no effect on the member. The stains probably appeared when the beams were installed, due to the charred ends scraping against another beam. These stains could probably be found in both floors but have been removed in the upper floor during refurbishment. An example of a charred beam edge at a support can be seen in Figure 7.1, these were of further interest in the material testing.

Figure 7.1 *One of several charred beam edges at supports (Left) and the thickness of the charring is revealed by the crack (Right).*

Stains that indicate earlier moisture exposure could also be seen, both at supports as well as between the supports. The most notable presence of the stains was on primary

beam 1 in the lower floor, near the ventilation equipment (below secondary beam O). Greyish discolourations could be seen throughout the lower floor structure. At places it seemed to have run from the top of the beam while at other places the beam is thoroughly greyish. These stains were suspected to have been caused by waste from earlier refurbishment.

White plaster-like specks could be found throughout the lower floor structure, pictured in Figure 7.*2*. Additionally yellow-green specks were found at some outer wall supports of the lower floor which raised concern. The specks were present at beams, sill plates and at the masonry. Both types of speck were suspected to have been caused by waste from refurbishment rather than being old fruiting bodies from fungal attack, despite the sometimes unexpected locations. Further inspection of the removed part from the beam P revealed fungal growth within the timber, adjacent to damaged earlywood which can be seen in Figure 7.2. Due to this find the origin of the specks as well as accompanying discoloration was reconsidered as possible fungal attack.

Figure 7.2 *White specks and discolouration in the lower floor (Left) and piece from the removed part of beam P showing damage on the earlywood and fungal growth (grey spots, right)).*

Major deterioration was noted at the staircase support of beam K in span 3. Suspected deterioration was noted along the edge of beam E and L. The latter beam also showed a group of holes, ~1-1.5 mm in diameter, similar holes were found at the support of beam D as well. Further inspection revealed signs of insect attack, visible in Figure 7.3. It was suspected that the damage was caused by common furniture beetle (*Anobium punctatum*) or old-house borer (*Hylotrupes bajules*). The former attacks sapwood but not heartwood leaving residual holes of 1-2 mm in diameter (Ridout, 2000), whereas the latter leaves holes of 6-10 mm in diameter.

Figure 7.3 *Damaged region at wall support of beam D in span 1 in lower floor. Several smooth holes (one visible near the centre of the image) raised concern about eventual damage close to the surface and the bottom face. After probing with a screwdriver the damage was revealed and explained as an insect attack.*

7.2 Detailed inspection and moisture measurements

The detailed mapping was prepared in advance by establishing document sheets, both for the overview and for individual members, where essential data is filled in (see Appendix A). For the lower floor measurements of cross-section and spacing of the beams had to be established. However, for the upper floor this information was found in the documentary search, hence the validity had to be verified. During this verification it was decided to establish plane drawings for both floors though. The final mapping is illustrated in Figure 7.4 and Figure 7.5 for the lower floor and in Figure 7.6 and Figure 7.7 for the upper floor. The plane drawings were used to communicate positions of measurements and damages in the proceeding of the assessment.

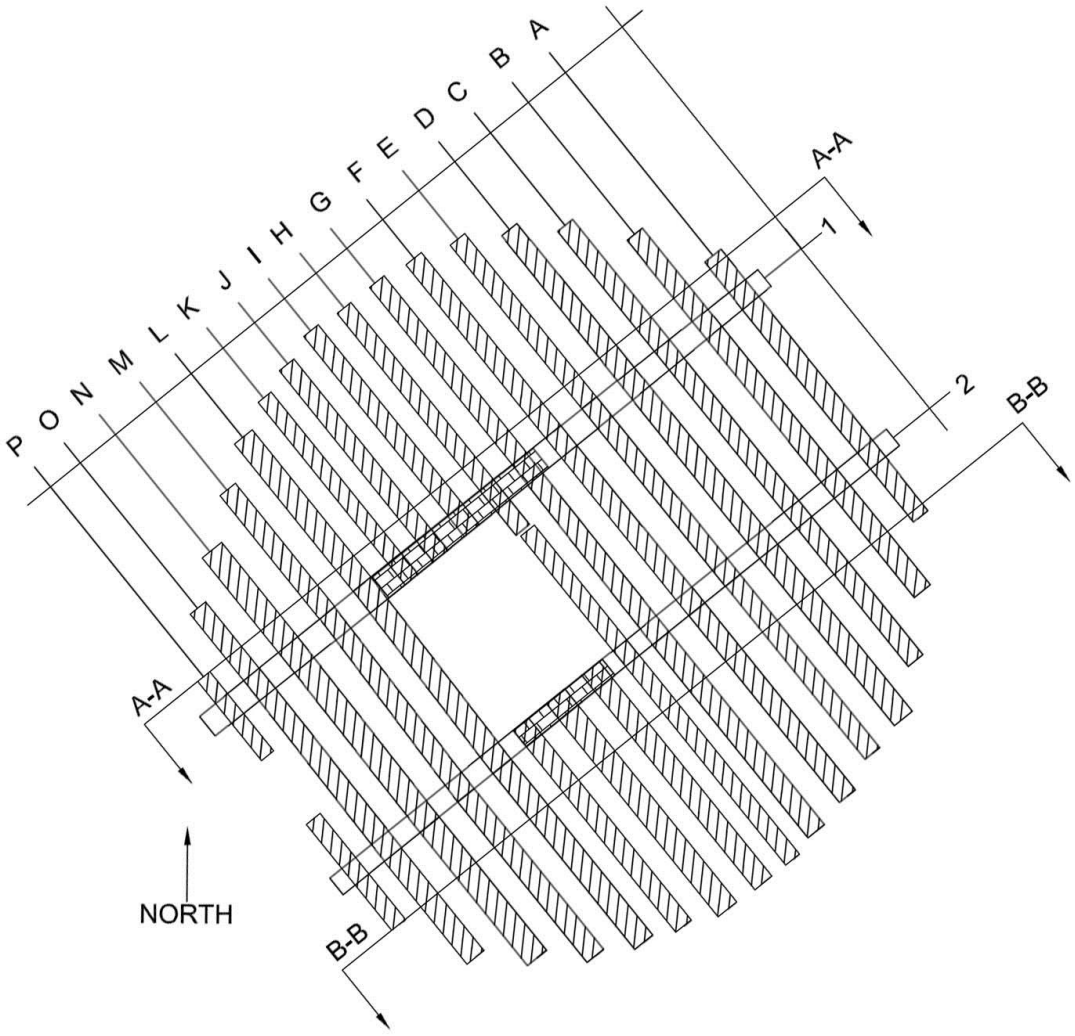

Figure 7.4 *Established plane drawing of first artillery floor (lower floor) with named primary beams (1-2) and secondary beams (A-P).*

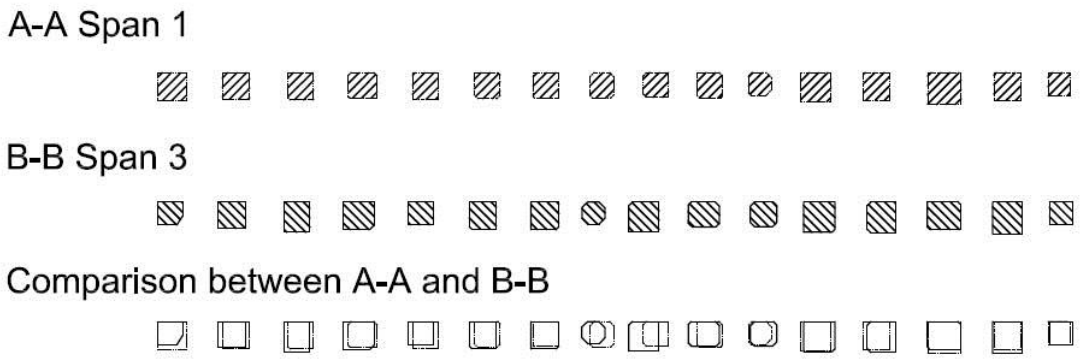

Figure 7.5 *Illustration of sections in the plane drawing of first artillery floor, top) section A-A, middle section B-B and below the illustration of the deviation between section A-A and section B-B.*

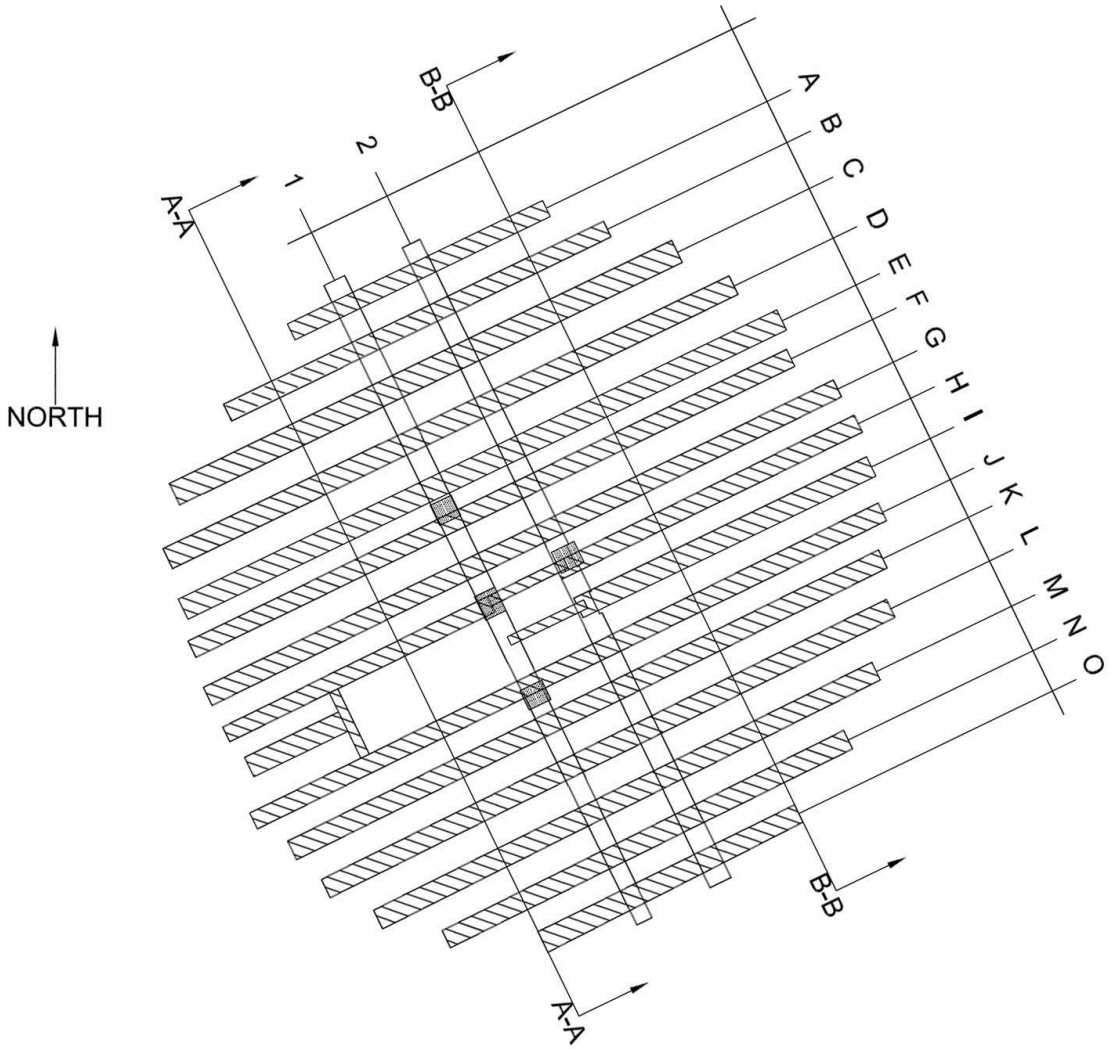

Figure 7.6 *Established plane drawing of second artillery floor (upper floor) with named primary beams (1-2) and secondary beams (A-O).*

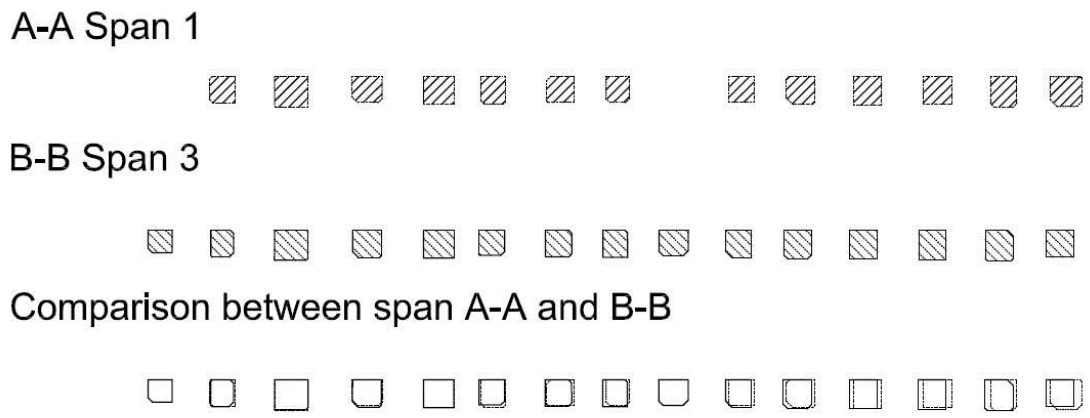

Figure 7.7 *Illustration of sections in the plane drawing of second artillery floor, top) section A-A, middle) section B-B and below the illustration of the deviation between section A-A and section B-B.*

During the detailed inspection, significant cracks and changes in geometry of the beams were recorded for each beam, in addition to the global geometry. The width and height of each beam was measured with a digital calliper or yardstick. The trim and depth of cracks were measured with a yardstick. Spans and edge-to-edge distances between members were measured with a laser rangefinder. The cross-sections for the secondary beams were measured near the middle of each span at a point that was considered representative of the general cross-section of each span. In general the average cross-section was 30 x 30 [in cm]. For the primary beams, measurements were made at both the middle of the spans as well as at the edges of the supports, indicating a slightly larger cross-section than for the secondary beams. Reductions of the cross-section from trimmed corners were noted by measuring the diagonal of the removed area, which was assumed to have an inclination of 45°, see Figure 7.8. The numbers here were also used to identify faces of the beam, e.g. 1-2 corresponds to the right-hand face when looking from span 1 towards span 2. The supports of the beams were documented with photographs as well as notifications about the contact between primary and secondary beams, which affects the structural response. In the lower floor, the length of the support could be measured at some locations. In general this length is about 50 cm for secondary beams and 90 cm, not including the additional reinforcement, for primary beams. For the upper floor these lengths were available in existing drawings.

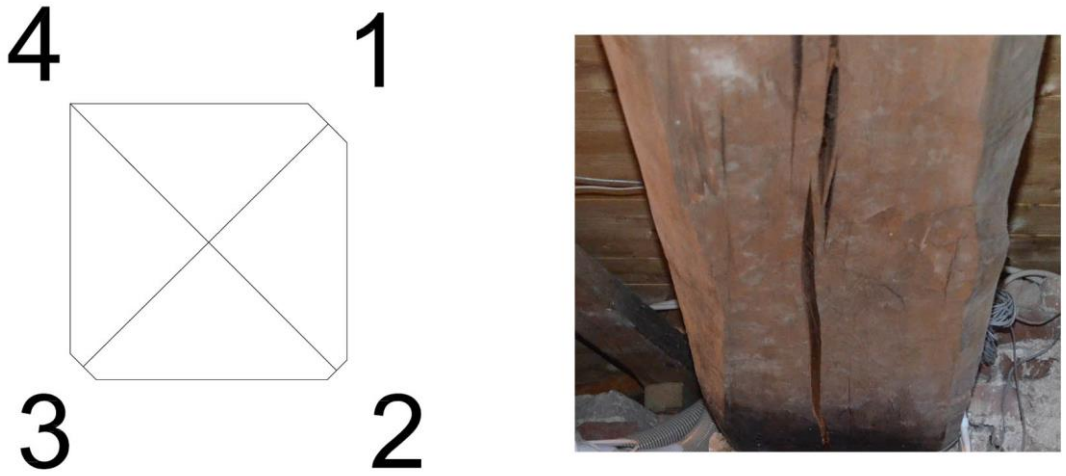

Figure 7.8 *Definition of nomenclature for trimmed corners seen in the direction from beam 1 towards beam 2 regarding secondary beams and from beam A towards beam B regarding primary beams (Left) and example of real trimmed corners (Right).*

In addition, the moisture content in the lower floor was measured with a resistive moisture meter. The moisture content varied between 10-12% throughout the beams and slightly higher in the sill plates in the outer wall. Therefore any moisture correction was not needed for the X-ray and stress wave measurements. Measurements were taken at the outer wall supports due to the risk for moisture ingress due to the masonry (ISCARSAH, 2003), as well as further into the spans. At the stained section of primary beam 1 in the lower floor measurements showed 10.5%, proving that any possible previous moisture have dried out. There was one

measurement of 15.6% in the lower sill plate for beam P, further measurements showed a moisture content of 13.1% in the upper sill plate and 10.7% in the actual beam. It was concluded that any moisture related deterioration had happened earlier and was not an on-going process. This includes the damage suspected to have been caused by common furniture beetle, since it favours moisture contents above 13.5% (Ridout, 2000).

7.3 Tested locations

The tested locations were planned in forehand but also improvised in-situ. The main idea for the testing was to thoroughly map both floors with the use of stress wave and obtain X-ray images for interesting regions identified in the detailed inspection, as well as sound timber regions for comparison. Further on, resistance drilling should be performed in the vicinity of X-rayed regions and where stress wave testing indicated some lack of material quality. The plan drawings of tested locations are illustrated in Figure 7.9 and Figure 7.10 for the lower and upper floor, respectively. In these all transverse stress wave measurements, all X-ray images and all resistance drillings are included, but the longitudinal stress wave measurements that were performed on all members, are excluded. However, a complete documentation with all in-situ tests can be found in Appendix B.

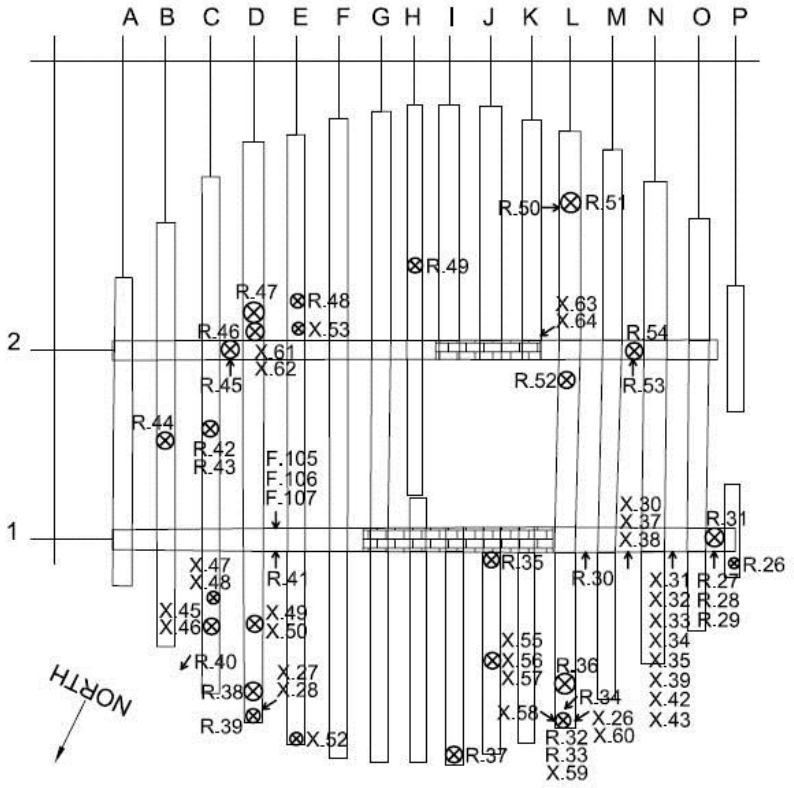

Figure 7.9 Tested locations in the lower floor.

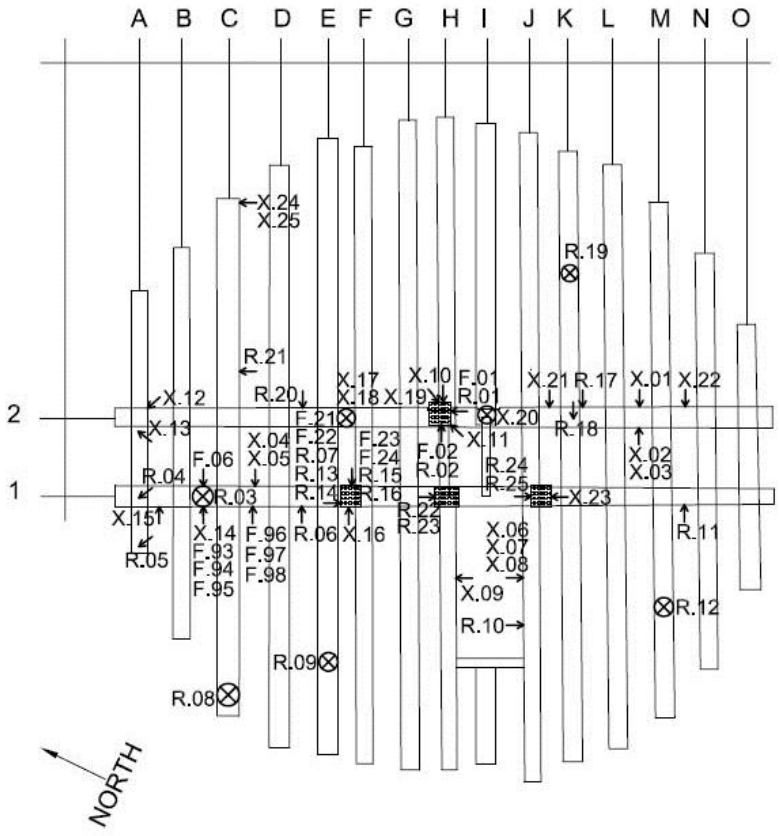

Figure 7.10 Tested locations in the upper floor.

7.4 X-ray

As X-ray imaging provides more comprehensive information than the other two conducted tests, it was consequently, in this case, more demanding in terms of portability and time of testing. However, it is interesting to discuss whether the advantages of excessive information may overweigh the drawbacks of effort or not. The X-ray testing in-situ was performed on both the first and second artillery floor in Skansen Lejonet, however the extent varied slightly between the two due to different conditions. According to the adapted strategy the common issue for both floors was to test locations with identified possible damages and some location that seemed to be sound. In next section, the procedure of the X-ray testing is presented in detail.

7.4.1 Procedure of in-situ X-ray imaging

In this case study the X-ray device Inspector XR200 was used (Golden Engineering Inc.). This device was part of equipment which besides this device consists of phosphor plates, scanner and a laptop computer. The idea of this testing technique was to attach a plate behind an interesting member and to place the X-ray device on a tripod on the opposite side irradiating the member (see Section 3.1). The plate then registered the residual energy of the rays after attenuation in the material and by removing the plate and inserting it into the scanner, it was possible to analyze the greyscale data in the computer. Two imaging types were distinguished; imaging of

interior condition and imaging for density measurements. To enable density measurements in the radiograph, a timber piece (hereafter called calibration wedge) had to be included in the image. By mounting this wedge on the tested member and attaching the plate such that it had adequate coverage and almost in contact with the wedge, to minimize the poor sharpness, the registered greyscale data for the member region could be compared with the corresponding data for the calibration region (for further information about this calibration, see Lechner et al. (2011)). The quadratic cross-section of the piece meant that it could be rotated arbitrarily when mounted on a member. However, the long side of the piece should always point towards the X-ray device, in order to hit the X-rays as perpendicular as possible.

7.4.2 Analyses of radiographs

Analyses of radiographs were distinguished by analysis of interior condition radiographs and analysis of density measurements radiographs. The latter were more demanding in terms of accuracy of greyscale values in order to properly calculate densities. These values might be measured instantly in-situ as a pre-analysis using the software ImageJ to ensure adequate image quality for the subsequent evaluation.

Image quality depends on the energy distribution of the X-rays on the plate and this distribution may be uneven, which affect the accuracy of the density evaluation. This more or less uneven distribution had to be corrected by using an image plate exposed to the X-rays alone, the resulting radiograph is called a background image (Kruglowa, 2012). Since lighter regions indicate lower density and vice versa, it was important that there was no coinciding of higher density parts of the calibration wedge and lighter areas on the background image for a certain setup. If that was the case, the differences between higher and lower densities were compensated to some extent, or even overcompensated, yielding inadequate greyscale values for further density calculation.

As the in-situ tested members deviated from the conditions of the calibration wedge, it was crucial to consider this calibration by means of adjusting the measured greyscale value of the member in the radiograph. In the analyses of radiographs this was done by applying correction factors when deviating thicknesses and moisture contents were prevailing in-situ. The used calibration wedge consisted of eight different timber pieces with different densities glued together and its cross-section was quadratic with the dimension of 30 mm. Regarding the calibration, thickness of the member was of major importance which needed to be considered. Further, the wedge was conditioned to a moisture content of 12% in laboratory, since the reference densities were measured at that moisture content. However, the moisture content could be neglected due to its minor importance in the interval 8-16%. Tables of correction factors for different thicknesses and moisture contents were available (Lechner et al., 2011).

The analysis of a radiograph at the office comprehended the already mentioned greyscale evaluation using the software ImageJ. The greyscale values were taken for the eight different timber pieces in the calibration wedge and for the timber member itself, according to Figure 7.11 avoiding inaccurate values at the borders of each region. These mean values were then adjusted with the correction factor regarding thickness before being matched to corresponding densities. From these values a linear regression between density and greyscale was performed to establish the density of the tested member (see Appendix C for an example of an evaluated radiograph).

Regarding the necessary procedure of correcting an original radiograph due to the uneven energy distribution, this was carried out in ImageJ where it was possible to divide the greyscale of the original radiograph being evaluated with the greyscale of a matching background image. After that the resulting image was multiplied by an arbitrary and appropriate factor to obtain a clear image again. By following this procedure, correct calculations of density could be performed. This procedure is further explained in Kruglowa (2012). To complement the X-ray measurements an approximate density of 420 kg/m^3 was estimated for a small sample, from the removed part of beam P in the lower floor. This density value was determined in laboratory (for calculation see Appendix D).

It is important to keep in mind that radiographs intended for density measurements may not be adjusted with regard to brightness or contrast and should be saved in a lossless file format, i.e. no data is lost. A radiograph affected by such alterations, whether it is for interior condition estimation or density measurements, may only be studied regarding the interior conditions.

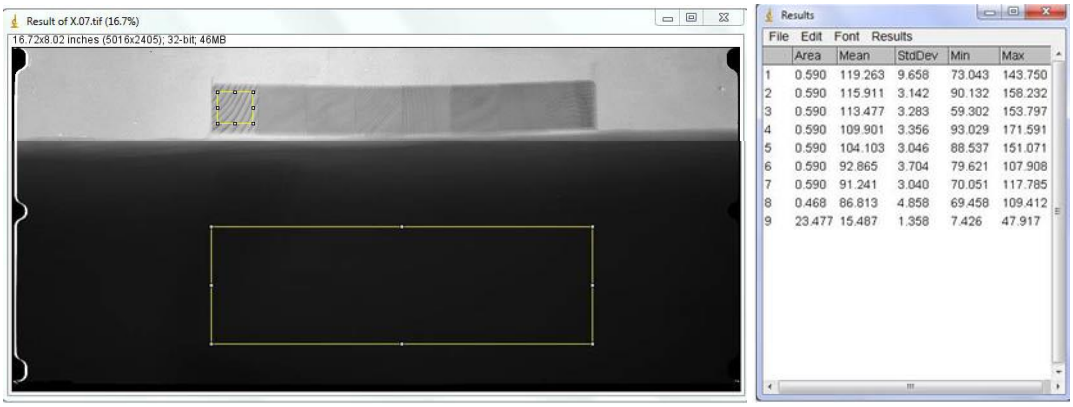

Figure 7.11 *Screenshot from ImageJ illustrating the process for analysing a corrected radiograph (X.07). Starting to measure mean greyscale value within the box, in the leftmost piece (lowest density) in the calibration wedge and tabulate the value, proceeding with same measuring towards the rightmost piece (highest density), measure mean greyscale value for the investigated member, drawing a box approximately as wide as the calibration wedge.*

7.4.3 Summary of X-ray imaging results

The density results of the analyses are summarized and presented in Table 7.1. The mean densities from radiographs were calculated separately for primary and secondary beams. Beams in different floors were also separated in this calculation which is presented in Table 7.2.

Table 7.1 Summary of density results from evaluated radiographs.

Radiograph	Floor	Beam	Density	R^2
X.04	Upper	Primary 1	424 kg/m^3	0,90
X.06	Upper	Secondary J	405 kg/m^3	0,98
X.07	Upper	Secondary J	474 kg/m^3	0,98
X.17	Upper	Primary 2	462 kg/m^3	0,94
X.30	Lower	Primary 1	458 kg/m^3	0,96
X.37	Lower	Primary 1	492 kg/m^3	0,97
X.43	Lower	Primary 1	476 kg/m^3	0,98
X.48	Lower	Secondary C	480 kg/m^3	0,97
X.55	Lower	Secondary J	434 kg/m^3	0,98

Table 7.2 Mean densities based on the results presented in Table 7.1.

	Lower floor		Upper floor	
	Primary	**Secondary**	**Primary**	**Secondary**
Mean density	475 kg/m^3	457 kg/m^3	424 kg/m^3	440 kg/m^3

As a verification of the density results, the radiographs yielded densities in the same spectrum as the expected sample density. However, densities from X-ray measurements become larger than the sample density, for all beams in both floor structures. The densities from radiographs were used in the subsequent structural analysis. Values of MOE, based on density, were calculated with the following expression for air-dried timber given by Dinwoodie (2000):

$E = 25{,}186 \cdot G^{0{,}9454}$

where E [GPa] is the modulus of elasticity and G is the specific gravity.

A qualitative radiograph taken of a charred support revealed the grain structure of the timber to be intact; therefore suspicions of any thorough deterioration of the charred cross-sections were eliminated. Any local weakening of the timber close to the

charring could not be determined and required further investigation. Additionally the outer wall was slightly damaged at the support of beam L in span 1 in the lower floor, which allowed radiographs to be taken a slight distance into the wall. A radiograph taken at that location showed no damage to the member, which otherwise was suspected due to the risk of unfavourable moisture conditions. Further radiographs of the same beam, at a position close to where deterioration was found with resistance drilling, did not show any signs of deterioration. Although a radiograph of beam H in the upper floor showed signs of similar deterioration as drilling results indicated for beam L in the lower floor, see Figure 7.12. In general, the qualitative radiographs showed the grain structure of the members to be intact.

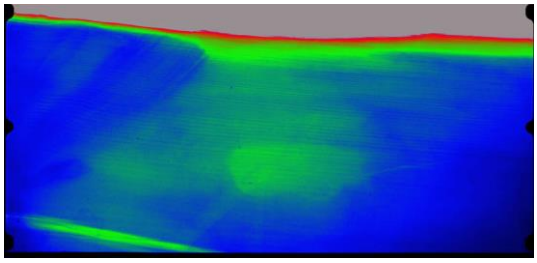

Figure 7.12 *A qualitative radiograph (X.09) of beam H in the upper floor (modified contrast and colourized) indicates similar deterioration (in the centre) as drilling results indicated for beam L in the lower floor (cf. Figure 7.21).*

Radiographs of connections showed that the nails were generally in good condition at the inspected locations, except at the wall support in span 1 for primary beam 1 in the upper floor. There, an iron bar was attached to the top of the beam with three nails which can be seen in Figure 7.13. The outline of the leftmost nail was not as sharp as the other nails which is a sign of corrosion, i.e. moisture problems, additionally it should be noted that the rightmost nail appeared to have failed. The connection between column 5 and primary beam 1 in the upper floor is also pictured in Figure 7.13 as an example of a connection without damage. The nails were part of two iron details which connected the column to the beam.

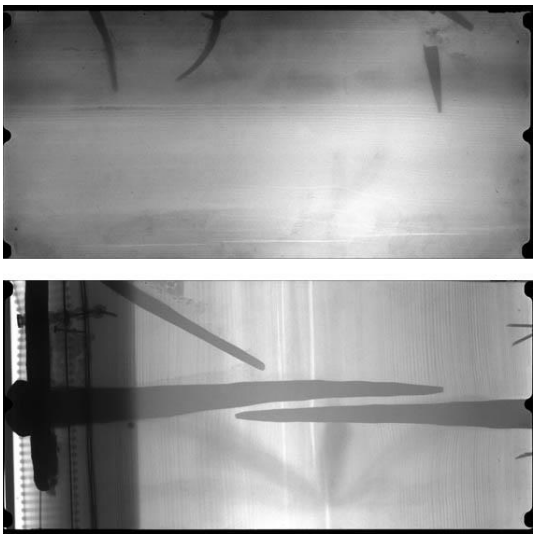

Figure 7.13 Radiograph X.15 modified showing detail of primary beam at wall support (Top) and radiograph X.23 modified showing nails at beam-column connection (Bottom).

7.5 Stress wave

The device that was used for the stress wave measurements was FAKOPP Microsecond Timer (FAKOPP Enterprise). The longitudinal stress wave measurements were performed in every span of each beam in the lower floor and in span 1 and 3 in the upper floor, except the two outermost secondary beams in both floors due to the almost absent span 1 and span 3 in those beams. Generally, these measurements embodied whole spans or the middle of the spans. Due to limited accessibility and convenience there were some deviations in this general strategy in-situ.

7.5.1 Procedure of in-situ stress wave measurements

Part of the test setup of the stress wave equipment is illustrated in Figure 5.1. Tests were performed on a face of the beam that was considered appropriate by means of accessibility. The spikes of the transducers should be inserted in such a way that the angle to the timber surface is preferably 45° and below 60° to ensure reliable measurements (Fakopp-Enterprise, 2013).

Transverse stress wave measurements were also performed, but not as comprehensive as the longitudinal ones. The main idea of the transverse testing was to provide supplementary information about a certain cross-section. One common issue for both longitudinal and transverse stress wave testing was the execution technique. When the start and stop transducers had been hammered into place with a rubber hammer, the distance between them were measured. Then a signal was generated by hitting the head of the start transducer with a small metal hammer. The time of flight was displayed in microseconds on the FAKOPP device. By pressing the reset button and repeating the simple procedure several times, enabled to establish a mean value of the time of flight, which was related to the distance to give the velocity (see FAKOPP-tests in Appendix B). If any measurement in-situ deviated substantially from the

relevant sound reference velocity, the studied region was investigated in more detail in order to take advantage of the possibility to map the extent of damage.

7.5.2 Analyses of stress wave results

When analyzing the results of the FAKOPP tests it was necessary to know that reasonable velocities for sound timber are approximately 1000 m/s and 4000-5500 m/s in the transverse and longitudinal directions, respectively (Ross et al., 2004). The dynamic modulus of elasticity was calculated according to the formula given in Section 3.2, once the density of the region was known. According to the same section, the static modulus of elasticity was then calculated with a and b values in the linear formula as given by Ìñiguez (2007):

$E_s = 579{,}5 + 0{,}7548 \cdot E_d$ (Íñiguez, 2007)

where E_s and E_d are in [MPa] and E_d was calculated according to the expression given in Section 3.2.

7.5.3 Summary of stress wave results

The longitudinal FAKOPP measurements in Appendix B were extracted and complemented with MOE calculations in Appendix E. In Table 7.3 the minimum and maximum values of MOE are summarized for both the sample density and densities from radiographs.

Table 7.3 Summary of stress wave results, depending on density.

Material property	**Lower floor**			
	Primary		**Secondary**	
ρ	420 kg/m^3	475 kg/m^3	420 kg/m^3	457 kg/m^3
MOE	5,4-9,3 GPa	6,7 -10,8 GPa	6,5-10,2 GPa	7,1-11,1 GPa
	Upper floor			
	Primary		**Secondary**	
ρ	420 kg/m^3	424 kg/m^3	420 kg/m^3	440 kg/m^3
MOE	7,4-10,2 GPa	7,4-10,3 GPa	6,7-10,4 GPa	7,0-10,9 GPa

The average velocity of the longitudinal measurements throughout both timber floors was calculated to 4969 m/s, matching the velocity for sound wood. Overviews of velocities for the lower and upper floor are illustrated in Figure 7.14 and Figure 7.15, respectively.

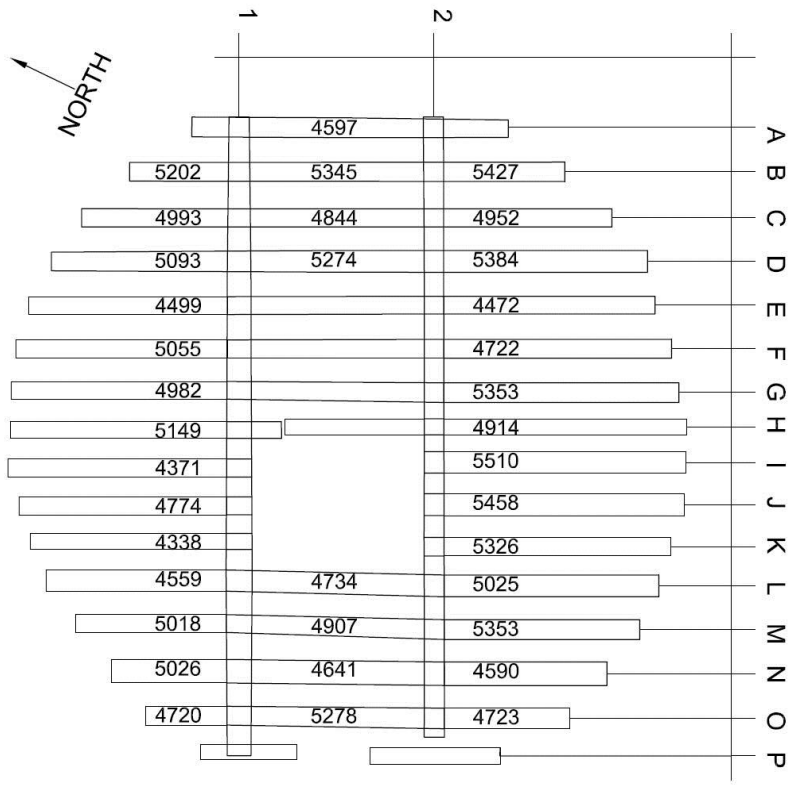

Figure 7.14 *Illustration of stress wave velocities [m/s] from FAKOPP measurements in the lower floor.*

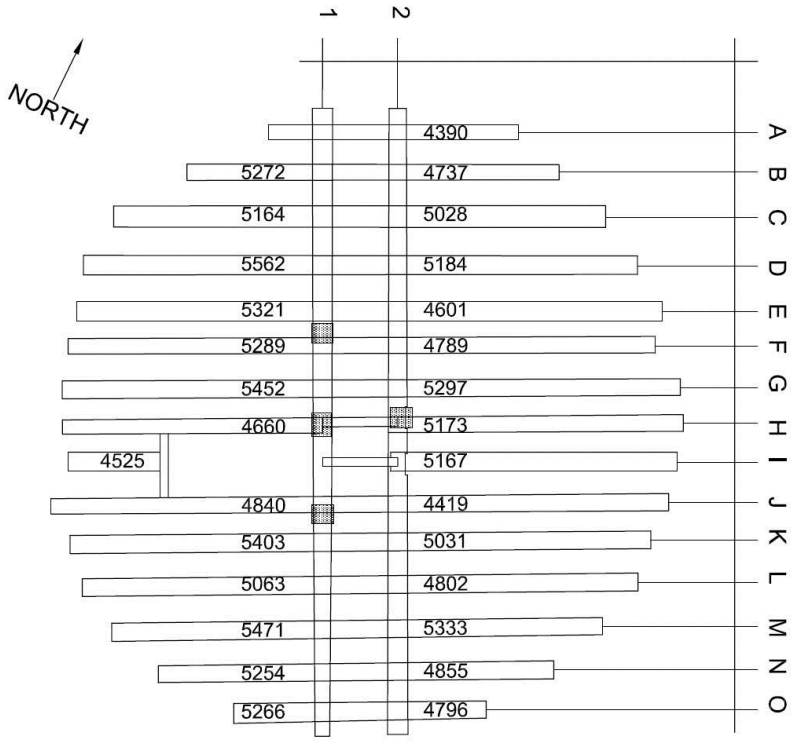

Figure 7.15 *Illustration of stress wave velocities [m/s] from FAKOPP measurements in the upper floor.*

The principle of detecting eventual deterioration with the use of FAKOPP measurements, as described in Figure 5.1, was performed on primary beam 1 in the upper and lower floor. The results of these measurements for the upper floor are illustrated in Figure 7.16, showing that the velocities were rather constant for all measurements with a slight decrease near the column. Therefore, primary beam 1 showed no signs of deterioration in span 1 for the upper floor.

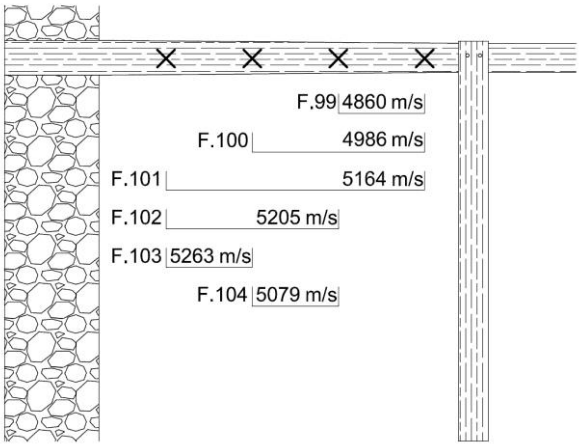

Figure 7.16 Illustration of FAKOPP principle applied in-situ on beam 1 in the upper floor, including velocity results. The measuring numbers refer to longitudinal stress wave measurements.

Regarding primary beam 1 in the lower floor, this procedure implied, by comparison to average and sound velocities, that there was deterioration within the support region where the velocity is 3916 m/s (see Figure 7.17). This velocity was about 20% lower than the velocity for sound wood, which could be compared to the common relationship that 30% decrease in velocity, indicates a 50% loss in strength (Ross et al., 2004).

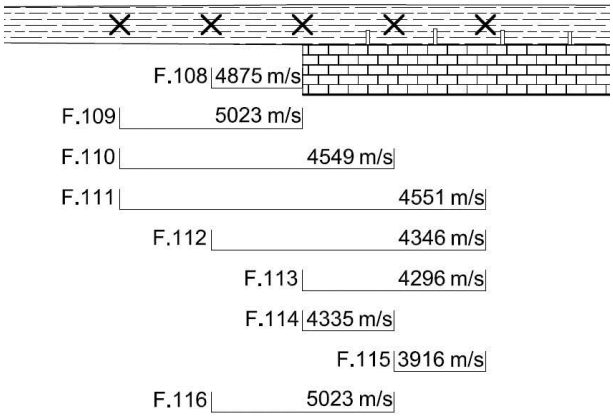

Figure 7.17 Illustration of FAKOPP principle applied in-situ on beam 1 in the lower floor, including velocity results. The measuring numbers refer to longitudinal stress wave measurements.

7.6 Resistance drilling

Although resistance drilling causes tiny holes it is considered as an NDT since these holes negligibly influence the capacity of the timber. However, resistance drilling is very local and needs several holes to map an area. Due to these two statements it is from an aesthetically point of view preferable to properly plan the procedure of resistance drilling in-situ, in order to minimize the amount of holes and hence the interventions on the structure. Therefore it is appreciated to conduct resistance drilling after that X-ray imaging and stress wave measurements have been performed, which hopefully have indicated all critical and suspected positions in a structure. This sequence was followed in-situ.

7.6.1 Procedure of in-situ resistance drilling

The arrangement of the in-situ drilling considered the crucial aspects of resistance drilling, according to Section 3.3, before the drilling was initiated. It was important to be aware of all the crucial aspects in order to obtain adequate accurace of the measurements. To maintain such accuracy the very first thing to be considered was to use a modern electrical resistance drill (see Figure 7.18) without any resonance effects. It was important to be aware of the low stiffness of the drill due to the small drill diameter in relation to its length, which might cause it to deviate. It was also crucial to ensure that no slipping occurred when pushing the machine against the timber surface as orthogonal as possible, implying that a pre-check of the stiffness and flatness of the member, at the interesting location, is recommended.

Figure 7.18 *Electrical resistance drilling device driven perpendicular to the timber surface of a column during the in-situ testing.*

Upon execution of the drilling it was also important to understand the timber species studied and the annular ring orientation, in order to not make incorrect interpretations of the timber interior. For example, the pith with its certain spread will result in a lower density which should not be confused with any type of damage. This decrease in density near the centre is more pronounced for softwoods than for hardwoods. If the drilling is performed radially the risk of deviation of the drill due to the annular rings is reduced substantially, the extent of information about the rings is maximized and identification of decay is simplified.

7.6.2 Analyses of resistance drilling results

The resistance drilling yielded graphs showing the relative resistance along the lengths of the drilled holes, where lower relative resistance indicated some deterioration. Generally the tested locations showed that regions close to the surfaces had significantly lower relative resistances than the inner regions, why the cross-section dimensions were reduced according to Figure 7.19 for affected members. The same reduction was assumed for face 12 and 34. Similarly face 23 and 14 were assigned the same reduction. The reduction for opposing faces were added together and distributed evenly between the two faces.

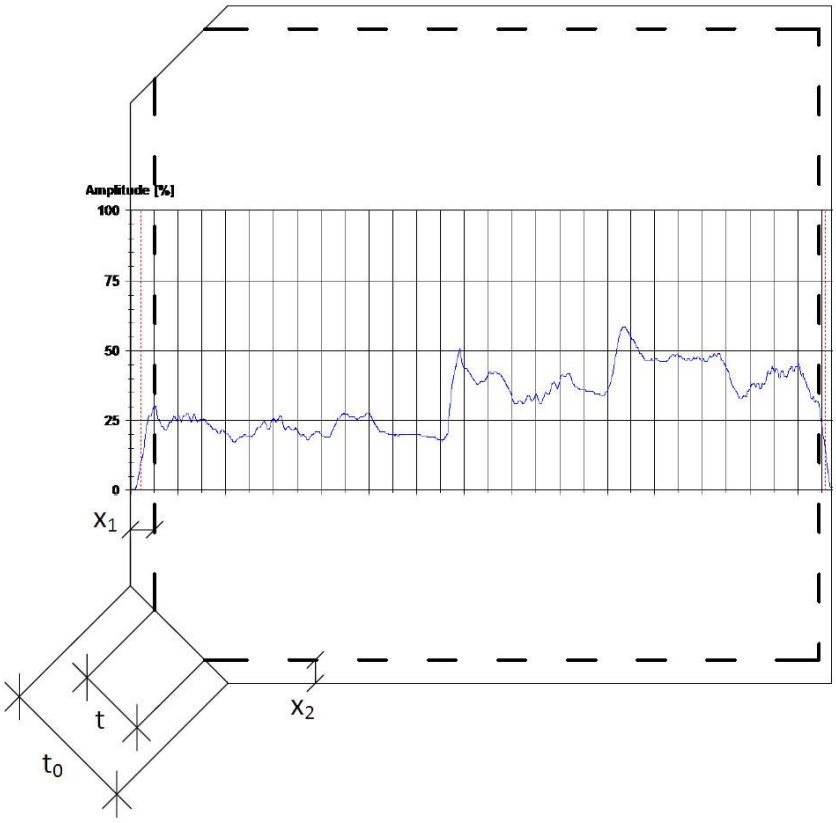

Figure 7.19 *Principle of reduction of the cross-section dimensions as a result of the low relative resistances at the faces illustrated in the graph. Dashed line indicates reduced cross-section.*

The procedure of reduction of cross-section dimensions implied that the trims at corners had to be reduced as well. With Figure 7.19 in mind the new trim t was calculated according to the following formulas:

$$t = t_0 - 2\sqrt{2} \cdot x \qquad for\ x_1 = x_2$$

$$t = t_0 - \sqrt{2} \cdot x_1 - \sqrt{2} \cdot x_2 \qquad for\ x_1 \neq x_2$$

where t_0 is the original trim, x_1 and x_2 are the reductions of faces 12 and 34 and faces 23 and 14, respectively. This meant that the effect of trim might vanish. The resistance drilling implied that the cross-section dimensions of all tested members had to be reduced due to regions with deterioration. Cross-section dimensions of members

subjected to resistance drilling were reduced with dimensions obtained from evaluated graphs for the respective member. The mean value of the reduction of all drilled members in both floors, were assigned to all faces of all undrilled members. This reduction value was calculated to approximately 5 mm per face. A summary of reductions for all tested members in both timber floors can be found in Appendix F. The total reduction, both horizontally and vertically, was 1cm in each direction for undrilled members.

7.6.3 Summary of resistance drilling results

The reduction values given in the previous section were used in the calculation of reduced cross-sectional areas and second moments of area. In Table 7.4 and Table 7.5 it is exemplified how the reduction affected secondary beams B and D in the lower floor, respectively.

Table 7.4 *Summary of original measured and reduced cross-sectional areas and second moments of area for secondary beam B in the lower floor, based on reduction values given in Appendix F. For this beam the reduction was 10 mm.*

Area			**Second moment of area**		
Original	**Reduced**	**Difference**	**Original**	**Reduced**	**Difference**
977 cm^2	915 cm^2	6,3%	$8{,}07 \cdot 10^8$ mm^4	$7{,}09 \cdot 10^8$ mm^4	12,2%
972 cm^2	912 cm^2	6,2%	$7{,}72 \cdot 10^8$ mm^4	$6{,}79 \cdot 10^8$ mm^4	12,0%
992 cm^2	930 cm^2	6,3%	$7{,}84 \cdot 10^8$ mm^4	$6{,}88 \cdot 10^8$ mm^4	12,2%

Table 7.5 *Summary of original measured and reduced cross-sectional areas and second moments of area for secondary beam D in the lower floor, based on reduction values given in Appendix F. For this beam the reduction was 13 to 18 mm.*

Area			**Second moment of area**		
Original	**Reduced**	**Difference**	**Original**	**Reduced**	**Difference**
920 cm^2	82 4cm^2	10,5%	$6{,}88 \cdot 10^8$ mm^4	$5{,}51 \cdot 10^8$ mm^4	19,9%
1120 cm^2	1026 cm^2	8,5%	$9{,}13 \cdot 10^8$ mm^4	$7{,}61 \cdot 10^8$ mm^4	16,7%
1180 cm^2	1095 cm^2	7,2%	$10{,}3 \cdot 10^8$ mm^4	$8{,}84 \cdot 10^8$ mm^4	14,2%

Resistance drilling was performed at a charred support in the lower floor which revealed that the member had not suffered any additional damage from the charring, when compared to other beams. The graph for the measurement performed at the charred support is pictured in Figure 7.20.

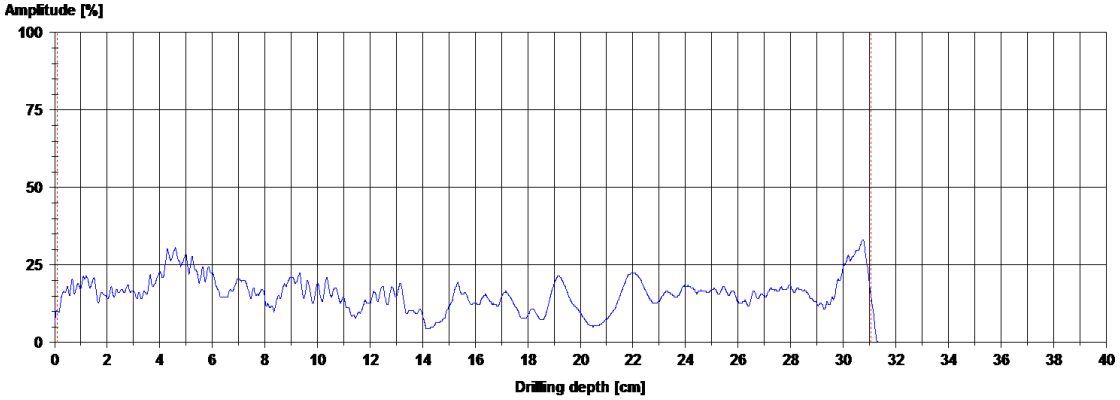

Figure 7.20 *Resistance drilling graph R.35 indicating no interior deterioration in beam J in the lower floor at the charred support.*

At the secondary beam L, interior deterioration was found in span 1, which can be seen in Figure 7.21. The measurement was taken from below which meant that the height of the deteriorated area was close to 10 cm, other nearby measurements did not show the same deterioration implying that the damage was local.

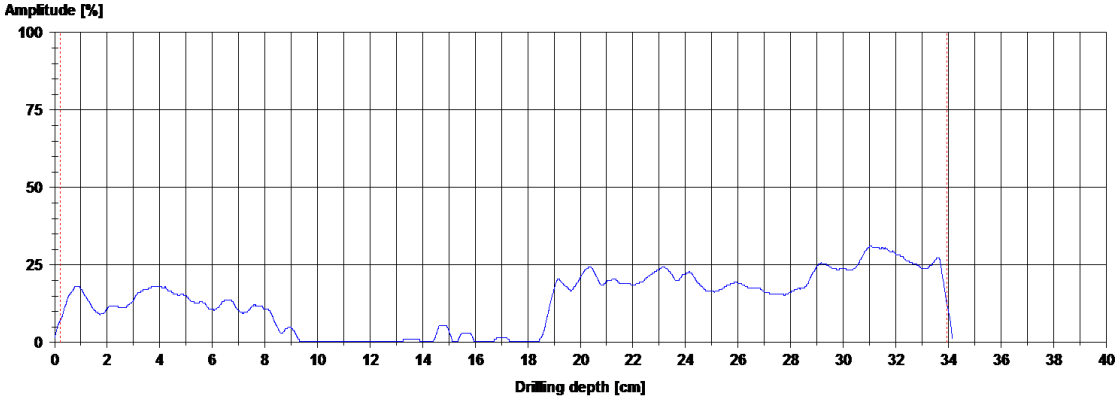

Figure 7.21 *Resistance drilling graph R.32 indicating interior deterioration in beam L in the lower floor.*

8 Structural analysis of floor structures

Each of the floor structures consist of two primary beams on which a number of secondary beams are placed. The beams are, with some exceptions, continuous elements of timber crossing the room. The function of the floor structures are explained in detail in Sections 8.1 and 8.2, evaluated in Section 8.3 and the results are presented in Section 8.4.

8.1 First artillery floor

In the lower floor both primary beams are supported at the ends and continuously supported over the brick masonry staircase. At the end supports, the beams are placed on rock masonry and continue about 1 meter into the outer wall in addition to 30 cm of visible support in the room. There are flat iron mounts at the staircase that attach to the bottom of the beams. In the primary beam 1 four sockets have been made for these mounts, while in the primary beam 2 there are spacers between the beam and mounts. The supports for the primary beam 1 at the staircase (see Figure 8.1) have been reinforced with additional bricks below both primary beams. Corresponding support for the primary beam 2 has been even further reinforced, but the support length is substantially shorter there.

Figure 8.1 *Photography of primary beam 1 in first artillery floor, supported by the masonry structure (Left) close up view of the anchorage detail for the rightmost secondary beam K (Right), cf. Figure 8.2.*

There are 16 secondary beams which cross the room perpendicular to the primary beams and are supported at the walls and by the primary beams (see Figure 7.4). At the outer wall, the beams continue into the wall about 50 cm and are placed on timber sill plates. At some points, flat iron details were visible some distance into the masonry, suggesting that the beams were anchored in the wall. Secondary beam A completely lacked contact with the primary beams while the other beams were either in full contact or in partial contact by added stone or timber pieces.

The beams crossing the staircase (H-K) differ from the other beams. These beams consist of two separate beams spanning from the outer wall to the staircase where there was a flat iron anchorage connecting it to the primary beam (see Figure 8.2). For beams I-K this separation was done in order to maintain accessibility in the staircase. However, for beam H it could be seen that the beam continues 50 cm into the staircase where it ends and the assumed end of the other part is visible. Beam G at the edge of the staircase is either of the same type as beam H or a continuous beam. The lack of

anchorage could be an indication of that it is a single continuous beam, why it is further on considered as such. Additionally beam P has had a section removed in span 2, due to refurbishing, causing it to act as two separate beams.

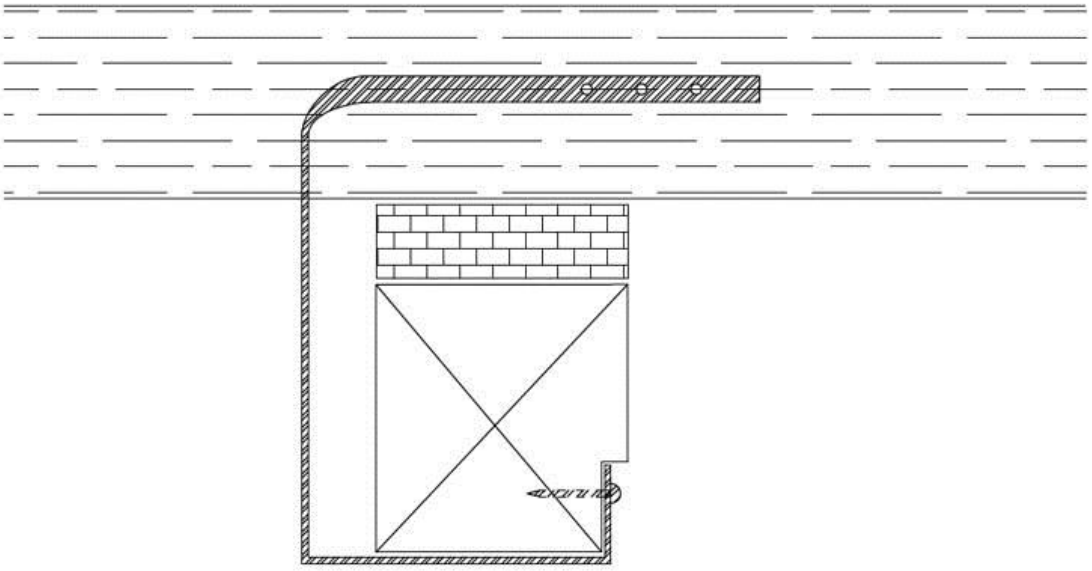

Figure 8.2 *Illustration of anchorage of the upper secondary beam to the lower primary beam with brick in between.*

Among the four columns in the upper floor, two columns could be seen in the lower floor. The base of column 3 could be seen on top of the masonry above secondary beam I at primary beam 1 and the base of column 5 could be seen directly on top of secondary beam J at primary beam 2. Column 4 is standing directly on the staircase masonry which could be seen when standing in the staircase. The support of column 6 was not visible, but assumed to stand directly on the staircase masonry.

8.2 Second artillery floor

The primary beams in the upper floor are supported by four columns in the middle of the room and by the outer wall at the ends. These end supports, for both primary and secondary beams, were not as visible as in the lower floor due to refurbishment of the masonry. Although, it was a reasonable assumption that the same design as in the lower floor had been used. In Bernung & Bengtsson (1993) there is a drawing of the floor structure which shows varying lengths for which the beams continue into the wall.

Sides of the columns rectangular cross-sections vary between 35 cm and 40 cm and the height of the columns is 3.7 m. Three of the columns support primary beam 1 with a spacing of 1.2 m, the last column is placed approximately at the middle of primary beam 2. Where the beams are connected to the columns, a portion of the beam has been removed due to the design of the connection (see Figure 8.3). Additionally primary beam 2 is missing a corresponding portion beneath secondary beam I.

In the upper floor, there are 15 secondary beams, oriented perpendicularly to the primary beams with a slight deviation. Five of the secondary beams lack contact with one or both primary beams. Towards the centre of the room there have previously

been two openings which cause discontinuities in some secondary beams. The original intended opening was 1 x 1.1 [in m] and located between the primary beams and secondary beams G and J, causing beams H and I to not be continuous across the whole room. Later, these beams have been spliced between the primary beams with members of approximately the same height but half the width. There has also been another opening, 2.2 x 1.1 [in m], in span 1 between beams H and J, centred along beam I. Due to this opening, beam I is shorter than span 1 and is therefore supported by beams H and J via the connecting member shown in Figure 8.3. Notches for previous connecting member between H and J were found in the middle of the opening.

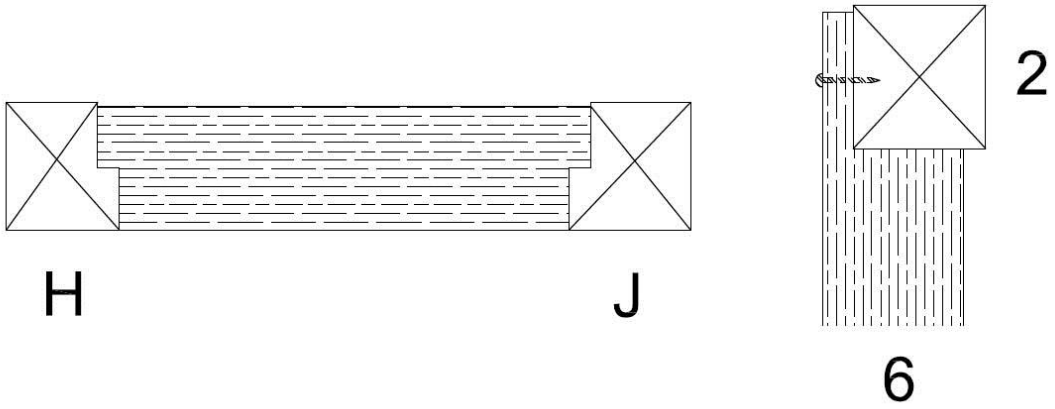

Figure 8.3 *Illustration of connecting member (Left), principle of fixation of primary beam to column (Right).*

8.3 Computer modelling

The timber floor structures were modelled in the software RSTAB 5.16 with beam elements. In the analysis of the floor structures, both of them were joined into one single structure. This was made for the purpose of a convenient overview and comparison between the behaviour of the two structures while analysing. However, this joining was not structurally necessary since the columns that connect the floors have little influence on the structural behaviour. This is due to that only two columns connect to the lower floor upon the stiff masonry staircase.

The main concept of establishing a model in this software was to define nodes, once the global geometry is known, and then add complementary input information. All available input categories are illustrated in Figure 8.4 together with the used input categories for this analysis. Relevant inputs were adjusted for the different models.

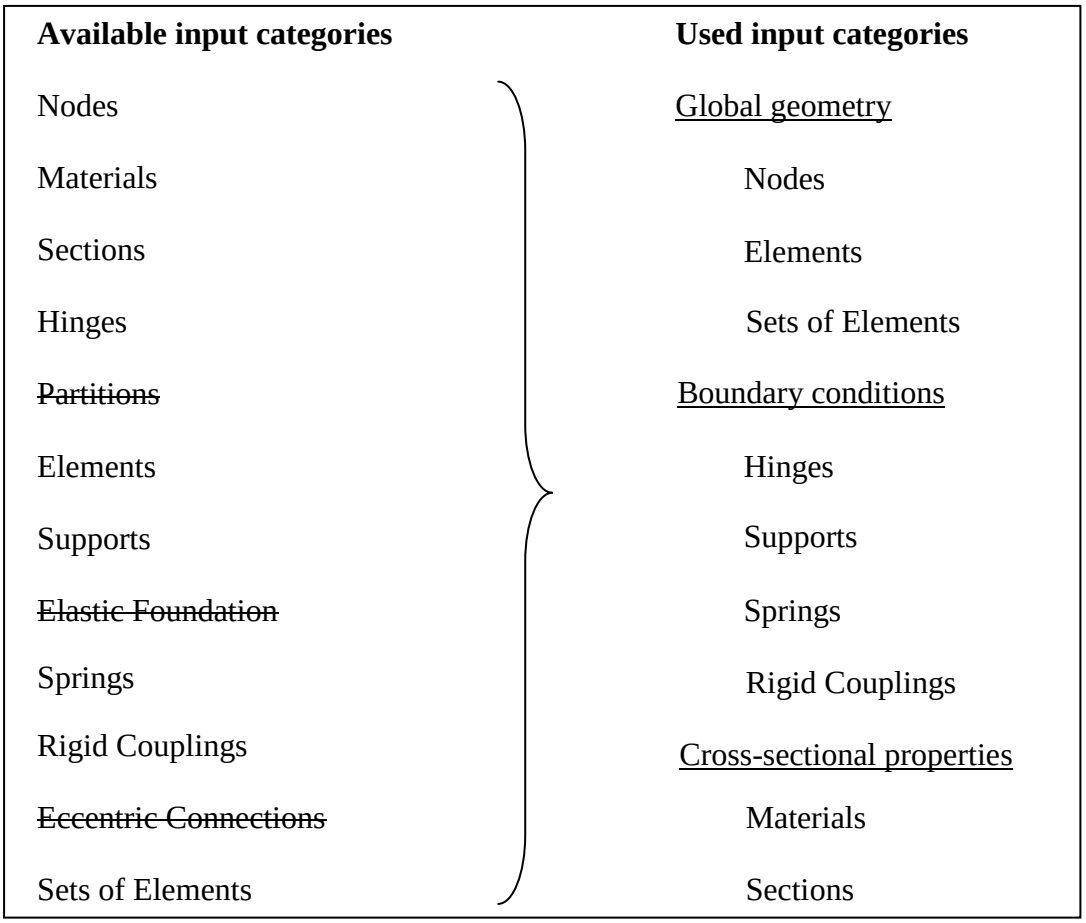

Figure 8.4 *Illustration of available input categories in RSTAB and the used input categories for this case study. Categories being strikethrough were left out.*

Once the detailed inspection had been performed it was possible to define the global geometry in terms of nodes in a coordinate system. Then elements could be defined with a start and end node allowing for varying cross-section, although the software requires that the material properties must be constant within each element. Also certain elements were joined by defining sets of elements in order to facilitate the interpretation of results.

With the global geometry established it was appropriate to insert information regarding boundary conditions. The observed boundary conditions in-situ was interpreted as the beams being simply supported, as well as there being no moment transfer between secondary and primary beams. The supports at the outer walls for both primary and secondary beams in both floors were modelled as supports in RSTAB only allowing for rotation about the 2nd local axis (see Figure 8.5). In order to reflect the load paths, the secondary beam elements were offset arbitrarily 300mm from the primary beam elements and connected to them in different ways, depending on whether there was contact or lack of contact between the primary and secondary beam. Where it was contact, springs with large longitudinal spring constants were used while where it was lack of contact rigid couplings with no stiffness were used (so called dummy elements, required due to the software). Information regarding contact conditions between primary and secondary beams can be found in Appendix A. In order to reflect the behaviour of the connecting beams at the old openings in the upper floor, hinges were defined at the ends of these beams since there is no moment transfer between these beams and the original secondary beams. Further, the

stabilizing effect of the flooring on both timber floors was neglected since it was difficult to quantify. It is on the safe side to neglect this contribution, since it is favourable.

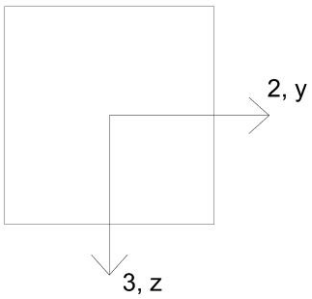

Figure 8.5 Definition of local axes for each member in RSTAB.

A challenging part to deal with in the models was the long masonry supports in the lower floor. In order to reflect a realistic behaviour of the primary beams here, where also columns are coming down from the upper floor, the boundary conditions had to be considered carefully. Although this scenario was difficult to completely reflect realistically, a reasonable set of boundary conditions was chosen. Primary beam 1 was modelled as being simply supported at the nodes on the edges of the masonry and fixed at the next node over the masonry. This was due to the masonry on top of the beam (see Figure 8.1), which was assumed to provide fixation after a certain distance, allowing rotation at the edges. Primary beam 2 was modelled as being simply supported at the two outer nodes of the masonry with no support in the middle, this choice was made due to the major addition of new masonry and lack of old masonry (see Figure 8.6) due to damage.

Figure 8.6 Middle support for primary beam 2 in the lower floor.

Regarding the columns, the lower ends were observed to miss anchorage and therefore considered as pinned connections. Columns 4 and 6 were placed on supported nodes corresponding to the masonry, while columns 3 and 5 were placed on observed locations. Connections of the columns to the primary beams in the upper floor were also considered as pinned connections. The fact that it is a timber structure together with the design of the connections argued for this choice.

Once the in-situ testing had been carried out, the model was complemented with cross-sectional properties such as material and section information, for those models being dependent on such. Otherwise this information could be added directly after the detailed inspection, in case of assumed material properties. Since the inspection generated several section measurements along a member, sections were created

through interpolation for nodes where needed. Then each element was assigned its start and end section, in order to account for changes in the real local geometry. For example the section calculations of torsion and bending moments of inertia and total cross-sectional areas, included the effects of trimmed corners. Regarding the models being dependent on results of the resistance drilling, the geometrical section values were adjusted. Regarding the models being dependent on non-assumed material values, the material constants are adjusted according to the results and evaluation of the in-situ testing.

As an initial investigation, the structure was subjected solely to 2 kN/m^2, corresponding to the smallest imposed load besides the self-weight. Due to the lack of contact at both primary beams, the secondary beams B and D in the upper floor deflected approximately 5 mm and 19 mm respectively. The deflections exceeded the corresponding gaps over primary beam 2 (the gaps were measured in-situ when the self-weight already acts). Therefore springs were inserted instead of rigid couplings at these locations in order to reflect the real behaviour when the structure is loaded. After this modification of the model actual deflections could be recorded as well as maximum moments, maximum shear forces and normal forces in columns.

8.3.1 Comparison between test methods

In order to compare and evaluate the NDTs and to suggest appropriate survey strategies with sequences of applied NDTs being used, different models and scenarios were analyzed in terms of utilization ratios. By modelling the floor structures digitally, it was possible to efficiently perform these analyses. The different models reflected different combinations of applied NDTs (e.g. values of density, MOE and cross-sections) and can be seen in Table 8.1.

Table 8.1 Input sources for different computer models, with references to MOE sources.

Model	Cross-section	Density	MOE	Notes
1	Measured	Sample	Assumed	Mohager (1987)
2	Measured	Sample	FAKOPP	
3	Measured	X-ray	Correlated	Dinwoodie (2011)
4	Measured	X-ray	FAKOPP	
5	Reduced	Sample	Assumed	Mohager (1987)
6	Reduced	Sample	FAKOPP	
7	Reduced	X-ray	Correlated	Dinwoodie (2011)
8	Reduced	X-ray	FAKOPP	
9	Reduced	X-ray	FAKOPP	Average

The first model was used as a reference model, with no NDTs applied. Instead this model was assigned the measured cross-sections from the detailed inspection, the sample density as well as MOE (independent of density) from Mohager (1987). This initial model was then modified in order to compare the different in-situ measurements.

Input information regarding material properties can be found in Table 8.2 for all nine models. For the FAKOPP models MOE is given as an interval, showing the minimum and maximum values, except for model 9 where an average value was used for all members in order to investigate the effect of assigning an average global MOE instead of varying MOE. Values for all members can be found in Appendix E. Cross-sectional dimensions were the same for models 1 to 4, but reduced for models 5 to 9 according to resistance drilling results given in Section 7.6.2.

Table 8.2 Material properties input for all models.

	Material property	**Lower floor**		**Upper floor**	
		Primary	**Secondary**	**Primary**	**Secondary**
Model 1 and 5	**ρ**	420 kg/m^3	420 kg/m^3	420 kg/m^3	420 kg/m^3
	MOE	10,5 GPa	10,5 GPa	10,5 GPa	10,5 GPa
Model 2 and 6	**ρ**	420 kg/m^3	420 kg/m^3	420 kg/m^3	420 kg/m^3
	MOE	5,4-9,3 GPa	6,5-10,2 GPa	7,4-10,2 GPa	6,7-10,4 GPa
Model 3 and 7	**ρ**	475 kg/m^3	457 kg/m^3	424 kg/m^3	440 kg/m^3
	MOE	12,6 GPa	12,0 GPa	11,2 GPa	11,6 GPa
Model 4 and 8	**ρ**	475 kg/m^3	457 kg/m^3	424 kg/m^3	440 kg/m^3
	MOE	6,7-10,8 GPa	7,1-11,1 GPa	7,4-10,3 GPa	7,0-10,9 GPa
Model 9	**ρ**	4755 kg/m^3	457 kg/m^3	424 kg/m^3	440 kg/m^3
	MOE	9,2 GPa	9,2 GPa	9,2 GPa	9,2 GPa

Regarding load scenarios, there were two considered load combinations in ULS as stated in Section 5.2. For the comparison between testing methods, the following load combination was considered:

Load combination according to Eurocode 1: $1{,}35 \cdot G + 1{,}5 \cdot 4\ kN/m^2$

The load combination according to Eurocode 1 included floor self-weight and a uniformly distributed load corresponding to the appropriate load class for the current

use of Skansen Lejonet. The distributed load was applied on secondary beams by transforming it into line loads based on tributary areas, disregarding that the load distribution could be affected by member stiffness as well as span length, i.e. contact with primary beams. The tributary area for each secondary beam was chosen as half the distance to adjacent members, cf. Figure 8.7.

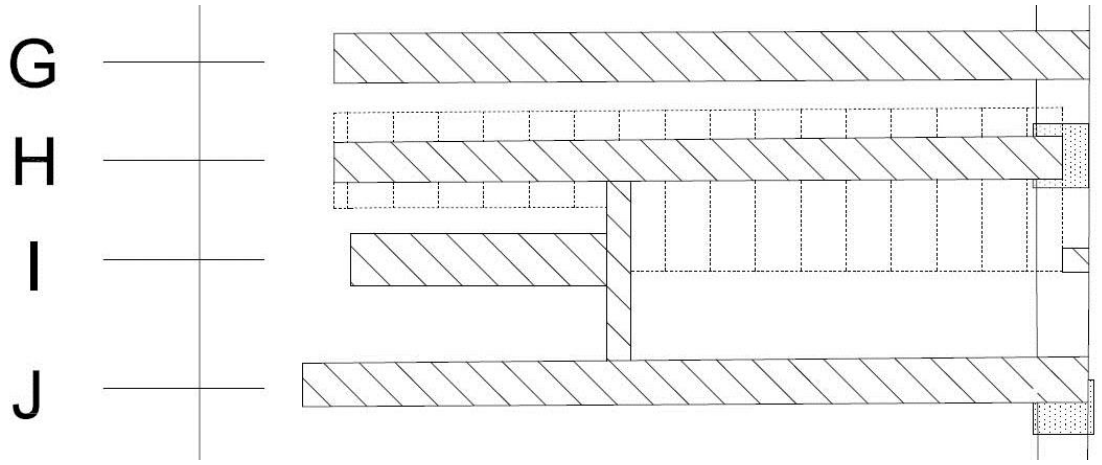

Figure 8.7 *Illustration of tributary area for secondary beam H in span 1 in the upper floor.*

Also a ULS design calculation was performed on model 8. This analysis was conducted by calculating the maximum utilization ratios with regard to moment and shear force, in both floors separately, with first only the self-weight $1{,}35 \cdot G$ applied and thereafter an imposed load of $1{,}5 \cdot 1\ kN/m^2$. An increase of the imposed load was assumed to increase stresses linearly, the maximum load was therefore determined from the remaining capacity after self-weight had been applied. The calculation of utilization ratios for bending stresses and shear stresses can be found in Appendices G while the calculations for buckling of columns can be found in Appendix H. A calculation predicting the maximum load capacity can be found in Appendix I.

8.3.2 Intended use

The original intended use of Skansen Lejonet, including cannon loads, was represented by the following load combination, cf. Eurocode 1:

$$\text{Original intended load combination: } 1{,}35 \cdot G + 1{,}5 \cdot P_{cannons} + 2\ kN/m^2$$

where the weight of the ammunition was seen as part of the distributed imposed load. This load combination was applied only on model 8, which utilized results from all NDTs. The reason to this choice was that this model was considered to reflect the current structural condition most accurately. Also this ULS analysis considered the removal of primary beams in the upper floor, examining the redundancy of the floor structure (see Appendix G). Removal of the primary beams caused the cantilever parts of beams H and I to be removed due to the assumption of not being able to carry any load as a cantilever.

The cannon load consists of the cannon itself together with the mount, assumed to weigh half of the cannon. Therefore the total load of one 12-pound cannon was approximately 25.0 kN and 13.2 kN for one 6-pound cannon. The mounts had an assumed size of 1 x 2 [in m] and the total load was distributed equally between the four wheels, resulting in four point loads. Two placements of the cannons were considered, in each of the of the placements, the 12-pound cannon and seven 6-pound cannons were positioned on the investigated floor with the five remaining 6-pound cannons placed on the other floor. The load configuration including the 12-pound cannon is illustrated for the lower and upper floor in Figure 8.8 and Figure 8.9, respectively.

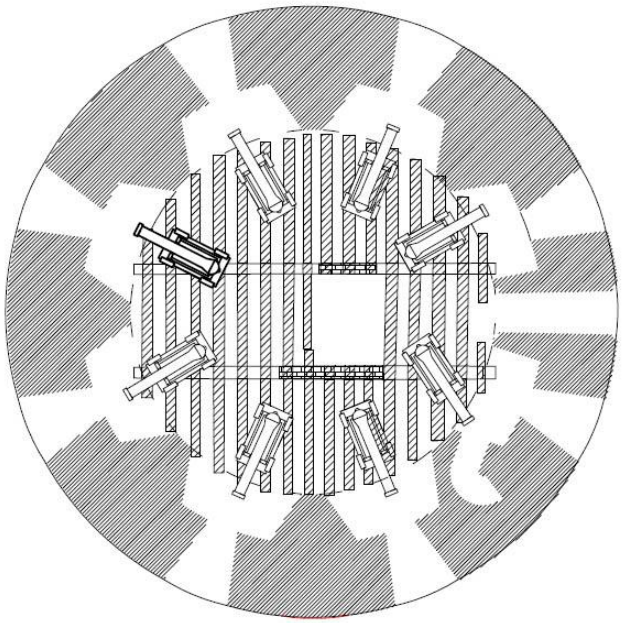

Figure 8.8 *Load configuration of cannons in the lower floor, where the bolded cannon represents the 12-pound cannon.*

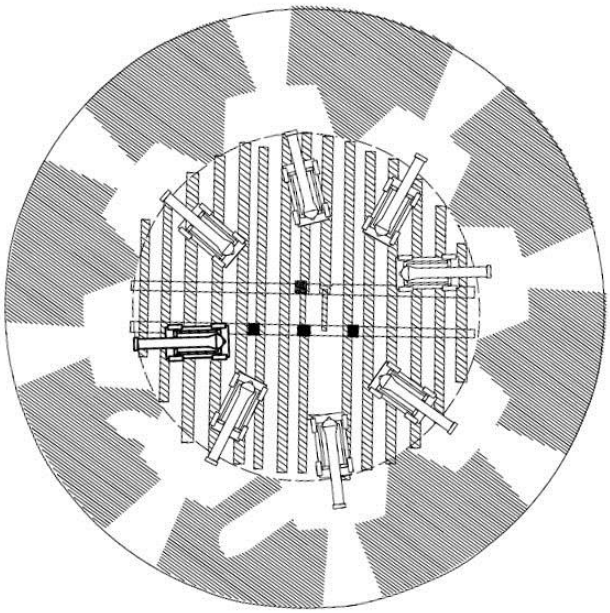

Figure 8.9 *Load configuration of cannons in the upper floor, where the bolded cannon represents the 12-pound cannon.*

8.3.3 Verification of structural performance

Once the results were recorded for the behaviour of the floor structures, utilization ratios were calculated for all members in both floors. For these calculations the bending strength $f_{m,k}$ (MOR) and shear strength $f_{v,k}$ were needed, which were calculated according to Dinwoodie (2000) and Glos (1995), respectively. The expressions are:

$f_{m,k} = 0{,}002065 \cdot E_s$ (Dinwoodie, 2000)

$f_{v,k} = 0{,}2 \cdot f_{m,k}^{0,8}$ (Glos, 1995)

These strength values are presented in Appendix E. All members have more or less rectangular cross-sections, depending on the trims, therefore bending stresses σ_{moment} and shear stresses τ_{shear} were calculated according to the following formulas, respectively:

$$\sigma_{moment} = \frac{M}{I} \cdot z = \frac{M}{I} \cdot \frac{h}{2}$$

$$\tau_{shear} = \frac{3 \cdot V}{2 \cdot A}$$

where M is the moment, I is the second moment of area, z is the distance from the neutral axis, h is the height of the member, V is the shear force and A is the cross-sectional area of the member. All stress values were calculated with the same cross-section as in the maximum moment and maximum shear force section, respectively. Regarding the shear stresses, the reduction factor k_{crack} was not applied.

Furthermore, the normal forces in the four columns in Skansen Lejonet were investigated with regard to buckling. The buckling was investigated by calculating the theoretical Euler buckling load N_{cr}:

$$N_{cr} = \frac{\pi^2 \cdot E \cdot I}{L_e^2}$$

where L_e is the effective buckling length, taken as $1{,}00 \cdot L_{column}$ since the columns were modelled as pinned in both ends, as stated in Section 8.3. These calculations resulted in low utilization ratios, why more accurate calculations including reduction factor due to for example imperfections, were not performed. The perfect column in Euler's theory was therefore considered to adequately compare the different ratios.

Finally, with all load effects and strength parameters known it was straightforward to calculate the aforementioned utilization ratios, as following:

$$\mu_{moment} = \frac{\sigma_{moment}}{f_{m,k}}$$

$$\mu_{shear} = \frac{\tau_{shear}}{f_{v,k}}$$

$$\mu_{buckling} = \frac{N}{N_{cr}}$$

The first and second ratios were calculated for all beams and the third ratio was calculated for all columns. Due to the variation in cross-section dimensions, the

locations of maximum bending and shear stresses were not necessarily equal to the maximum bending moment and shear force locations, respectively.

8.4 Results of structural analysis

According to the modelling of the load combination according to Eurocode 1, the general behaviour of the timber floor structures was that the maximum bending moment and maximum shear force appeared at the masonry support areas for primary beams in the lower floor. Meanwhile, in the upper floor corresponding maximum values appeared at the columns, except column 4. Furthermore, the capacity of the secondary beams in both floors was only utilized to a small extent and the primary beams to a larger extent. The general moment distribution of both floors can be seen in Figure 8.10 while the general deformed model is illustrated in Figure 8.11. In the lower floor the largest deflections appeared in the first span of primary beam 2, while the corresponding position in the upper floor varied between the shortened beam at the opening in the floor and the first span of primary beam 2. The largest deflection with the load combination according to Eurocode 1 was 15.3 mm (beam H in the upper floor) and appeared in model 6 cf. Table 8.1.

The application of NDTs changed the structural behaviour in individual members, but the general global behaviour remained unchanged. For models where stress wave test data had been applied, except model 9, the maximum bending moment for primary beam 1 in the upper floor was located in the middle of span 1. Corresponding moment was found at column 3 in the other models. A thorough documentation of all maximum bending moments and maximum shear forces with corresponding locations and utilization ratios is available in Appendix G.

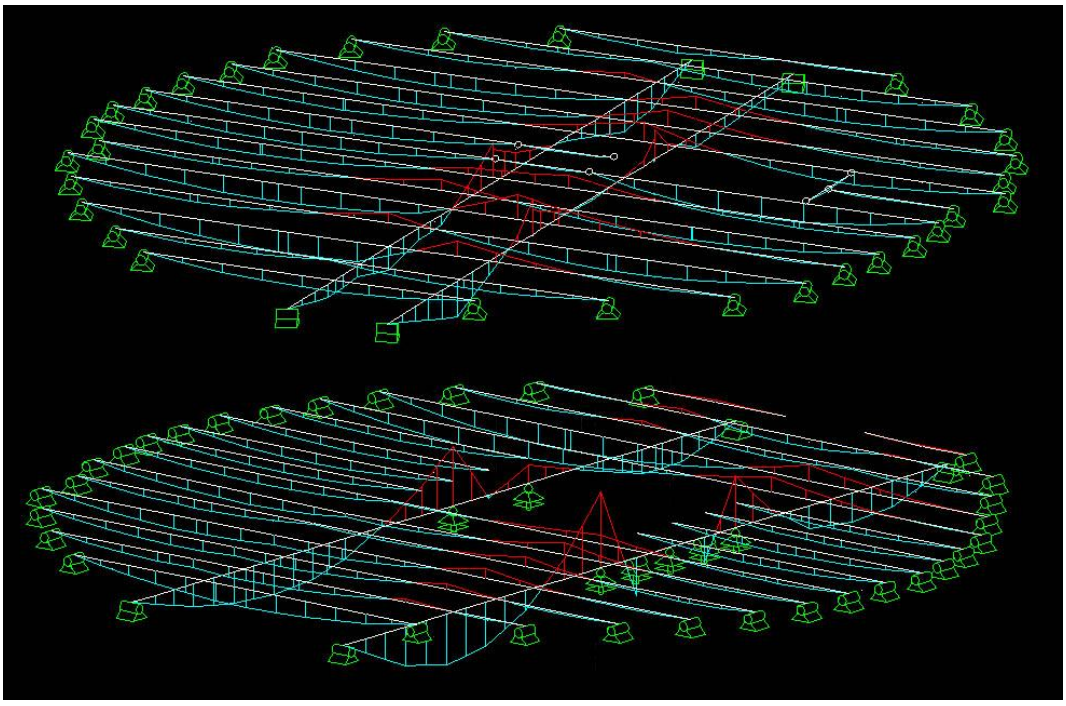

Figure 8.10 Moment distribution for model 8 (load combination acc. to Eurocode 1) in the upper floor (Top) and moment distribution for model 8 (load combination

acc. to Eurocode 1) in the lower floor (Bottom). Note that the orientation relative each other is not the actual orientation.

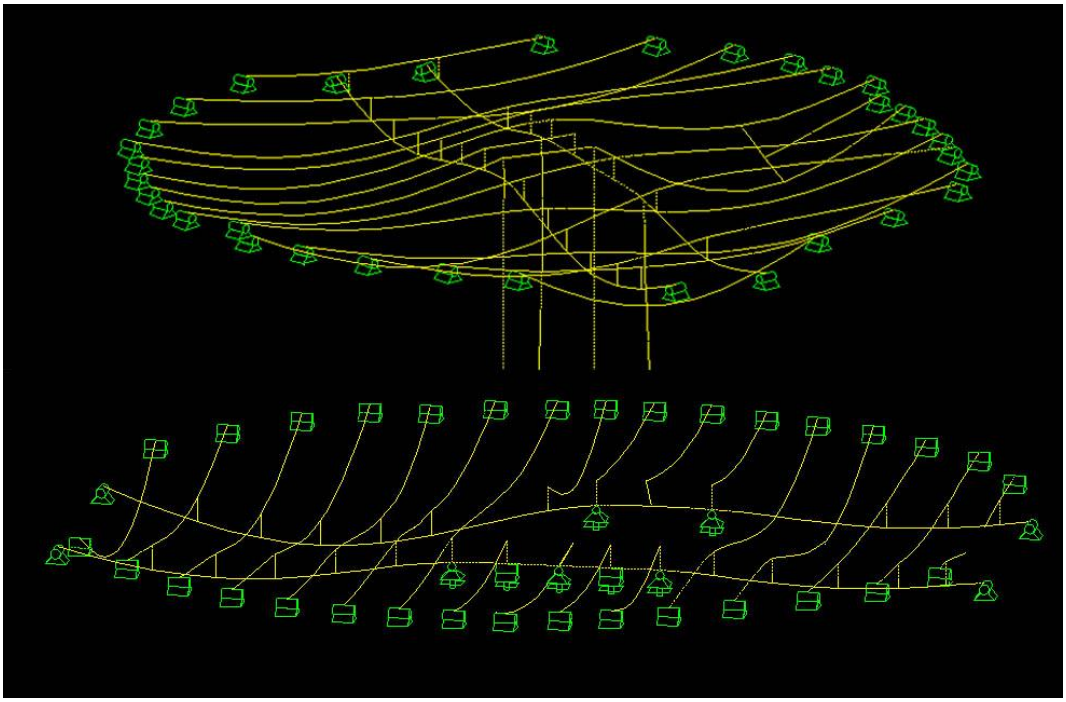

Figure 8.11 *Deflections for model 8 (load combination acc. to Eurocode 1) in the upper floor (Top) and deflections for model 8 (load combination acc. to Eurocode 1) in the lower floor (Bottom). Note that the orientation relative each other is not the actual orientation.*

In order to present the differences between the models in a comprehensible and relevant manner average values of utilization ratios μ_{moment} and μ_{shear} were determined. These values for primary beams are presented and compared between different computer models in Table 8.3. Corresponding values for secondary beams can be found in Table 8.4. Finally, values for secondary beam H in the lower floor are presented in Table 8.5, this beam was chosen since it is regarded as simply supported and spans between two fixed supports in the model.

Table 8.3 *Differences in utilization ratios regarding primary beams in both floors for different computer models (load combination acc. to Eurocode 1).*

Model	μ_{moment}	1	2	3	4	5	6	7	8	9
1	0,35									
2	0,44	0,09								
3	0,28	-0,06	-0,15							
4	0,40	0,06	-0,04	0,12						
5	0,37	0,03	-0,07	0,09	-0,03					
6	0,46	0,11	0,02	0,18	0,06	0,09				
7	0,30	-0,04	-0,13	0,02	-0,10	-0,07	-0,16			
8	0,42	0,08	-0,02	0,14	0,02	0,05	-0,04	0,12		
9	0,42	0,08	-0,01	0,14	0,02	0,05	-0,04	0,12	0,00	
Model	μ_{shear}	**1**	**2**	**3**	**4**	**5**	**6**	**7**	**8**	**9**
1	0,40									
2	0,49	0,09								
3	0,34	-0,06	-0,14							
4	0,47	0,07	-0,02	0,13						
5	0,42	0,02	-0,07	0,08	-0,05					
6	0,52	0,12	0,04	0,18	0,05	0,11				
7	0,36	-0,05	-0,13	0,01	-0,12	-0,06	-0,17			
8	0,49	0,09	0,00	0,15	0,02	0,07	-0,04	0,13		
9	0,51	0,11	0,03	0,17	0,04	0,09	-0,01	0,16	0,02	

Table 8.4 Differences in utilization ratios regarding secondary beams in both floors for different computer models (load combination acc. to Eurocode 1).

Model	μ_{moment}	1	2	3	4	5	6	7	8	9
1	0,13									
2	0,16	0,03								
3	0,12	-0,01	-0,04							
4	0,15	0,02	-0,01	0,03						
5	0,14	0,01	-0,02	0,02	-0,01					
6	0,17	0,04	0,01	0,05	0,02	0,03				
7	0,12	-0,01	-0,04	0,00	-0,03	-0,02	-0,05			
8	0,16	0,03	0,00	0,04	0,01	0,02	-0,01	0,04		
9	0,16	0,03	0,00	0,04	0,01	0,02	-0,01	0,04	0,00	
Model	μ_{shear}	**1**	**2**	**3**	**4**	**5**	**6**	**7**	**8**	**9**
1	0,10									
2	0,11	0,01								
3	0,09	-0,01	-0,02							
4	0,10	0,00	-0,01	0,01						
5	0,10	0,00	-0,01	0,01	0,00					
6	0,12	0,02	0,01	0,03	0,02	0,02				
7	0,09	-0,01	-0,02	0,00	-0,01	-0,01	-0,03			
8	0,11	0,01	0,00	0,02	0,01	0,01	-0,01	0,02		
9	0,12	0,02	0,01	0,03	0,02	0,02	0,00	0,03	0,01	

Table 8.5 Differences in utilization ratios regarding beam H (span 1) in the lower floor for different computer models (load combination acc. to Eurocode 1).

Model	μ_{moment}	1	2	3	4	5	6	7	8	9
1	0,10									
2	0,12	0,02								
3	0,09	-0,01	-0,03							
4	0,11	0,01	-0,01	0,02						
5	0,10	0,00	-0,02	0,01	-0,01					
6	0,12	0,02	0,00	0,03	0,01	0,02				
7	0,09	-0,01	-0,03	0,00	-0,02	-0,01	-0,03			
8	0,11	0,01	-0,01	0,02	0,00	0,01	-0,01	0,02		
9	0,11	0,01	-0,01	0,02	0,00	0,01	-0,01	0,02	0,00	
Model	μ_{shear}	**1**	**2**	**3**	**4**	**5**	**6**	**7**	**8**	**9**
1	0,07									
2	0,08	0,01								
3	0,06	-0,01	-0,02							
4	0,07	0,00	-0,01	0,01						
5	0,07	0,00	-0,01	0,01	0,00					
6	0,08	0,01	0,00	0,02	0,01	0,01				
7	0,07	0,00	-0,01	0,01	0,00	0,00	-0,01			
8	0,08	0,01	0,00	0,02	0,01	0,01	0,00	0,01		
9	0,08	0,01	0,00	0,02	0,01	0,01	0,00	0,01	0,00	

The ULS analysis resulted in a maximum imposed load of 7.5 kN/m^2 when the same load was applied on both floors. The governing stress was shear stress at the masonry support of primary beam 2 in the lower floor (cf. Figure 8.6), without considering the reduction factor $k_{crack} = 0{,}67$ in Eurocode 5. If k_{crack} had been considered the critical utilization ratio would be 0.90, therefore further significant increase of the load is not possible. For the applied load the utilization ratio was 0.98. The results for the original intended load combination resulted in maximum utilization ratios of 0.32 (beam 1) for bending moment and 0.57 (beam 2) for shear force with the 12-pound cannon loading the lower floor. The corresponding utilization ratios were 0.35 (beam 2) and 0.63 (beam 1) when the cannon loaded the upper floor.

Regarding the redundancy of the upper floor, removal of primary beam 1 resulted in that bending stresses due to load effect in primary beam 2 exceeds the bending capacity of this beam by 2%. Removal of both beams resulted in exceeding the capacity for investigated secondary beams G and J, with 28% and 45%, respectively. The deflections in the non-failing model, i.e. primary beam 2 removed, is illustrated in Figure 8.12 where the maximum deflection was 13.75 mm in secondary beam G.

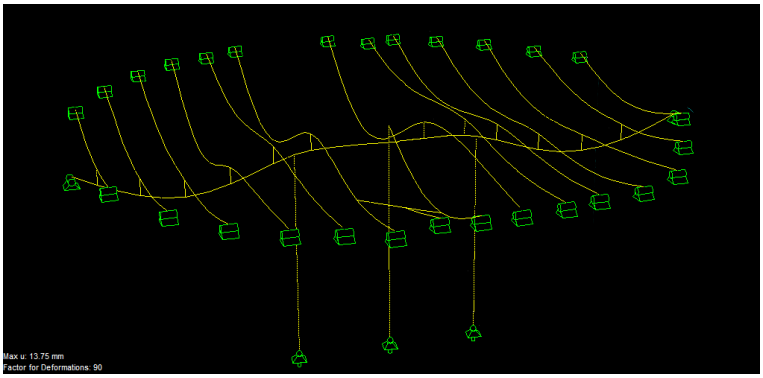

Figure 8.12 *Deflections in the upper floor (original intended load combination) when primary beam 2 was removed.*

9 Discussion

The deterioration was revealed in different ways for the different NDTs. Since resistance drilling produces information related to extremely local conditions, it is difficult to discover interior deterioration without any indication of it. Such indicators could be radiographs or lower velocities from stress wave tests in addition to traditional deterioration signs. With regard to effort and time it would be preferable to initially map the longitudinal velocities to locate regions of lower wood quality rather than using X-ray imaging. It would be suitable to conduct global measurements to identify characteristic velocities for the investigated structure, to identify members requiring further investigation. An advantage from this is that the characteristic velocity can be used as a reference value rather than general values for sound timber. The measured average velocity at Skansen Lejonet was relatively high. This implied that the original quality of the timber was superior to modern construction timber, since there are damage in the joists that have degraded the quality of the timber over the years.

Furthermore, with the results from longitudinal velocities it is appropriate to proceed the investigation with local transverse stress wave testing at the suspected deteriorated regions. A good suggestion is to arrange these measurements in a grid over the region, with appropriate resolution in order to accurately measure the extent of deterioration. Using the variations of local values to determine the extent is preferable rather than comparing to a global transverse velocity, since the sound timber regions may have initially been of lower quality due to natural variations in the member. Combining the results from the grid region with a radiograph of the region, would allow for a good measurement of the deterioration as well as defining how deterioration appears in a radiograph. Since this will only determine the extent in two directions it is appropriate to measure the depth with resistance drilling. This could also be done with further transverse tests perpendicular to the original grid, although it is more efficient to just drill through the decay rather than doubling the number of stress wave measurements.

In this investigation, the massive size of the members reduced the influence of cross-sectional reduction based on resistance drilling. Furthermore, the irregularities in the geometry might have affected the measured cross-section to a greater extent than the resistance drilling, if the cross-section had been measured at a different position. However, in structures with a well-defined geometry and higher utilization ratios, i.e. modern structural designs, slight differences in reductions can be decisive for limit state verifications.

The close spacing of the secondary beams in Skansen Lejonet affected the quality and extent of X-ray imaging and resistance drilling. At most locations, perpendicular resistance drilling was limited to the bottom face of the beam due to the length of the unit. Regarding the X-ray imaging, the source had to be placed sometimes close to the members. However, a longer distance would be preferable in order to obtain radiographs with even exposure which facilitates and increases the accuracy in the subsequent density evaluation. Contrary, stress wave measurements did not require a lot of space, implying that it can be used in most assessments.

As seen in the obtained utilization ratios, the current structural capacity fulfills the requirements for the load combination according to Eurocode 1. Since none of the models produce exceeding design stresses, a detailed analysis which takes local defects such as major knots, where the members are in tension, into consideration was not deemed necessary. Furthermore, the effect of local interior deterioration was

neglected due to difficulties to quantify the extent accurately, since it was only found in a few timber members, it would be inaccurate to reduce all members for it. An extreme way of accounting for it would be to disregard the members where it was found, and with such an approach the capacity would still probably be sufficient. A general difference, between the models with a global MOE and those with varying MOE within the members, was noticed for the maximum moment in primary beam 1 in the upper floor. For the models with global MOE the maximum moment was positioned at column 3, while for the models with varying MOE the maximum moment was positioned in the adjacent span 1, although with no major differences in magnitude. This might imply that if all varying MOE data within each member was simplified into an average value or assumed value, there is a risk of predicting an inaccurate structural behaviour.

Regarding the original intended load combination, when applied on the upper floor, it should be noted that secondary beam I had not been shortened at the time when cannons were used at Skansen Lejonet. Furthermore, the cases with removed primary beams are very unlikely to happen in reality. A possible situation is that the columns had been damaged, by some impact load, resulting in failure of the beams due to the column-beam connections. A slightly more likely event is that the primary beams lose the support from the columns without failure, i.e. spanning over the entire diameter of the tower.

If NDT measurements are accurately applied by considering their crucial aspects and limitations, it is possible to obtain reliable results. This increases the ability to prolong the service life of buildings instead of constructing new ones, as a part of sustainable development. One might think that the applications of NDTs lower the capacity of a structure since the utilization ratios in general are higher than for the initial model. The reason to this is that the initial guessed model overestimated the timber and that the NDTs provided more accurate information about the actual timber. However, one should keep in mind the uncertainties in the mathematical correlations between NDT outputs and strength parameters, especially for timber compared to clear wood. The correlation of dynamic MOE to static MOE used in this thesis was somewhat conservative, providing static values below 90% of dynamic values. Following this significant reduction, bending and shear strengths were also reduced. This correlation led to an underestimation of the capacity. For an accurate assessment it would be suitable to have correlations based on comparable specimens, i.e. old timber specimens tested to failure.

10 Conclusions

The main results from the field measurements and analyses are shown in Table 10.1 and Table 10.2, respectively.

Table 10.1 Summary of main results from field measurements.

		Mean density from X-ray	Mean FAKOPP MOE	
			X-ray density	Sample density
Lower floor	**Primary beams**	475 kg/m^3	10,4 GPa	7,6 GPa
	Secondary beams	457 kg/m^3	9,1 GPa	8,4 GPa
Upper floor	**Primary beams**	424 kg/m^3	8,6 GPa	8,5 GPa
	Secondary beams	440 kg/m^3	9,1 GPa	8,7 GPa

Table 10.2 Summary of main results from Ultimate Limit State analyses (load combination acc. to Eurocode 1). Numbers within parenthesis refer to model number where the stress occurs.

		Bending stress	Shear stress
Lower floor	**Primary beams**	-9,40 MPa (8)	1,31 MPa (7)
	Secondary beams	4,54 MPa (7-9)	0,34 MPa (5-9)
Upper floor	**Primary beams**	-9,12 MPa (5)	1,23 MPa (6, 9)
	Secondary beams	6,93 MPa (7-9)	0,53 MPa (5-9)

The major conclusions from this thesis are:

- The floor structures exposed to current climate conditions and use are of very good condition and fulfill the requirements according to the applied standards, cf. Eurocodes,. The uniformly-distributed imposed load in Ultimate Limit State could be increased to 7.5 kN/m^2 in both floors, disregarding k_{crack}.

- To prepare a systematic approach and documentation of the in-situ inspection and testing is crucial for an accurate and efficient assessment process.

- For the localization of interior damage, longitudinal stress wave testing is easy to perform and shows great promise.

- In order to assess the general quality of the timber, it is sufficient to apply stress wave measurements possibly together with resistance drilling.

- The extent of measurements should be adjusted with regard to structural condition and information.

- There are great opportunities to adapt NDT methods to minimize interventions while prolonging the service life of buildings.

References

Andersson, M. 2011. Drawing A-40.2-001. GAJD Arkitekter/Statens fasighetsverk.

Anthony, R. W. Examination of Connections and Deterioration in Timber Structures Using Digital Radioscopy. *In:* Bosela, P. A., Delatte, N. J. & Rens, K. L., eds. Third Forensic Engineering Congress, 19-21 October 2003 San Diego, CA. American Society of Civil Engineers, 320-328.

Anthony, R. W. 2007. Practice Points 03, Basics of Wood Inspection: Considerations for Historic Preservation. *APT Bulletin,* vol. 38, nr. 2/3**,** pp. 1-6.

ASCE, 2000. *Guideline for Structural Condition Assessment of Existing Buildings*.

Bernung, C. & Bengtsson, B.-O. 1993. *Vårdplan för Skansen Kronan och Skansen Lejonet i Göteborg.* Master thesis, Chalmers University of Technology, Gothenburg.

Bucur, V. & Böhnke, I. 1994. Factors affecting ultrasonic measurements in solid wood. *Ultrasonics*, vol. 32, nr. 5**,** pp. 385-390.

Dinwoodie, J. M. 2000. *Timber: Its nature and behaviour (2nd edition).* London, E & FN Spon.

Fakopp Enterprise 2013. *FAKOPP Microsecond Timer USER'S GUIDE* [Online]. Available: http://www.fakopp.com/site/downloads/Fakopp_MT_Guide.pdf Accessed 2013-05-03

Feio, A. J. d. O. 2006. *Inspection and Diagnosis of Historical Timber Structures: NDT Correlations and Structural Behaviour.* Ph.D thesis, University of Minho.

FPL 2001. Wood Handbook - Wood as an Engineering Material. Madison, WI: Forest Products Laboratory.

Glos, P. 1995. Solid timber - Strength classes. *In:* Blass, H. J., Aune, P., Choo, B. S., Görlacher, R., Griffiths, D. R., Hilson, B. O., Racher, P. & Steck, G. (eds.) *Timber Engineering - STEP 1.* Centrum Hout.

Granefelt, E., Fransson, S. A. & Grandien, B. R. s. 2011. Artilleriets materielutveckling under 1800- och 1900-talen. *In:* Granefelt, E. (ed.) *Svenska Artilleriets utveckling under 1800- och 1900-talen.* Stockholm: Militärhistoriska Förlaget.

Grenander, G. 1993. Artilleriets Pjäser och Ammunition. *In:* Ulfhielm, H. (ed.) *Karl XI:s och Karl XII:s tid.* Stockholm: Militärhistoriska Förlaget.

Grödinger, P., Brydolf, E., Eklund, D., et al. 1982. *Var virket bättre förr?* Stockholm, Nordiska museet, Riksantikvarieämbetet.

ICOMOS, 1999. *Principles for the preservation of historic timber structures*.

ICOMOS 2013. *ICOMOS' Mission* [Online]. Available: http://www.icomos.org/index.php/en/about-icomos/mission-and-vision/icomos-mission Accessed 6/3 2013.

Íñiguez, G. 2007. *Clasificación Mediante Técnicas No Destructivas y Evaluación de Las Propiedades de La Madera Aserrada de Coníferas de Gran Escuadría Para Uso Estructural.* Doctor thesis, Universidad Politécnica de Madrid.

ISCARSAH, 2003. *Recommendations for the analysis, conservation and structural restoration of architectural heritage*.

ISO13822, 2001. *Bases for design of structures - Assessment of existing structures*.

Kasal, B. & Anthony, R. W. 2004. Advances in *in situ* evaluation of timber structures. *Progress in Structural Enginnering and Materials,* vol. 6, nr. 2**,** pp. 94-103.

Kasal, B., Lear, G. & Anthony, R. 2010a. Radiography. *In:* Kasal, B. & Tannert, T. (eds.) *In-Situ Assessment of Structural Timber.* Springer.

Kasal, B., Lear, G. & Tannert, T. 2010b. Stress Waves. *In:* Kasal, B. & Tannert, T. (eds.) *In-Situ Assessment of Structural Timber.* Springer.

Kruglowa, T. 2012. *In-situ assessment of density and material properties in timber structures by non-destructive and semi-destructive testing.* Licentiate of engineering thesis, Chalmers University of Technology, Gothenburg.

Lear, G. 2005. *Improving the Assessment of In Situ Timber Members with the Use of Nondestructive and Semi-Destructive Testing Techniques.* Master thesis, North Carolina State University, Raleigh, NC.

Lear, G., Kasal, B. & Anthony, R. 2010. Resistance Drilling. *In:* Kasal, B. & Tannert, T. (eds.) *In-Situ Assessment of Structural Timber.* Springer.

Lechner, T., Sandin, Y. & Kliger, R. 2011. Assessment of Density in Timber Using X-Ray Equipment. *International Journal of Architectural Heritage: Conservation, Analysis, and Restoration,* vol. 7, nr. 4**,** pp. 416-433.

Lourenço, P. B. 2005. Assessment, diagnosis and strenghtening of Outerio Church, Portugal. *Construction and Building Materials,* vol. 19, nr.**,** pp. 634-645.

Magnus, L. 2008. *Historic Timber Roof Structures: Construction Technology and Structural Behaviour.* Master thesis, Katholieke Universiteit Leuven.

Mohager, S. 1987. *Studier av krypning hos trä: Med särskild hänsyn till inverkan av konstanta och cykilskt varierande fukttillstånd.* Ph.D thesis, Kungliga Tekniska Högskolan.

Palaia, L. Structural Failure Analysis of Timber Floors and Roofs in Ancient Buildings at Valencia (Spain). From Material to Structure - Mechanical Behaviour and Failures of the Timber Structures, 11-16 November 2007 Florence, Venice and Vicenza. ICOMOS International Wood Committee.

Ridout, B. 2000. *Timber Decay in Buildings: The Conservation Approach to Treatment (1st edition).* London, E & FN Spon.

Rinn, F. 2012. Basics of typical resistance-drilling profiles. *Western Arborist,* vol. 39, nr. 4**,** pp. 30-36.

Ross, R. J., Brashaw, B. K. & Wang, X. 2006. Structural Condition Assessment of In-Service Wood. *Forest Products Journal,* vol. 56, nr. 6**,** pp. 4-8.

Ross, R. J., Brashaw, B. K., Wang, X., et al. 2004. *Wood and Timber: Condition Assessment Manual.* Madison, WI, Forest Products Society.

Ross, R. J., DeGroot, R. C., Nelson, W. J., et al. 1997. The Relationship Between Stress Wave Transmission and The Compressive Strength of Biologically Degraded Wood. *Forest Products Journal,* vol. 47, nr. 5**,** pp. 89-93.

Ross, R. J. & Pellerin, R. F. 1994. Nondestructive Testing for Assessing Wood Members in Structures: A Review. Madison, WI: Forest Products Laboratory.

SIS, 2002. *SS-EN 1991-1-1 Eurokod 1: Laster på bärverk - Del 1-1: Allmänna laster - Tunghet, egentyngd, nyttig last för byggnader*.

SIS, 2004. *SS-EN 1995-1-1:2004 Eurokod 5: Dimensionering av träkonstruktioner - Del 1-1: Allmänt - Gemensamma regler och regler för byggnader*.

Soltis, L. A., Wang, X., Ross, R. J., et al. 2002. Vibration Testing of Timber Floor Systems. *Forest Products Journal,* vol. 52, nr. 10**,** pp. 75-81.

Weiss, H. F. 1915. *The Preservation of Structural Timber.* New York, McGraw-Hill Book Company, Inc.

Williams, J. R. 2009. Non-destructive assessment of timber in historic buildings. *Proceedings of the institution of Civil Engineers - Construction Materials,* vol. 162, nr. 4**,** pp. 175-180.

Appendices

A Used investigation data sheets

Inspection overview - First artillery floor

Beam	A	B	C	D	E	F	G	H	I	J	K	L	M	N	O	P	1	2
Discolouration/stain	X	X	X	X	X	X	X	X	X	X	X		X	X	X	X	X	X
Charing	X	X	X	X				X	X	X		X		X	X	X		
Cracking			X	X	X	X	X	X	X	X	X	X	X	X	X	X	X	X
Holes												X						
Frass or powder posting					X													
Fruiting bodies																		
Large deviations in geometry								X								X		
Contact with primary beam 1?		X	X	X	X	X	X	X	X	X	X	X	X	X	X	X		
Contact with primary beam 2?		X	X	X	X	X	X	X	X	X	X			X	X	X		

Edge to edge-distances between beams at end supports

Edge to edge-distance	Span 1	Span 3	[mm]
A-B	428	413	
B-C	462	458	
C-D	420	391	
D-E	431	397	
E-F	425	423	
F-G	389	410	
G-H	377	272	
H-I	342	280	
I-J	335	343	
J-K	309	362	
K-L	346	316	
L-M	391	381	
M-N	446	376	
N-O	388	379	
O-P	322	320	
1-2	2898	2885	

General crack opening a: 20

Inspection overview - Second artillery floor

Beam	A	B	C	D	E	F	G	H	I	J	K	L	M	N	O	1	2	Column	3	4	5	6
Discolouration/stain																						
Charing																						
Cracking																						
Holes																						
Frass or powder posting																						
Fruiting bodies																						
Large deviations in geometry																						
Contact with primary beam 1?			X		X	X	X	X	X	X	X	X			X							
Contact with primary beam 2?			X		X	X	X	X	X	X	X	X	X	X	X							

CC-distances between beams at end supports

CC-distance	Start	Stop	
A-B	454	432	
B-C	450	453	
C-D	501	500	
D-E	465	460	
E-F	446	430	
F-G	470	450	
G-H	370	339	
H-I	x	369	
I-J	x	392	H-J, span 3= 1116
J-K	369	356	
K-L	440	428	
L-M	464	468	
M-N	439	444	
N-O	379	375	O-Wall, ~25 cm
1-2	990	992	

General crack opening a: 20

Beam:	B			**Notes:**		
Length of whole beam				Corner 2 deteriorated?		
Length of span 1	2,195			Corner 1, deterioration over beam 1?		
Length of span 2						
Length of span 3	2,666					
Contact with primary beam 1?	no	Photography:				
Contact with primary beam 2?	no	Photography:				
Measurements at different coordinates						
Coordinate		span 3				span 1
Width		265				290
Height		300				295
Trimmed corner diagonal:						
4		50				
3		70				
2		25				60
1						45
Moisture content						

B Documentation of in-situ testing

Second artillery floor															
Measurement nr.	Member	Span	Location	Face	Direction	d [cm]	t_1 [µs]	t_2 [µs]	t_3 [µs]	t_4 [µs]	t_5 [µs]	t_6 [µs]	t_{mean} [µs]	v [m/s]
F.01	6	-	Bottom	14	Trans	37	388	356	349	361	348	351	355	1043
F.02	6	-	Bottom	12	Trans	38	454	451	438	444	444	450	443	858
F.03	6	-	Bottom	14	Long	154	316	306	308	307	304	309	304	5060
F.04	6	-	Bottom	12	Long	188	375	374	373	385	379	380	374	5031
F.05	1	1	Middle	23	Long	156	320	328	321	322	315		317	4918
F.06	1	1	B-C, middle	34	Trans	34	424	405	385	415	396		401	848
F.07	B	1	Whole	23	Long	163	318	318	308	313	309		309	5272
F.08	C	1	Whole	23	Long	195	378	384	385	381	380		378	5164
F.09	D	1	Mi-Prim	23	Long	200	370	351	369	367	361		360	5562
F.10	E	1	Mi-Prim	14	Long	159	320	306	297	301	297	296	299	5321
F.11	F	1	Mi-Prim	14	Long	152	292	291	292	290	292		287	5289
F.12	G	1	Middle	23	Long	141	265	266	261	262	259		259	5452
F.13	H	1	Middle	34	Long	100	223	223	213	211	223		215	4660
F.14	I	1	Middle	34	Long	82	186	188	184	188	180		181	4525
F.15	J	1	Mi/Prim	23	Long	103	214	219	220	220	211		213	4840
F.16	K	1	Middle	23	Long	142	274	265	266	265	264		263	5403
F.17	L	1	Mi/Prim	23	Long	140	283	277	284	288	272	279	277	5063
F.18	M	1	Mi/Prim	14	Long	123	226	230	229	232	228	228	225	5471
F.19	N	1	Mi/whole	14	Long	122	236	237	237	235	236		232	5254
F.20	O	1	Whole	14	Long	115	225	222	223	222	220		218	5266
F.21	3	-	Bottom	14	Trans	35	306	307	343	309	319		313	1119
F.22	3	-	Middle	14	Trans	35	243	241	243	242	246		239	1464
F.23	3	-	Bottom	12	Trans	37	310	304	322	320	320		311	1189
F.24	3	-	115 cm fr bot	12	Trans	37	324	336	322	326	319	327	322	1150
F.25	3	-	Bottom	12	Long	81	166	162	170	164	163		161	5031
F.26	3	-	Bo-Mid	14	Long	179	376	374	368	364	373	372	367	4875
F.27	O	3	Bottom	34	Long	54	117	116	118	116	116		113	4796
F.28	N	3	Bottom	34	Long	134	267	286	277	292	278		276	4855
F.29	M	3	Bottom	34	Long	117	220	228	220	219	230		219	5333
F.30	L	3	Middle	14	Long	114	249	252	253	253	200		237	4802
F.31	K	3	Middle		Long	122	242	238	235	262	252	250	243	5031
F.32	J	3	Middle	34	Long	114	260	268	259	265	258		258	4419
F.33	I	3	Middle	23	Long	130	256	260	255	254	253		252	5167
F.34	H	3	Middle	12	Long	105	204	205	205	205	205		201	5229
F.35	H	3	Middle	34	Long	118	236	235	235	235	232		231	5117
F.36	G	3	Middle	34	Long	110	210	212	216	212	212	208	208	5297
F.37	F	3	Middle	34	Long	116	244	246	246	248	247		242	4789
F.38	E	3	Middle	12	Long	143	315	309	316	313	316	320	311	4601
F.39	D	3	Mi-Prim	12	Long	121	235	238	244	236	234		233	5184
F.40	C	3	Mi-Prim	12	Long	104	211	206	206	212	212	218	207	5028
F.41	B	3	Mi-Prim	12	Long	75	160	162	162	163	164	163	158	4737
F.42	A	3	Mi-Prim	12	Long	78	175	181	187	180	180	187	178	4390
F.43	2	1	Middle	34	Long	203	475	442	446	434	432	430	439	4622
F.44	1	3	Middle	34	Long	170	363	367	375	362	369		363	4681
F.45	2	3	Middle	12	Long	168	325	316	320	319	320	322	316	5311
F.46	5	-	Bo-Mid	12	Long	169	308	309	313	309	315		307	5508
F.47	5	-	Bo-Mid	23	Long	150	283	290	278	277	280		278	5403
F.48	4	-	Bo-Mid	12	Long	137	272	268	268	270	270	267	265	5167
F.49	5	-	250 cm up, near 34	23	Long	242	471	478	477	477	465		470	5153
F.93	1	1	B-C, middle	12	Trans	34	228	222	214	225	224		219	1555
F.94	1	1	B-C, bottom half	12	Trans	34	249	256	256	237	247		245	1388
F.95	1	1	B-C, top half	12	Trans	34	302	303	303	312	289		298	1142
F.96	1	1	C-D, middle	12	Trans	34	211	216	210	217	219		211	1614
F.97	1	1	C-D, bottom half	12	Trans	34	255	265	266	260	249		255	1333
F.98	1	1	C-D, top half	12	Trans	34	212	220	218	210	214		211	1613
F.99	1	1	From column	12	Long	90	184	196	190	189	187		185	4860
F.100	1	1	Start from column	12	Long	180	366	366	364	362	366	366	361	4986
F.101	1	1	Start from column	12	Long	270	526	524	530	525	529		523	5164
F.102	1	1	Move start point 90 cm	12	Long	180	354	348	358	344	345		346	5205
F.103	1	1	Move start point 180 cm	12	Long	90	175	176	175	174	175		171	5263
F.104	1	1	"Middle 90 cm"	12	Long	90	180	182	182	182	180		177	5079
R.01	6	-	Bottom	23	Rad									
R.02	6	-	Bottom	12	Rad									
R.03	1	1	Middle	23	Rad									
R.04	1	1	End	23	Angle									
R.05	A	1	End	23	Angle									
R.06	1	1	Bott/Mid	12	Rad									
R.07	3	-	Top	14	Rad									
R.08	C	1	End	23	Rad									
R.09	E	1	Middle	23	Rad									
R.10	J	1	Bott/Mid	34	Rad									
R.11	1	3	Middle	12	Rad									
R.12	M	1	Near 14	23	Rad									
R.13	3	-	70 cm up	14	Rad									
R.14	3	-	130 cm up	14	Rad									
R.15	3	-	115 cm up	12	Rad									
R.16	3	-	40 cm up	12	Rad									
R.17	2	3	K-L, bottom	34	Rad									
R.18	2	3	K, top	34	Rad									
R.19	K	3	Near 12	23	Rad									
R.20	2	1	D-E, bottom	34	Rad									
R.21	C	3	Bottom	12	Rad									
R.22	4	-	120 cm up	14	Rad									
R.23	4	-	Under (mult. cracks)	14	Rad									
R.24	5	-	Bottom	12	Rad									
R.25	5	-	150 cm up	14	Rad									
X.01	2	3	L-M, bottom	34	Perp	36								
X.02	2	3	L-M, bottom	12	Perp	36								
X.03	2	3	L-M, bottom	12	Perp	36								
X.04	1	1	C-D, bottom	34	Perp	36								
X.05	1	1	C-D, bottom	34	Perp	36								
X.06	J	1	Middle	34	Perp	28								
X.07	J	1	Middle	34	Perp	28								
X.08	J	1	Middle	34	Perp	28								
X.09	H	1	Middle	12	Perp/Angle (quali)									
X.10	6 (joint)	-		34	Perp (quali)									
X.11	6 (joint)	-		14	Angle									
X.12	A	3	Near prim	12	Angle									
X.13	2	1	Start	12	Angle									

X.14	1	1	B-C	12	Perp (quali, suspected insect damage)										
X.15	1	1	B-C	12	Perp (quali, anchorage at top)										
X.16	3				Angle										
X.17	2	1	E-F	23	Perp	32									
X.18	2	1	E-F	23	Perp	32									
X.19	H	3		34	Angle										
X.20	2	3	Notch	23	Perp (quali)										
X.21	2	3	J-K	34	Perp (quali)										
X.22	2	3	M-N	34	Perp (quali)										
X.23	5	-	Under prim (joint)	23	Perp (quali)										
X.24	C	3	End	12	Angle										
X.25	C	3	Same as X.24, but better	12	Angle										

First artillery floor														
Measurement nr.	Member	Span	Location	Face	Direction	d [cm]	t_1 [µs]	t_2 [µs]	t_3 [µs]	t_4 [µs]	t_5 [µs]	t_6 [µs]	t_{mean} [µs]	v [m/s]
F.50	O	1	Middle	34	Long	86	178	196	177	180	180		182	4720
F.51	P	1	Middle	34	Long	51	105	108	105	106	106		106	4811
F.52	N	1	Middle	34	Long	156	304	307	325	307	309		310	5026
F.53	M	1	Middle	34	Long	196	387	390	388	397	391		391	5018
F.54	L	1	Middle	34	Long	209	460	457	457	464	454		458	4559
F.55	K	1	Middle	34	Long	175	406	406	404	404	397		403	4338
F.56	J	1	Middle	34	Long	186	387	394	391	386	390		390	4774
F.57	I	1	Middle	34	Long	164	363	374	386	374	379		375	4371
F.58	H	1	Middle	34	Long	173	339	338	338	331	334		336	5149
F.59	G	1	Middle	34	Long	163	333	325	325	326	327		327	4982
F.60	F	1	Middle	34	Long	165	328	328	327	321	328		326	5055
F.61	E	1	Middle	34	Long	166	372	367	364	372	370		369	4499
F.62	D	1	Middle	12	Long	169	326	330	331	336	336		332	5093
F.63	C	1	Middle	12	Long	149	286	298	308	302	298		298	4993
F.64	B	1	Middle	12	Long	121	234	234	232	232	231		233	5202
F.65	A	1	Middle	12	Long	139	306	306	301	301	298		302	4597
F.66	B	2	Middle	12	Long	237	445	442	441	442	448		444	5343
F.67	C	2	Middle	23	Long	209	432	433	438	433	430	423	432	4844
F.68	D	2	Middle	34	Long	178	333	334	336	342	337	343	338	5274
F.69	B	3	Middle	12	Long	127	234	232	235	232	237		234	5427
F.70	C	3	Middle	12	Long	185	375	375	376	372	370		374	4952
F.71	D	3	Middle	12	Long	153	284	284	288	282	282	285	284	5384
F.72	E	3	Middle	12	Long	164	346	342	352	342	345	357	347	4722
F.73	F	3	Middle	12	Long	191	384	386	393	399	384		389	4908
F.74	G	3	Middle	12	Long	214	411	404	396	394	394		400	5353
F.75	H	3	Middle	12	Long	188	374	384	384	385	386		383	4914
F.76	I	3	Middle	12	Long	199	357	358	355	364	370	363	361	5510
F.77	J	3	Middle	12	Long	186	338	338	349	340	339		341	5458
F.78	K	3	Middle	12	Long	230	427	429	434	434	435	432	432	5326
F.79	L	3	Middle	12	Long	199	398	397	397	397	391		396	5025
F.80	M	3	Middle	34	Long	185	351	345	340	354	338		346	5353
F.81	N	3	Middle	34	Long	121	264	266	261	266	261		264	4590
F.82	O	3	Middle	34	Long	92	199	193	193	194	195		195	4723
F.83	L	2	Middle	12	Long	121	262	252	256	249	259		256	4734
F.84	M	2	Middle	12	Long	147	297	302	303	295	301		300	4907
F.85	N	2	Middle	34	Long	168	356	368	368	362	356		362	4641
F.86	O	2	Middle	23	Long	163	309	308	312	306	309		309	5278
F.87	2	3	Middle	34	Long	135	258	258	260	260	258		259	5216
F.88	2	2	Middle	34	Long	87	183	180	182	181	180		181	4801
F.89	2	1	Middle	34	Long	287	543	542	547	555	542		546	5258
F.90	1	1	Middle	12	Long	325	640	637	644	643	637		640	5077
F.91	1	2	Middle	12	Long	280	606	603	606	600	591	613	603	4642
F.92	1	3	Middle	12	Long	224	477	480	483	480	481	481	480	4663
F.105	1	1	D, middle	34	Trans	39	224	230	226	225	223	224	225	1731
F.106	1	1	D, bottom half	34	Trans	39	357	363	372	358	337	362	358	1089
F.107	1	1	D, top half	34	Trans	39	260	268	270	272	277		269	1448
F.108	1	1	Start at masonry	12	Long	90	187	184	184	184	184		185	4875
F.109	1	1	180 (sp 1) 0 (sp 2)	12	Long	180	357	357	358	360	361	357	358	5023
F.110	1	1 & 2	180 (sp 1) 90 (sp 2)	12	Long	270	595	588	597	591	597		594	4549
F.111	1	1 & 2	180 in each sp 1 & 2	12	Long	360	793	787	787	792	796		791	4551
F.112	1	1 & 2	90 (sp 1) 180 (sp 2)	12	Long	270	646	608	615	624	613		621	4346
F.113	1	2	0 (sp 1) 180 (sp 2)	12	Long	180	420	415	420	414	423	422	419	4296
F.114	1	2	0 (sp 1) 90 (sp 2)	12	Long	90	208	206	207	211	206		208	4335
F.115	1	2	Start at 90 cm from masonry	12	Long	90	230	229	230	228	230	232	230	3916
F.116	1	1 & 2	90 in each sp 1 & 2	12	Long	180	417	414	397	306	308		368	4886
R.26	P	1	Middle	23	Rad									
R.27	1	3	Middle	12	Rad									
R.28	1	3	Middle	12	Rad									
R.29	1	3	Middle	12	Rad									
R.30	1	3	Mi-Bot	12	Rad									
R.31	1	3	Near 34	23	Rad									
R.32	L	1	Near 34	23	Rad									
R.33	L	1	Middle	23	Rad									
R.34	L	1	Middle	23	Angle									
R.35	J	1	Middle	23	Rad									
R.36	L	1	Middle	23	Rad									
R.37	I	1	Middle	23	Rad									
R.38	D	1	Middle	23	Rad									
R.39	D	1	Middle	23	Rad									
R.40	North sill	1			Rad									
R.41	1	1	D-E, 1/3 from bottom	34	Rad									
R.42	C	2	Middle, crack	23	Rad									
R.43	C	2	Near 34, crack	23	Rad									
R.44	B	2	Middle	23	Rad									
R.45	2	1	C-D, middle	12	Rad									
R.46	2	1	C-D, middle	23	Rad									
R.47	D	3	Middle	23	Rad									
R.48	E	3	Near 12	23	Rad									
R.49	H	3	Middle	23	Rad									
R.50	L	3	Bottom	34	Rad									
R.51	L	3	Middle	23	Rad									
R.52	L	2	Near 34	23	Rad									
R.53	2	3	Mi-Bot	12	Rad									
R.54	2	3	Middle	23	Rad									
X.26	L	1	Start	12	Angle									
X.27	D	1	Start	12	Angle									
X.28	D	1	Start	12	Angle									
X.29	1	3	Background image											
X.30	1	3	Healthy timber	12	Perp	39								
X.31	1	3	Discolouration and crack, with needle and paper	12	Perp	40								
X.32	1	3	Discolouration and crack, with needle and paper	12	Perp	40								

X.33	1	3	Discolouration and crack, be aware of needle and paper	12	Perp	40									
X.34	1	3	Discolouration and crack, without needle and paper	12	Perp	40									
X.35	1	3	Grain structure the disc and crack	12	Angle										
X.36	1	3	Background image												
X.37	1	3	Half healthy timber	12	Perp	41									
X.38	1	3	Half healthy timber	12	Perp	41									
X.39	1	3	Discolouration and crack	12	Perp	41									
X.40	1	3	Background image												
X.41	1	3	Background image												
X.42	1	3	Discolouration and crack	12	Perp	41									
X.43	1	3	Discolouration and crack	12	Perp	41									
X.44	C	1	Background image												
X.45	C	1	Cracked region, middle of span	23	Perp	32									
X.46	C	1	Cracked region, middle of span	23	Perp	32									
X.47	C	1	Healthy timber	23	Perp	33									
X.48	C	1	Healthy timber	23	Perp	33									
X.49	D	1	Plate along beam, middle of span	23	Perp (quali)										
X.50	D	1	Plate across beam, middle of span	23	Perp (quali)										
X.51	D	1	Background image												
X.52	E	1	At wall support		Perp	29									
X.53	E	3	Suspected damage		Perp	25									
X.54	(P)		Old piece from P	-	Perp	29									
X.55	J	1	Healthy timber, middle of span	23	Perp	29									
X.56	J	1	Healthy timber, middle of span	23	Perp	29									
X.57	J	1	Healthy timber, middle of span	23	Perp	29									
X.58	L	1	Damaged support at wall	34	Angle										
X.59	L	1	Support at wall	23	Perp	33									
X.60	L	1	Support at wall	12	Angle										
X.61	D	3	Towards span 2 and face 12	23	Perp	31									
X.62	D	3	Towards span 2 and face 12	23	Perp	31									
X.63	K	3	Support at masonry	12	Angle										
X.64	K	3	Support at masonry	12	Angle										

C Example of an evaluated radiograph for density determination

d=1m; Impulse=70; 300 dpi; 8-bit image depth

Image name: X.07.tif (corrected)

Date and Time
2013-05-14

No.	ρ [kg/m³]	Mean	Stdv	Min	Max	Area
55	432	119,3	9,87	73	244	0,689
65	492	116,0	3,16	90	158	0,689
75	526	113,3	3,23	59	154	0,689
95	560	109,8	3,40	93	172	0,689
105	574	104,1	3,01	89	151	0,689
115	728	92,9	3,71	78	108	0,689
135	758	91,1	3,13	70	118	0,689
125	775	86,1	5,21	69	109	0,508

Image no.	ρ	Avg. Greyscale	measured ρ	Diff [%]
2-mod	474	116,9		#VÄRDEFEL!

Linear relationship

x-term	-10,3
constant	1675,8
R^2	0,98

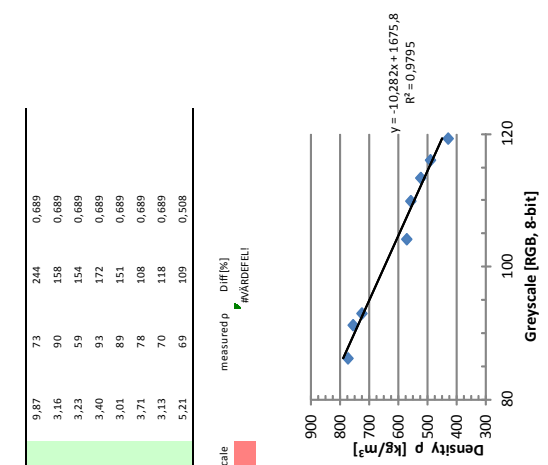

Calibration wedge:

55	65	75	95	105	115	135	125

No.	Area	Mean	Stdv	Min	Max
1	0,689	119,281	9,866	73	244
2	0,689	116,017	3,156	90	158
3	0,689	113,337	3,231	59	154
4	0,689	109,847	3,397	93	172
5	0,689	104,106	3,013	89	151
6	0,689	92,910	3,712	78	108
7	0,689	91,147	3,129	70	118
8	0,508	86,147	5,206	69	109
9	25,17	15,869	1,450	7	48

corrected with X.29, mult with 150

Thickness adjustment: 101,048 28 cm thick
moisture adjustment: 0

D Determination of sample density in Mathcad

Calculation of approximate expected timber density from an edge timber piece of removed part of beam P in first artillery floor. The dry mass of a sample were measured on a scale in laboratory. Then the sample were submerged in a beaker with a known volume of water. Then the new water level was noticed and the volume of the sample could be calculated and subsequently related to the dry mass.

Sample nr 1

$m_{dry1} := 15.28\,10^{-3}\,kg$

$m_{wet1} := 18.13\,10^{-3}\,kg$

$v_{abs1} := \frac{m_{wet1} - m_{dry1}}{1000\frac{kg}{m^3}} = 2.85\,ml$

$v_{water1} := 150\,ml$

$v_{total1} := 183\,ml$

$v_{sample1} := v_{total1} - v_{water1} + v_{abs1} = 0.036\,L$

$\rho_{sample1} := \frac{m_{dry1}}{v_{sample1}} = 426.22\frac{kg}{m^3}$

Sample nr 2

$m_{dry2} := 19.88\,10^{-3}\,kg$

$m_{wet2} := 23.64\,10^{-3}\,kg$

$v_{abs2} := \frac{m_{wet2} - m_{dry2}}{1000\frac{kg}{m^3}} = 3.76\,ml$

$v_{water2} := 150\,ml$

$v_{total2} := 194\,ml$

$v_{sample2} := v_{total2} - v_{water2} + v_{abs2} = 0.048\,L$

$\rho_{sample2} := \frac{m_{dry2}}{v_{sample2}} = 416.248\frac{kg}{m^3}$

Average (expected) density

$\rho_{mean} := \frac{\rho_{sample1} + \rho_{sample2}}{2} = 421.234\frac{kg}{m^3}$

E Calculation of MOE, f_m and f_v for models 2,4,6 and 8

Second artillery floor									Sample density					X-ray densities				
Measurement nr.	Member	Span	Location	Face	Direction	d [cm]	t_{mean} [µs]	v [m/s]	ρ [kg/m^3]	E_d [GPa]	E_s [GPa]	f_m [MPa]	f_v [MPa]	ρ [kg/m^3]	E_d [GPa]	E_s [GPa]	f_m [MPa]	f_v [MPa]
F.03	6	-	Bottom	14	Long	154	304	5060	420	10,8	8,7	18,0	2,02	424	10,9	8,8	18,1	2,03
F.04	6	-	Bottom	12	Long	188	374	5031	420	10,6	8,6	17,8	2,00	424	10,7	8,7	17,9	2,01
F.05	1	1	Middle	23	Long	156	317	4918	420	10,2	8,2	17,0	1,93	424	10,3	8,3	17,2	1,95
F.07	B	1	Whole	23	Long	163	309	5272	420	11,7	9,4	19,4	2,14	440	12,2	9,8	20,3	2,22
F.08	C	1	Whole	23	Long	195	378	5164	420	11,2	9,0	18,7	2,08	440	11,7	9,4	19,5	2,15
F.09	D	1	Mi-Prim	23	Long	200	360	5562	420	13,0	10,4	21,4	2,32	440	13,6	10,9	22,4	2,41
F.10	E	1	Mi-Prim	14	Long	159	299	5321	420	11,9	9,6	19,7	2,17	440	12,5	10,0	20,6	2,25
F.11	F	1	Mi-Prim	14	Long	152	287	5289	420	11,7	9,4	19,5	2,15	440	12,3	9,9	20,4	2,23
F.12	G	1	Middle	23	Long	141	259	5452	420	12,5	10,0	20,7	2,25	440	13,1	10,5	21,6	2,34
F.13	H	1	Middle	34	Long	100	215	4660	420	9,1	7,5	15,4	1,78	440	9,6	7,8	16,1	1,85
F.14	I	1	Middle	34	Long	82	181	4525	420	8,6	7,1	14,6	1,71	440	9,0	7,4	15,2	1,77
F.15	J	1	Mi/Prim	23	Long	103	213	4840	420	9,8	8,0	16,5	1,89	440	10,3	8,4	17,3	1,95
F.16	K	1	Middle	23	Long	142	263	5403	420	12,3	9,8	20,3	2,22	440	12,8	10,3	21,2	2,30
F.17	L	1	Mi/Prim	23	Long	140	277	5063	420	10,8	8,7	18,0	2,02	440	11,3	9,1	18,8	2,09
F.18	M	1	Mi/Prim	14	Long	123	225	5471	420	12,6	10,1	20,8	2,27	440	13,2	10,5	21,7	2,35
F.19	N	1	Mi/whole	14	Long	122	232	5254	420	11,6	9,3	19,3	2,13	440	12,1	9,7	20,1	2,21
F.20	O	1	Whole	14	Long	115	218	5266	420	11,6	9,4	19,3	2,14	440	12,2	9,8	20,2	2,22
F.25	3	-	Bottom	12	Long	81	161	5031	420	10,6	8,6	17,8	2,00	424	10,7	8,7	17,9	2,01
F.26	3	-	Bo-Mid	14	Long	179	367	4875	420	10,0	8,1	16,8	1,91	424	10,1	8,2	16,9	1,92
F.27	O	3	Bottom	34	Long	54	113	4796	420	9,7	7,9	16,3	1,86	440	10,1	8,2	17,0	1,93
F.28	N	3	Bottom	34	Long	134	276	4855	420	9,9	8,1	16,6	1,90	440	10,4	8,4	17,4	1,96
F.29	M	3	Bottom	34	Long	117	219	5333	420	11,9	9,6	19,8	2,18	440	12,5	10,0	20,7	2,26
F.30	L	3	Middle	14	Long	114	237	4802	420	9,7	7,9	16,3	1,86	440	10,1	8,2	17,0	1,93
F.31	K	3	Middle		Long	122	243	5031	420	10,6	8,6	17,8	2,00	440	11,1	9,0	18,6	2,07
F.32	J	3	Middle	34	Long	114	258	4419	420	8,2	6,8	14,0	1,65	440	8,6	7,1	14,6	1,71
F.33	I	3	Middle	23	Long	130	252	5167	420	11,2	9,0	18,7	2,08	440	11,7	9,4	19,5	2,15
F.34	H	3	Middle	12	Long	105	201	5229	420	11,5	9,2	19,1	2,12	440	12,0	9,7	19,9	2,19
F.35	H	3	Middle	34	Long	118	231	5117	420	11,0	8,9	18,3	2,05	440	11,5	9,3	19,2	2,12
F.36	G	3	Middle	34	Long	110	208	5297	420	11,8	9,5	19,6	2,16	440	12,3	9,9	20,4	2,24
F.37	F	3	Middle	34	Long	116	242	4789	420	9,6	7,9	16,2	1,86	440	10,1	8,2	16,9	1,92
F.38	E	3	Middle	12	Long	143	311	4601	420	8,9	7,3	15,1	1,75	440	9,3	7,6	15,7	1,81
F.39	D	3	Mi-Prim	12	Long	121	233	5184	420	11,3	9,1	18,8	2,09	440	11,8	9,5	19,6	2,16
F.40	C	3	Mi-Prim	12	Long	104	207	5028	420	10,6	8,6	17,7	2,00	440	11,1	9,0	18,5	2,07
F.41	B	3	Mi-Prim	12	Long	75	158	4737	420	9,4	7,7	15,9	1,83	440	9,9	8,0	16,6	1,89
F.42	A	3	Mi-Prim	12	Long	78	178	4390	420	8,1	6,7	13,8	1,63	440	8,5	7,0	14,4	1,69
F.43	2	1	Middle	34	Long	203	439	4622	420	9,0	7,4	15,2	1,76	424	9,1	7,4	15,3	1,77
F.44	1	3	Middle	34	Long	170	363	4681	420	9,2	7,5	15,5	1,80	424	9,3	7,6	15,7	1,81
F.45	2	3	Middle	12	Long	168	316	5311	420	11,8	9,5	19,7	2,17	424	12,0	9,6	19,8	2,18
F.46	5	-	Bo-Mid	12	Long	169	307	5508	420	12,7	10,2	21,1	2,29	424	12,9	10,3	21,2	2,31
F.47	5	-	Bo-Mid	23	Long	150	278	5403	420	12,3	9,8	20,3	2,22	424	12,4	9,9	20,5	2,24
F.48	4	-	Bo-Mid	12	Long	137	265	5167	420	11,2	9,0	18,7	2,08	424	11,3	9,1	18,8	2,09
F.49	5	-	250 cm up, near 34	23	Long	242	470	5153	420	11,2	9,0	18,6	2,07	424	11,3	9,1	18,7	2,09
F.99	1	1	From column	12	Long	90	185	4860	420	9,9	8,1	16,7	1,90	424	10,0	8,1	16,8	1,91
F.100	1	1	Start from column	12	Long	180	361	4986	420	10,4	8,5	17,5	1,97	424	10,5	8,5	17,6	1,99
F.101	1	1	Start from column	12	Long	270	523	5164	420	11,2	9,0	18,7	2,08	424	11,3	9,1	18,8	2,09
F.102	1	1	Move start point 90 cm	12	Long	180	346	5205	420	11,4	9,2	18,9	2,10	424	11,5	9,3	19,1	2,12
F.103	1	1	Move start point 180 cm	12	Long	90	171	5263	420	11,6	9,4	19,3	2,14	424	11,7	9,4	19,5	2,15
F.104	1	1	"Middle 90 cm"	12	Long	90	177	5079	420	10,8	8,8	18,1	2,03	424	10,9	8,8	18,2	2,04

First artillery floor									Sample density					X-ray densities				
Measurement nr.	Member	Span	Location	Face	Direction	d [cm]	t_{mean} [µs]	v [m/s]	ρ [kg/m^3]	E_d [GPa]	E_s [GPa]	f_m [MPa]	f_v [MPa]	ρ [kg/m^3]	E_d [GPa]	E_s [GPa]	f_m [MPa]	f_v [MPa]
F.50	O	1	Middle	34	Long	86	182	4720	420	9,4	7,6	15,8	1,82	457	10,2	8,3	17,1	1,94
F.51	P	1	Middle	34	Long	51	106	4811	420	9,7	7,9	16,4	1,87	457	10,6	8,6	17,7	1,99
F.52	N	1	Middle	34	Long	156	310	5026	420	10,6	8,6	17,7	2,00	457	11,5	9,3	19,2	2,13
F.53	M	1	Middle	34	Long	196	391	5018	420	10,6	8,6	17,7	1,99	457	11,5	9,3	19,1	2,12
F.54	L	1	Middle	34	Long	209	458	4559	420	8,7	7,2	14,8	1,73	457	9,5	7,8	16,0	1,84
F.55	K	1	Middle	34	Long	175	403	4338	420	7,9	6,5	13,5	1,61	457	8,6	7,1	14,6	1,71
F.56	J	1	Middle	34	Long	186	390	4774	420	9,6	7,8	16,1	1,85	457	10,4	8,4	17,4	1,97
F.57	I	1	Middle	34	Long	164	375	4371	420	8,0	6,6	13,7	1,62	457	8,7	7,2	14,8	1,73
F.58	H	1	Middle	34	Long	173	336	5149	420	11,1	9,0	18,6	2,07	457	12,1	9,7	20,1	2,20
F.59	G	1	Middle	34	Long	163	327	4982	420	10,4	8,4	17,4	1,97	457	11,3	9,1	18,9	2,10
F.60	F	1	Middle	34	Long	165	326	5055	420	10,7	8,7	17,9	2,01	457	11,7	9,4	19,4	2,14
F.61	E	1	Middle	34	Long	166	369	4499	420	8,5	7,0	14,4	1,69	457	9,2	7,6	15,6	1,80
F.62	D	1	Middle	12	Long	169	332	5093	420	10,9	8,8	18,2	2,04	457	11,9	9,5	19,7	2,17
F.63	C	1	Middle	12	Long	149	298	4993	420	10,5	8,5	17,5	1,98	457	11,4	9,2	19,0	2,10
F.64	B	1	Middle	12	Long	121	233	5202	420	11,4	9,2	18,9	2,10	457	12,4	9,9	20,5	2,24
F.65	A	1	Middle	12	Long	139	302	4597	420	8,9	7,3	15,0	1,75	457	9,7	7,9	16,2	1,86
F.66	B	2	Middle	12	Long	237	444	5343	420	12,0	9,6	19,9	2,19	457	13,0	10,4	21,5	2,33
F.67	C	2	Middle	23	Long	209	432	4844	420	9,9	8,0	16,6	1,89	457	10,7	8,7	17,9	2,01
F.68	D	2	Middle	34	Long	178	338	5274	420	11,7	9,4	19,4	2,14	457	12,7	10,2	21,0	2,29
F.69	B	3	Middle	12	Long	127	234	5427	420	12,4	9,9	20,5	2,24	457	13,5	10,7	22,2	2,39
F.70	C	3	Middle	12	Long	185	374	4952	420	10,3	8,4	17,2	1,95	457	11,2	9,0	18,7	2,08
F.71	D	3	Middle	12	Long	153	284	5384	420	12,2	9,8	20,2	2,21	457	13,2	10,6	21,8	2,36
F.72	E	3	Middle	12	Long	164	347	4722	420	9,4	7,6	15,8	1,82	457	10,2	8,3	17,1	1,94
F.73	F	3	Middle	12	Long	191	389	4908	420	10,1	8,2	17,0	1,93	457	11,0	8,9	18,4	2,05
F.74	G	3	Middle	12	Long	214	400	5353	420	12,0	9,7	20,0	2,19	457	13,1	10,5	21,6	2,34
F.75	H	3	Middle	12	Long	188	383	4914	420	10,1	8,2	17,0	1,93	457	11,0	8,9	18,4	2,05
F.76	I	3	Middle	12	Long	199	361	5510	420	12,8	10,2	21,1	2,29	457	13,9	11,1	22,8	2,44
F.77	J	3	Middle	12	Long	186	341	5458	420	12,5	10,0	20,7	2,26	457	13,6	10,9	22,4	2,41
F.78	K	3	Middle	12	Long	230	432	5326	420	11,9	9,6	19,8	2,18	457	13,0	10,4	21,4	2,32
F.79	L	3	Middle	12	Long	199	396	5025	420	10,6	8,6	17,7	2,00	457	11,5	9,3	19,2	2,13
F.80	M	3	Middle	34	Long	185	346	5353	420	12,0	9,7	20,0	2,19	457	13,1	10,5	21,6	2,34
F.81	N	3	Middle	34	Long	121	264	4590	420	8,8	7,3	15,0	1,74	457	9,6	7,8	16,2	1,86
F.82	O	3	Middle	34	Long	92	195	4723	420	9,4	7,7	15,8	1,82	457	10,2	8,3	17,1	1,94
F.83	L	2	Middle	12	Long	121	256	4734	420	9,4	7,7	15,9	1,83	457	10,2	8,3	17,2	1,94
F.84	M	2	Middle	12	Long	147	300	4907	420	10,1	8,2	17,0	1,93	457	11,0	8,9	18,3	2,05
F.85	N	2	Middle	34	Long	168	362	4641	420	9,0	7,4	15,3	1,77	457	9,8	8,0	16,5	1,89
F.86	O	2	Middle	23	Long	163	309	5278	420	11,7	9,4	19,4	2,15	457	12,7	10,2	21,0	2,29
F.87	2	3	Middle	34	Long	135	259	5216	420	11,4	9,2	19,0	2,11	475	12,9	10,3	21,3	2,31
F.88	2	2	Middle	34	Long	87	181	4801	420	9,7	7,9	16,3	1,86	475	11,0	8,8	18,3	2,04
F.89	2	1	Middle	34	Long	287	546	5258	420	11,6	9,3	19,3	2,14	475	13,1	10,5	21,7	2,34
F.90	1	1	Middle	12	Long	325	640	5077	420	10,8	8,7	18,1	2,03	475	12,2	9,8	20,3	2,22
F.91	1	2	Middle	12	Long	280	603	4642	420	9,1	7,4	15,3	1,77	475	10,2	8,3	17,2	1,94
F.92	1	3	Middle	12	Long	224	480	4663	420	9,1	7,5	15,4	1,79	475	10,3	8,4	17,3	1,96
F.108	1	1	Start at masonry	12	Long	90	185	4875	420	10,0	8,1	16,8	1,91	475	11,3	9,1	18,8	2,09
F.109	1	1	180 (sp 1) 0 (sp 2)	12	Long	180	358	5023	420	10,6	8,6	17,7	1,99	475	12,0	9,6	19,9	2,19
F.110	1	1 & 2	180 (sp 1) 90 (sp 2)	12	Long	270	594	4549	420	8,7	7,1	14,7	1,72	475	9,8	8,0	16,5	1,89
F.111	1	1 & 2	180 in each sp 1 & 2	12	Long	360	791	4551	420	8,7	7,1	14,8	1,72	475	9,8	8,0	16,5	1,89
F.112	1	1 & 2	90 (sp 1) 180 (sp 2)	12	Long	270	621	4346	420	7,9	6,6	13,6	1,61	475	9,0	7,4	15,2	1,76
F.113	1	2	0 (sp 1) 180 (sp 2)	12	Long	180	419	4296	420	7,8	6,4	13,3	1,58	475	8,8	7,2	14,9	1,73
F.114	1	2	0 (sp 1) 90 (sp 2)	12	Long	90	208	4335	420	7,9	6,5	13,5	1,60	475	8,9	7,3	15,1	1,76
F.115	1	2	Start at 90 cm from masonry	12	Long	90	230	3916	420	6,4	5,4	11,2	1,39	475	7,3	6,1	12,5	1,51
F.116	1	1 & 2	90 in each sp 1 & 2	12	Long	180	368	4886	420	10,0	8,1	16,8	1,91	475	11,3	9,1	18,9	2,10

F Reduction values based on resistance drilling graphs

Second artillery floor						
Measurement nr.	Member	Span	Location	Face	Direction	Total reduction [mm]
R.01	6	-	Bottom	23	Rad	5
R.02	6	-	Bottom	12	Rad	0
R.03	1	1	Middle	23	Rad	5
R.04	1	1	End	23	Angle	14
R.05	A	1	End	23	Angle	5
R.06	1	1	Bott/Mid	12	Rad	10
R.07	3	-	Top	14	Rad	5
R.08	C	1	End	23	Rad	0
R.09	E	1	Middle	23	Rad	8
R.10	J	1	Bott/Mid	34	Rad	10
R.11	1	3	Middle	12	Rad	0
R.12	M	1	Near 14	23	Rad	13
R.13	3	-	70 cm up	14	Rad	5
R.14	3	-	130 cm up	14	Rad	10
R.15	3	-	115 cm up	12	Rad	25
R.16	3	-	40 cm up	12	Rad	10
R.17	2	3	K-L, bottom	34	Rad	5
R.18	2	3	K, top	34	Rad	5
R.19	K	3	Near 12	23	Rad	10
R.20	2	1	D-E, bottom	34	Rad	5
R.21	C	3	Bottom	12	Rad	10
R.22	4	-	120 cm up	14	Rad	20
R.23	4	-	Under (mult. cracks)	14	Rad	20
R.24	5	-	Bottom	12	Rad	5
R.25	5	-	150 cm up	14	Rad	10

First artillery floor						
Measurement nr.	Member	Span	Location	Face	Direction	Total reduction [mm]
R.26	P	1	Middle	23	Rad	20
R.27	1	3	Middle	12	Rad	5
R.28	1	3	Middle	12	Rad	3
R.29	1	3	Middle	12	Rad	5
R.30	1	3	Mi-Bot	12	Rad	0
R.31	1	3	Near 34	23	Rad	5
R.32	L	1	Near 34	23	Rad	15
R.33	L	1	Middle	23	Rad	35
R.34	L	1	Middle	23	Angle	14
R.35	J	1	Middle	23	Rad	8
R.36	L	1	Middle	23	Rad	13
R.37	I	1	Middle	23	Rad	15
R.38	D	1	Middle	23	Rad	15
R.39	D	1	Middle	23	Rad	18
R.40	North sill	1			Rad	0
R.41	1	1	D-E, 1/3 from bottom	34	Rad	5
R.42	C	2	Middle, crack	23	Rad	10
R.43	C	2	Near 34, crack	23	Rad	15
R.44	B	2	Middle	23	Rad	10
R.45	2	1	C-D, middle	12	Rad	0
R.46	2	1	C-D, middle	23	Rad	5

R.47	D	3	Middle	23	Rad	13
R.48	E	3	Near 12	23	Rad	15
R.49	H	3	Middle	23	Rad	10
R.50	L	3	Bottom	34	Rad	10
R.51	L	3	Middle	23	Rad	5
R.52	L	2	Near 34	23	Rad	10
R.53	2	3	Mi-Bot	12	Rad	10
R.54	2	3	Middle	23	Rad	5

G Calculation of utilization ratios regarding moments and shear forces

Model 1 - Load case 1 - Second artillery floor															
Beam	Max bending moment [kNm]	Span	Height [mm]	Second moment of area [cm^4]	σ_{moment} [MPa]	f_m [MPa]	μ_{moment}	Max shear force [kN]	Span	Area [cm^2]	τ_{shear} [MPa]	f_v [MPa]	μ_{shear}	Max deformation [mm]
A	12,33	3	250	33886	4,548	21,7	0,21	11,31	1	702	0,242	2,34	0,10	7,31
B	8,66	1	295	59492	2,147	21,7	0,10	9,4	1	841	0,167	2,34	0,07	4,9
C	21,76	3	335	116820	3,120	21,7	0,14	30,56	1	1258	0,364	2,34	0,16	6,94
D	15,95	1	290	64458	3,588	21,7	0,17	17,86	3	945	0,283	2,34	0,12	11,03
E	-24,33	1	305	80389	-4,615	21,7	0,21	30,79	1	1037	0,445	2,34	0,19	9,16
F	13,52	1	305	62822	3,282	21,7	0,15	15,73	3	803	0,294	2,34	0,13	8,81
G	-13,15	1	290	61161	-3,118	21,7	0,14	14,08	1	888	0,238	2,34	0,10	5,79
H	21,3	1	290	47728	6,471	21,7	0,30	19,32	1	707	0,410	2,34	0,17	9,91
I	14,23	3	285	59269	3,421	21,7	0,16	11,65	3	912	0,192	2,34	0,08	6,53
J	-22,07	1	285	52086	-6,038	21,7	0,28	25,4	1	770	0,495	2,34	0,21	5,47
K	-16,7	1	310	74465	-3,476	21,7	0,16	18,8	1	964	0,293	2,34	0,12	5,77
L	-15,46	1	320	83521	-2,962	21,7	0,14	19,78	1	987	0,301	2,34	0,13	6,58
M	13,67	1	310	79443	2,667	21,7	0,12	14,54	3	990	0,220	2,34	0,09	7,49
N	11,65	1	340	90612	2,186	21,7	0,10	10,84	3	1045	0,156	2,34	0,07	5,01
O	9,04	3	300	61843	2,193	21,7	0,10	9,81	1	1117	0,132	2,34	0,06	1,76
1	-37,43	1	344	114063	-5,644	21,7	0,26	75,07	col 3	1095	1,028	2,34	0,44	5,35
2	-43,18	1	325	84585	-8,296	21,7	0,38	44,59	1	953	0,702	2,34	0,30	9,85

Model 1 - Load case 1 - First artillery floor														
Beam	Max bending moment [kNm]	Span	Height [mm]	Second moment of area [cm^4]	σ_{moment} [MPa]	f_m [MPa]	μ_{moment}	Max shear force [kN]	Span	Area [cm^2]	τ_{shear} [MPa]	f_v [MPa]	μ_{shear}	Max deformation [mm]
A	18,93	2	300	75150	3,778	21,7	0,17	14,44	end of 1	1058	0,205	2,34	0,09	8,24
B	12,13	2	309	77223	2,427	21,7	0,11	12	end of 1	975	0,185	2,34	0,08	7,19
C	14,44	3	338	96709	2,523	21,7	0,12	14,41	end of 1	969	0,223	2,34	0,10	9,36
D	15,31	3	321	96141	2,556	21,7	0,12	14,87	end of 1	1038	0,215	2,34	0,09	9,87
E	-10,9	1	315	77879	-2,204	21,7	0,10	12,64	end of 1	932	0,203	2,34	0,09	9,17
F	12,99	3	319	84582	2,450	21,7	0,11	13,93	end of 1	916	0,228	2,34	0,10	7,38
G	11,08	3	323	89151	2,007	21,7	0,09	11,48	end of 1	862	0,200	2,34	0,09	4,41
H1	8,15	1	298	55271	2,197	21,7	0,10	8,56	1	789	0,163	2,34	0,07	2,33
H3	9,72	3	262	29369	4,336	21,7	0,20	9,25	3	604	0,230	2,34	0,10	7,09
I1	8,23	1	292	58317	2,060	21,7	0,10	8,56	1	855	0,150	2,34	0,06	2,28
I3	10,23	3	345	116908	1,509	21,7	0,07	9,75	3	1210	0,121	2,34	0,05	1,68
J1	7,27	1	298	63522	1,705	21,7	0,08	7,94	1	878	0,136	2,34	0,06	1,68
J3	9,57	3	292	68799	2,031	21,7	0,09	9,2	3	1029	0,134	2,34	0,06	2,55
K1	6,44	1	271	31557	2,765	21,7	0,13	7,4	1	612	0,181	2,34	0,08	2,7
K3	8,52	3	289	54478	2,260	21,7	0,10	8,64	3	853	0,152	2,34	0,06	2,65
L	18,2	3	353	132400	2,426	21,7	0,11	14,5	1	1214	0,179	2,34	0,08	6,41
M	21,97	3	362	126233	3,150	21,7	0,15	20,44	1	961	0,319	2,34	0,14	8,62
N	7,46	2	350	132877	0,982	21,7	0,05	10,54	3	1235	0,128	2,34	0,05	2,75
O	10,54	2	354	121663	1,533	21,7	0,07	12,65	3	1293	0,147	2,34	0,06	2,69
P	-2,09	3	265	41872	-0,661	21,7	0,03	3,95	3	706	0,084	2,34	0,04	2,4
1	-84,96	end of 1	394	206117	-8,120	21,7	0,37	87,86	end of 1	1597	0,825	2,34	0,35	5,37
2	-56,48	end of 1	358	125646	-8,046	21,7	0,37	94,6	end of 1	1178	1,205	2,34	0,51	9,74

Model 2 - Load case 1 - Second artillery floor														
Beam	Max bending moment [kNm]	Span	Height [mm]	Second moment of area [cm^4]	σ_{moment} [MPa]	f_m [MPa]	μ_{moment}	Max shear force [kN]	Span	Area [cm^2]	τ_{shear} [MPa]	f_v [MPa]	μ_{shear}	Max deformation [mm]
A	12,33	3	250	33886	4,548	13,8	0,33	11,31	1	702	0,242	1,63	0,15	11,46
B	8,76	1	295	59492	2,172	19,4	0,11	9,5	1	841	0,169	1,83	0,09	6,07
C	22,78	3	335	116820	3,266	17,7	0,18	32,29	1	1258	0,385	2,08	0,19	8,8
D	16,58	1	290	64458	3,730	21,4	0,17	17,59	3	945	0,279	2,32	0,12	12,7
E	-25,77	1	305	80389	-4,889	19,7	0,25	30,24	1	1037	0,437	2,17	0,20	12,05
F	13,74	1	305	62822	3,335	19,5	0,17	15,64	3	803	0,292	2,15	0,14	10,38
G	-13,72	1	290	61161	-3,253	20,7	0,16	14,21	1	888	0,240	2,25	0,11	6,64
H	21,3	1	290	47728	6,471	15,4	0,42	19,32	1	707	0,410	1,78	0,23	13,86
I	14,23	3	285	59269	3,421	18,7	0,18	11,65	3	912	0,192	2,08	0,09	10,13
J	-24,64	1	285	52086	-6,741	16,5	0,41	25,3	1	770	0,493	1,89	0,26	7,74
K	-17,75	1	310	74465	-3,695	20,3	0,18	19,88	1	964	0,309	2,22	0,14	7,13
L	-14,76	1	320	83521	-2,828	18,0	0,16	18,09	1	987	0,275	2,02	0,14	8,01
M	14,14	1	310	79443	2,759	20,8	0,13	14,33	3	990	0,217	2,18	0,10	8,48
N	11,65	1	340	90612	2,186	19,3	0,11	10,84	1	968	0,168	1,90	0,09	5,81
O	7,88	3	300	61843	1,911	16,3	0,12	8,13	3	866	0,141	2,14	0,07	2,08
1	38,8	1	344	114063	5,851	18,1	0,32	75,4	col 3	1095	1,033	1,80	0,57	4,91
2	-42,33	1	325	84585	-8,132	15,2	0,54	43,11	col 6	953	0,679	1,76	0,39	9,1

Model 2 - Load case 1 - First artillery floor														
Beam	Max bending moment [kNm]	Span	Height [mm]	Second moment of area [cm^4]	σ_{moment} [MPa]	f_m [MPa]	μ_{moment}	Max shear force [kN]	Span	Area [cm^2]	τ_{shear} [MPa]	f_v [MPa]	μ_{shear}	Max deformation [mm]
A	18,93	2	300	75150	3,778	15,0	0,25	14,44	end of 1	1058	0,205	1,75	0,12	11,85
B	13,02	2	309	77223	2,605	19,9	0,13	12	end of 1	975	0,185	2,10	0,09	8,56
C	12,82	3	356	96709	2,360	17,2	0,14	13,58	end of 1	969	0,210	1,98	0,11	11,15
D	15,93	3	325	96141	2,693	20,2	0,13	14,99	end of 1	1038	0,217	2,04	0,11	11,69
E	-9,89	1	315	77879	-2,000	14,4	0,14	12,1	end of 1	932	0,195	1,69	0,12	10,77
F	-12,35	1	309	70600	-2,703	17,9	0,15	13,41	end of 1	916	0,220	2,01	0,11	8,74
G	11,38	3	323	89151	2,062	20,0	0,10	11,51	end of 1	862	0,200	1,97	0,10	5,09
H1	8,15	1	298	55271	2,197	18,6	0,12	8,56	1	789	0,163	2,07	0,08	2,72
H3	9,72	3	262	29369	4,336	17,0	0,25	9,25	3	604	0,230	1,93	0,12	8,98
I1	8,23	1	292	58317	2,060	13,7	0,15	8,56	1	855	0,150	1,62	0,09	3,59
I3	10,23	3	345	116908	1,509	21,1	0,07	9,75	3	1210	0,121	2,29	0,05	1,73
J1	7,27	1	298	63522	1,705	16,1	0,11	7,94	1	878	0,136	1,85	0,07	2,25
J3	9,57	3	292	68799	2,031	20,7	0,10	9,2	3	1029	0,134	2,26	0,06	2,64
K1	6,44	1	271	31557	2,765	13,5	0,20	7,4	1	612	0,181	1,61	0,11	4,34
K3	8,52	3	289	54478	2,260	19,8	0,11	8,64	3	853	0,152	2,18	0,07	2,91
L	18,47	3	353	132400	2,462	17,7	0,14	14,4	1	1214	0,178	1,73	0,10	8,29
M	22,24	3	362	126233	3,189	20,0	0,16	20,34	1	961	0,317	1,99	0,16	10,38
N	7,54	2	350	132877	0,993	15,3	0,06	11,19	3	1235	0,136	1,74	0,08	3,6
O	11,75	2	354	121663	1,709	19,4	0,09	14,19	3	1293	0,165	1,82	0,09	3,43
P	-2,09	3	265	41872	-0,661	16,4	0,04	3,95	3	706	0,084	1,87	0,04	3,25
1	-79,06	end of 1	394	206117	-7,556	16,8	0,45	84,87	end of 1	1597	0,797	1,91	0,42	6,61
2	-58,4	end of 1	361	125646	-8,390	19,3	0,43	93,87	end of 1	1178	1,195	2,14	0,56	11,64

Model 3 - Load case 1 - Second artillery floor														
Beam	Max bending moment [kNm]	Span	Height [mm]	Second moment of inertia [cm^4]	σ_{moment} [MPa]	f_m [MPa]	μ_{moment}	Max shear force [kN]	Span	Area [cm^2]	τ_{shear} [MPa]	f_v [MPa]	μ_{shear}	Max deformation [mm]
A	12,37	2	250	33886	4,563	23,9	0,19	11,35	1	702	0,243	2,54	0,10	6,65
B	8,78	2	300	59492	2,214	23,9	0,09	9,5	start of 1	841	0,169	2,54	0,07	4,55
C	22,02	3	335	116820	3,157	23,9	0,13	30,63	end of 1	1258	0,365	2,54	0,14	6,43
D	16,07	1	290	64458	3,615	23,9	0,15	17,92	end of 2	945	0,284	2,54	0,11	10,17
E	-24,69	end of 1	305	80389	-4,684	23,9	0,20	31,37	end of 1	1037	0,454	2,54	0,18	8,48
F	13,61	1	305	62822	3,304	23,9	0,14	15,79	end of 2	803	0,295	2,54	0,12	8,11
G	-13,29	end of 1	290	61161	-3,151	23,9	0,13	14,17	end of 1	888	0,239	2,54	0,09	5,32
H	21,36	1	290	47728	6,489	23,9	0,27	19,36	end of 1	707	0,411	2,54	0,16	9,01
I	14,3	3	285	59269	3,438	23,9	0,14	11,71	3	912	0,193	2,54	0,08	6,68
J	-22,2	end of 1	285	52086	-6,074	23,9	0,25	25,48	end of 1	770	0,496	2,54	0,20	5,01
K	-16,48	end of 1	310	74465	-3,430	23,9	0,14	19,05	end of 1	964	0,296	2,54	0,12	5,29
L	-15,47	end of 1	320	83521	-2,964	23,9	0,12	19,92	end of 1	987	0,303	2,54	0,12	6,02
M	13,81	1	310	79443	2,694	23,9	0,11	14,58	end of 2	990	0,221	2,54	0,09	6,86
N	11,83	1	340	90612	2,219	23,9	0,09	10,95	start of 1	968	0,170	2,54	0,07	4,6
O	9,21	end of 2	300	61843	2,234	23,9	0,09	9,8	end of 1	1117	0,132	2,54	0,05	1,62
1	-37,66	col 3	327	114063	-5,398	23,1	0,23	75,82	col 3	1095	1,039	2,47	0,42	3,69
2	-42,75	col 6	325	84585	-8,213	23,1	0,36	44,19	col 6	953	0,696	2,47	0,28	6,62

Model 3 - Load case 1 - First artillery floor														
Beam	Max bending moment [kNm]	Span	Height [mm]	Second moment of area [cm^4]	σ_{moment} [MPa]	f_m [MPa]	μ_{moment}	Max shear force [kN]	Span	Area [cm^2]	τ_{shear} [MPa]	f_v [MPa]	μ_{shear}	Max deformation [mm]
A	19,1	2	319	75150	4,054	24,8	0,16	14,57	1	1089	0,201	2,61	0,08	7,27
B	11,01	2	309	77223	2,203	24,8	0,09	12,26	end of 1	975	0,189	2,61	0,07	5,47
C	13,29	3	338	96709	2,322	24,8	0,09	14,41	end of 1	976	0,221	2,61	0,08	7,16
D	14,35	3	321	96141	2,396	24,8	0,10	14,64	end of 1	1048	0,210	2,61	0,08	7,6
E	-10,85	end of 1	315	77879	-2,194	24,8	0,09	12,41	end of 1	942	0,198	2,61	0,08	7,16
F	-12,39	end of 1	309	70600	-2,711	24,8	0,11	13,39	end of 1	916	0,219	2,61	0,08	5,76
G	10,7	3	323	89151	1,938	24,8	0,08	11,44	end of 1	866	0,198	2,61	0,08	3,54
H1	8,22	1	298	55271	2,216	24,8	0,09	8,64	1	797	0,163	2,61	0,06	2,06
H3	9,78	3	262	29369	4,362	24,8	0,18	9,31	3	707	0,198	2,61	0,08	6,18
I1	8,31	1	292	58317	2,080	24,8	0,08	8,64	1	864	0,150	2,61	0,06	2,01
I3	10,37	3	345	116908	1,530	24,8	0,06	9,88	3	1232	0,120	2,61	0,05	1,49
J1	7,34	1	298	63522	1,722	24,8	0,07	8,02	1	878	0,137	2,61	0,05	1,48
J3	9,68	3	292	68799	2,054	24,8	0,08	9,31	3	1075	0,130	2,61	0,05	2,26
K1	6,49	1	271	31557	2,787	24,8	0,11	7,45	1	619	0,180	2,61	0,07	2,38
K3	8,6	3	289	54478	2,281	24,8	0,09	8,72	3	905	0,145	2,61	0,06	2,34
L	18,39	3	353	132400	2,452	24,8	0,10	14,78	end of 1	1214	0,183	2,61	0,07	5,6
M	22,01	3	362	126233	3,156	24,8	0,13	20,71	end of 1	969	0,321	2,61	0,12	7,39
N	6,63	2	350	132877	0,873	24,8	0,04	10,42	end of 2	1249	0,125	2,61	0,05	2,03
O	9,77	2	354	121663	1,421	24,8	0,06	12,74	end of 2	1301	0,147	2,61	0,06	2,02
P	-2,11	3	265	41872	-0,668	24,8	0,03	3,98	3	716	0,083	2,61	0,03	1,78
1	-86,41	end of 1	394	206117	-8,259	31,3	0,26	88,82	end of 1	1575	0,846	3,15	0,27	3,8
2	-61,67	end of 1	361	125646	-8,859	31,3	0,28	98,89	end of 1	1174	1,264	3,15	0,40	7,6

Model 4 - Load case 1 - Second artillery floor														
Beam	Max bending moment [kNm]	Span	Height [mm]	Second moment of area [cm^4]	σ_{moment} [MPa]	f_m [MPa]	μ_{moment}	Max shear force [kN]	Span	Area [cm^2]	τ_{shear} [MPa]	f_v [MPa]	μ_{shear}	Max deformation [mm]
A	12,37	3	250	33886	4,563	14,5	0,32	11,35	1	702	0,243	1,69	0,14	9,5
B	8,85	1	295	59492	2,194	20,2	0,11	9,5	start of 1	841	0,170	1,89	0,09	4,94
C	23,13	3	335	116820	3,316	18,6	0,18	32,6	1	1258	0,389	2,15	0,18	7,17
D	16,73	1	290	64458	3,763	22,5	0,17	17,64	3	945	0,280	2,16	0,13	10,22
E	-26,12	1	305	80389	-4,955	20,7	0,24	30,76	1	1037	0,445	2,25	0,20	9,81
F	13,84	1	305	62822	3,360	20,4	0,16	15,7	3	803	0,293	1,92	0,15	8,3
G	-13,91	1	290	61161	-3,298	21,7	0,15	14,3	1	888	0,242	2,34	0,10	5,36
H	21,36	1	290	47728	6,489	16,1	0,40	19,36	1	707	0,411	1,85	0,22	11,33
I	14,3	3	285	59269	3,438	19,4	0,18	11,71	3	912	0,193	2,15	0,09	8,25
J	-21,78	1	285	52086	-5,959	17,3	0,34	25,39	1	770	0,495	1,95	0,25	6,33
K	-17,99	1	310	74465	-3,745	21,3	0,18	20,25	1	964	0,315	2,30	0,14	5,78
L	-14,8	1	320	83521	-2,835	18,8	0,15	18,2	1	987	0,277	2,09	0,13	6,5
M	14,28	1	310	79443	2,786	21,7	0,13	14,37	3	990	0,218	2,34	0,09	6,87
N	11,81	1	340	90612	2,216	20,0	0,11	10,94	start of 1	968	0,170	2,26	0,08	4,72
O	8,01	3	300	61843	1,943	16,9	0,11	8,24	end of 3	866	0,143	1,96	0,07	1,7
1	38,87	1	344	114063	5,861	18,2	0,32	76,75	col 3	1095	1,051	1,81	0,58	4,04
2	-41,74	col 6	325	84585	-8,019	17,6	0,46	42,59	1	953	0,670	1,77	0,38	7,43

Model 4 - Load case 1 - First artillery floor														
Beam	Max bending moment [kNm]	Span	Height [mm]	Second moment of area [cm^4]	σ_{moment} [MPa]	f_m [MPa]	μ_{moment}	Max shear force [kN]	Span	Area [cm^2]	τ_{shear} [MPa]	f_v [MPa]	μ_{shear}	Max deformation [mm]
A	19,1	2	300	75150	3,812	16,2	0,24	14,58	1	1058	0,207	1,86	0,11	9,04
B	11,8	2	309	77223	2,361	21,5	0,11	12,34	1	975	0,190	2,24	0,08	5,49
C	12,11	3	338	96709	2,116	18,7	0,11	13,69	1	976	0,210	2,10	0,10	7,2
D	15,09	3	321	96141	2,519	21,8	0,12	14,9	1	1048	0,213	2,17	0,10	7,62
E	-9,74	end of 1	315	77879	-1,970	15,6	0,13	11,81	1	942	0,188	1,80	0,10	7,24
F	-12,01	end of 1	309	70600	-2,628	19,4	0,14	13,05	1	916	0,214	2,14	0,10	5,87
G	11,09	3	323	89151	2,009	21,6	0,09	11,51	1	866	0,199	2,10	0,09	3,52
H1	8,22	1	298	55271	2,216	20,1	0,11	8,64	1	797	0,163	2,20	0,07	2,04
H3	9,78	3	262	29369	4,362	18,4	0,24	9,31	3	707	0,198	2,05	0,10	6,7
I1	8,31	1	292	58317	2,080	14,8	0,14	8,64	1	864	0,150	1,73	0,09	2,76
I3	10,37	3	345	116908	1,530	22,8	0,07	9,88	3	1232	0,120	2,44	0,05	1,29
J1	7,34	1	298	63522	1,722	17,4	0,10	8,02	1	878	0,137	1,97	0,07	1,71
J3	9,68	3	292	68799	2,054	22,4	0,09	9,31	3	1075	0,130	2,41	0,05	1,97
K1	6,49	1	271	31557	2,787	14,6	0,19	7,45	1	619	0,180	1,71	0,11	3,33
K3	8,6	3	289	54478	2,281	21,4	0,11	8,72	3	905	0,145	2,32	0,06	2,17
L	18,47	3	353	132400	2,462	19,2	0,13	14,75	1	1214	0,182	1,84	0,10	6,47
M	22,17	3	362	126233	3,179	21,6	0,15	20,66	1	969	0,320	2,12	0,15	7,72
N	6,69	2	350	132877	0,881	16,5	0,05	10,9	2	1249	0,131	1,89	0,07	2,31
O	10,15	2	354	121663	1,477	21,0	0,07	14,16	2	1043	0,204	2,29	0,09	2,31
P	-2,11	3	265	41872	-0,668	17,7	0,04	3,98	3	716	0,083	1,99	0,04	2,08
1	-80,61	end of 1	394	206117	-7,704	18,3	0,42	86,13	end of 1	1597	0,809	2,05	0,39	3,95
2	-61,93	end of 1	361	125646	-8,897	22,2	0,40	98,31	end of 1	1174	1,256	2,39	0,53	7,61

Model 5 - Load case 1 - Second artillery floor														
Beam	Max bending moment [kNm]	Span	Height [mm]	Second moment of area [cm^4]	σ_{moment} [MPa]	f_m [MPa]	μ_{moment}	Max shear force [kN]	Span	Area [cm^2]	τ_{shear} [MPa]	f_v [MPa]	μ_{shear}	Max deformation [mm]
A	12,3	3	245	31686	4,755	21,7	0,22	11,28	1	676	0,250	2,34	0,11	7,82
B	8,54	1	285	53422	2,278	21,7	0,11	9,3	3	734	0,191	2,34	0,08	5,3
C	21,41	3	325	104460	3,331	21,7	0,15	30,37	1	1195	0,381	2,34	0,16	7,52
D	15,83	1	280	58428	3,793	21,7	0,17	17,81	3	896	0,298	2,34	0,13	11,99
E	-24,04	1	298	72958	-4,910	21,7	0,23	30,27	1	989	0,459	2,34	0,20	9,91
F	13,42	1	295	56199	3,522	21,7	0,16	15,65	3	753	0,312	2,34	0,13	9,7
G	-12,88	1	280	54438	-3,312	21,7	0,15	13,96	1	837	0,250	2,34	0,11	6,34
H	21,23	1	280	43021	6,909	21,7	0,32	19,26	1	667	0,433	2,34	0,18	10,95
I	14,15	3	275	53699	3,623	21,7	0,17	11,59	3	869	0,200	2,34	0,09	7,14
J	-21,85	1	275	45060	-6,668	21,7	0,31	25,27	1	715	0,530	2,34	0,23	5,99
K	-16,67	1	300	67447	-3,707	21,7	0,17	18,81	1	917	0,308	2,34	0,13	6,22
L	-15,45	1	310	74318	-3,222	21,7	0,15	19,48	1	929	0,315	2,34	0,13	7,12
M	13,3	1	298	67472	2,937	21,7	0,14	14,54	3	913	0,239	2,34	0,10	8,21
N	11,51	1	330	82605	2,299	21,7	0,11	10,75	end of 1	919	0,175	2,34	0,07	5,33
O	8,98	3	290	56355	2,311	21,7	0,11	9,97	1	1071	0,140	2,34	0,06	1,86
1	-37,09	1	339	107283	-5,860	21,7	0,27	74,25	col 3	1049	1,062	2,34	0,45	4,13
2	-45,12	1	320	79159	-9,120	21,7	0,42	45,12	1	915	0,740	2,34	0,32	7,69

Model 5 - Load case 1 - First artillery floor														
Beam	Max bending moment [kNm]	Span	Height [mm]	Second moment of area [cm^4]	σ_{moment} [MPa]	f_m [MPa]	μ_{moment}	Max shear force [kN]	Span	Area [cm^2]	τ_{shear} [MPa]	f_v [MPa]	μ_{shear}	Max deformation [mm]
A	18,82	2	290	65850	4,144	21,7	0,19	14,35	end of 1	994	0,217	2,34	0,09	9,38
B	11,68	2	299	67941	2,570	21,7	0,12	12,08	end of 1	913	0,198	2,34	0,08	7,76
C	13,76	3	325	82965	2,695	21,7	0,12	14,26	end of 1	896	0,239	2,34	0,10	10,14
D	14,72	3	308	83418	2,718	21,7	0,13	14,61	end of 1	957	0,229	2,34	0,10	10,72
E	-10,5	1	300	63900	-2,465	21,7	0,11	12,14	end of 1	942	0,193	2,34	0,08	10,07
F	-12,92	end of 1	299	64625	-2,989	21,7	0,14	13,79	end of 1	872	0,237	2,34	0,10	8,05
G	10,92	3	313	79550	2,148	21,7	0,10	11,36	end of 1	805	0,212	2,34	0,09	4,83
H1	8,11	1	288	51687	2,259	21,7	0,10	8,53	1	756	0,169	2,34	0,07	2,48
H3	9,68	3	247	26509	4,510	21,7	0,21	9,22	3	582	0,238	2,34	0,10	7,82
I1	8,16	1	277	50554	2,236	21,7	0,10	8,49	1	784	0,162	2,34	0,07	2,65
I3	10,13	3	330	100816	1,658	21,7	0,08	9,65	3	1121	0,129	2,34	0,06	1,93
J1	7,24	1	291	58680	1,792	21,7	0,08	7,9	1	842	0,141	2,34	0,06	1,81
J3	9,54	3	285	65287	2,079	21,7	0,10	9,17	3	1001	0,137	2,34	0,06	2,67
K1	6,44	1	256	31217	2,641	21,7	0,12	7,4	1	608	0,183	2,34	0,08	2,73
K3	8,48	3	303	51347	2,502	21,7	0,12	8,61	3	824	0,157	2,34	0,07	2,8
L	18,39	3	348	124275	2,575	21,7	0,12	14,21	1	1079	0,198	2,34	0,08	7,01
M	21,88	3	352	115603	3,331	21,7	0,15	20,3	1	900	0,338	2,34	0,14	9,4
N	7,21	2	340	121419	1,009	21,7	0,05	10,35	3	1181	0,131	2,34	0,06	2,91
O	10,24	2	344	108250	1,627	21,7	0,08	12,49	3	1222	0,153	2,34	0,07	2,87
P	-2,06	3	245	30638	-0,824	21,7	0,04	3,88	3	603	0,097	2,34	0,04	2,58
1	-84,25	end of 1	389	195916	-8,364	21,7	0,39	86,95	end of 1	1557	0,838	2,34	0,36	5,6
2	-57,37	end of 1	353	117798	-8,596	21,7	0,40	95,22	end of 1	1136	1,257	2,34	0,54	10,72

Model 6 - Load case 1 - Second artillery floor													
Beam	Max bending moment [kNm]	Span	Height [mm]	Second moment of area [cm^4]	σ_{moment} [MPa]	f_m [MPa]	μ_{moment}	Max shear force [kN]	Span	Area [cm^2]	τ_{shear} [MPa]	f_v [MPa]	μ_{shear}	Max deformation [mm]
A	12,3	3	245	31686	4,755	13,8	0,34	11,28	1	676	0,250	1,63	0,15	12,25
B	8,64	1	285	53422	2,305	19,4	0,12	9,4	start of 1	795	0,177	1,83	0,10	6,57
C	22,41	3	325	104460	3,486	17,7	0,20	32,11	1	1195	0,403	2,08	0,19	9,53
D	16,45	1	280	58428	3,942	21,4	0,18	17,54	3	896	0,294	2,32	0,13	13,79
E	-25,44	1	298	72958	-5,196	19,7	0,26	29,75	1	989	0,451	2,17	0,21	13,04
F	13,63	1	295	56199	3,577	19,5	0,18	15,56	3	753	0,310	2,15	0,14	11,4
G	-13,44	1	280	54438	-3,456	20,7	0,17	14,08	1	837	0,252	2,25	0,11	7,26
H	21,23	1	280	43021	6,909	15,4	0,45	19,26	1	667	0,433	1,78	0,24	15,33
I	14,15	3	275	53699	3,623	18,7	0,19	11,59	3	869	0,200	2,08	0,10	11,34
J	-21,4	1	275	45060	-6,530	16,5	0,40	25,18	1	715	0,528	1,89	0,28	8,51
K	-17,69	1	300	67447	-3,934	20,3	0,19	19,85	1	917	0,325	2,22	0,15	7,71
L	-14,77	1	310	74318	-3,080	18,0	0,17	17,82	1	929	0,288	2,02	0,14	8,76
M	13,73	1	298	67472	3,032	20,8	0,15	14,35	3	913	0,236	2,18	0,11	9,35
N	11,52	1	330	82605	2,301	19,3	0,12	10,75	start of 1	919	0,175	1,90	0,09	6,26
O	7,83	3	290	56355	2,015	16,3	0,12	8,24	1	1071	0,115	2,14	0,05	2,23
1	38,6	1	339	107283	6,099	18,1	0,34	74,96	3	912	1,233	1,80	0,68	5,18
2	-42,9	1	320	79159	-8,671	15,2	0,57	43,64	1	915	0,715	1,76	0,41	9,8

Model 6 - Load case 1 - First artillery floor													
Beam	Max bending moment [kNm]	Span	Height [mm]	Second moment of area [cm^4]	σ_{moment} [MPa]	f_m [MPa]	μ_{moment}	Max shear force [kN]	Span	Area [cm^2]	τ_{shear} [MPa]	f_v [MPa]	μ_{shear}	Max deformation [mm]
A	18,82	2	290	65850	4,144	15,0	0,28	14,35	end of 1	994	0,217	1,75	0,12	13,49
B	12,53	2	299	67941	2,757	19,9	0,14	12,08	end of 1	913	0,198	2,10	0,09	9,22
C	12,3	3	325	82965	2,409	17,2	0,14	13,44	end of 1	896	0,225	1,98	0,11	12,06
D	15,28	3	308	83418	2,821	20,2	0,14	14,72	end of 1	957	0,231	2,04	0,11	12,68
E	-9,57	1	300	63900	-2,246	14,4	0,16	11,65	end of 1	942	0,186	1,69	0,11	11,8
F	-12,31	1	299	64625	-2,848	17,9	0,16	13,27	end of 1	872	0,228	2,01	0,11	9,52
G	11,2	3	313	79550	2,203	20,0	0,11	11,39	end of 1	805	0,212	1,97	0,11	5,56
H1	8,11	1	288	51687	2,259	18,6	0,12	8,53	1	756	0,169	2,07	0,08	2,9
H3	9,68	3	247	26509	4,510	17,0	0,27	9,22	3	582	0,238	1,93	0,12	9,9
I1	8,16	1	277	50554	2,236	13,7	0,16	8,49	1	784	0,162	1,62	0,10	4,19
I3	10,13	3	330	100816	1,658	21,1	0,08	9,65	3	1121	0,129	2,29	0,06	1,99
J1	7,24	1	291	58680	1,792	16,1	0,11	7,9	1	842	0,141	1,85	0,08	2,43
J3	9,54	3	285	65287	2,079	20,7	0,10	9,17	3	1001	0,137	2,26	0,06	2,77
K1	6,44	1	256	31217	2,641	13,5	0,20	7,4	1	608	0,183	1,61	0,11	4,38
K3	8,48	3	303	51347	2,502	19,8	0,13	8,61	3	824	0,157	2,18	0,07	3,08
L	18,63	3	348	124275	2,608	17,7	0,15	14,11	1	1079	0,196	1,73	0,11	9,07
M	22,14	3	352	115603	3,371	20,0	0,17	20,21	1	900	0,337	1,99	0,17	11,31
N	7,3	2	340	121419	1,022	15,3	0,07	10,99	3	1181	0,140	1,74	0,08	3,81
O	11,43	2	344	108250	1,816	19,4	0,09	14,01	3	1222	0,172	1,82	0,09	3,66
P	-2,06	3	245	30638	-0,824	16,4	0,05	3,88	3	603	0,097	1,87	0,05	3,5
1	-78,48	end of 1	389	195916	-7,791	16,8	0,46	84,05	end of 1	1557	0,810	1,91	0,42	6,93
2	-59,25	end of 1	353	117798	-8,878	19,3	0,46	94,44	end of 1	1136	1,247	2,14	0,58	12,64

Model 7 - Load case 1 - Second artillery floor														
Beam	Max bending moment [kNm]	Span	Height [mm]	Second moment of area [cm^4]	σ_{moment} [MPa]	f_m [MPa]	μ_{moment}	Max shear force [kN]	Span	Area [cm^2]	τ_{shear} [MPa]	f_v [MPa]	μ_{shear}	Max deformation [mm]
A	12,34	3	245	31686	4,771	23,9	0,20	11,32	1	676	0,251	2,54	0,10	7,11
B	8,65	1	290	53422	2,348	23,9	0,10	9,38	start of 1	795	0,177	2,54	0,07	4,92
C	21,64	3	325	104460	3,366	23,9	0,14	30,45	end of 1	1195	0,382	2,54	0,15	6,96
D	15,95	1	280	58428	3,822	23,9	0,16	17,86	end of 2	896	0,299	2,54	0,12	11,04
E	-24,37	end of 1	298	72958	-4,977	23,9	0,21	30,83	end of 1	989	0,468	2,54	0,18	9,16
F	13,5	1	295	56199	3,543	23,9	0,15	15,71	end of 2	753	0,313	2,54	0,12	8,9
G	-13,02	end of 1	280	54438	-3,348	23,9	0,14	14,04	end of 1	837	0,252	2,54	0,10	5,82
H	21,29	1	280	43021	6,928	23,9	0,29	19,31	end of 1	667	0,434	2,54	0,17	9,96
I	14,22	3	275	53699	3,641	23,9	0,15	11,65	3	869	0,201	2,54	0,08	7,47
J	-21,96	end of 1	275	45060	-6,701	23,9	0,28	25,35	end of 1	715	0,532	2,54	0,21	5,5
K	-16,8	end of 1	300	67447	-3,736	23,9	0,16	19,06	end of 1	917	0,312	2,54	0,12	5,74
L	-15,47	end of 1	310	74318	-3,226	23,9	0,13	19,62	end of 1	929	0,317	2,54	0,12	6,58
M	13,43	1	298	67472	2,966	23,9	0,12	14,58	end of 2	913	0,240	2,54	0,09	7,59
N	11,69	1	330	82605	2,335	23,9	0,10	10,85	start of 1	919	0,177	2,54	0,07	4,96
O	9,15	end of 2	290	56355	2,354	23,9	0,10	9,96	end of 1	1071	0,139	2,54	0,05	1,74
1	-37,32	col 3	339	107283	-5,896	23,1	0,26	74,98	col 3	1049	1,072	2,47	0,43	3,9
2	-43,36	col 6	320	79159	-8,764	23,1	0,38	44,72	col 6	915	0,733	2,47	0,30	7,15

Model 7 - Load case 1 - First artillery floor														
Beam	Max bending moment [kNm]	Span	Height [mm]	Second moment of area [cm^4]	σ_{moment} [MPa]	f_m [MPa]	μ_{moment}	Max shear force [kN]	Span	Area [cm^2]	τ_{shear} [MPa]	f_v [MPa]	μ_{shear}	Max deformation [mm]
A	18,97	2	290	65850	4,177	24,8	0,17	14,48	1	994	0,219	2,61	0,08	8,28
B	10,61	2	299	67941	2,335	24,8	0,09	12,29	end of 1	913	0,202	2,61	0,08	5,9
C	12,67	3	325	82965	2,482	24,8	0,10	14,2	end of 1	896	0,238	2,61	0,09	7,74
D	13,76	3	308	83418	2,540	24,8	0,10	14,34	end of 1	957	0,225	2,61	0,09	8,25
E	-10,41	end of 1	300	63900	-2,444	24,8	0,10	11,91	end of 1	942	0,190	2,61	0,07	7,85
F	-12,34	end of 1	299	64625	-2,855	24,8	0,12	13,24	end of 1	872	0,228	2,61	0,09	6,28
G	10,54	3	313	79550	2,074	24,8	0,08	11,32	end of 1	805	0,211	2,61	0,08	3,87
H1	8,18	1	288	51687	2,279	24,8	0,09	8,6	1	756	0,171	2,61	0,07	2,19
H3	9,74	3	247	26509	4,538	24,8	0,18	9,28	3	582	0,239	2,61	0,09	6,81
I1	8,23	1	277	50554	2,255	24,8	0,09	8,56	1	784	0,164	2,61	0,06	2,34
I3	10,25	3	330	100816	1,678	24,8	0,07	9,77	3	1121	0,131	2,61	0,05	1,71
J1	7,31	1	291	58680	1,809	24,8	0,07	7,98	1	842	0,142	2,61	0,05	1,6
J3	9,65	3	285	65287	2,103	24,8	0,08	9,27	3	1001	0,139	2,61	0,05	2,36
K1	6,49	1	256	31217	2,661	24,8	0,11	7,45	1	608	0,184	2,61	0,07	2,41
K3	8,56	3	303	51347	2,526	24,8	0,10	8,69	3	824	0,158	2,61	0,06	2,48
L	18,58	3	348	124275	2,601	24,8	0,10	14,46	end of 1	1079	0,201	2,61	0,08	6,14
M	21,92	3	352	115603	3,337	24,8	0,13	20,55	end of 1	900	0,343	2,61	0,13	8,06
N	6,41	2	340	121419	0,897	24,8	0,04	10,24	end of 2	1181	0,130	2,61	0,05	2,14
O	9,51	2	344	108250	1,511	24,8	0,06	12,58	end of 2	1222	0,154	2,61	0,06	2,15
P	-2,08	3	245	30638	-0,832	24,8	0,03	3,92	3	603	0,098	2,61	0,04	1,92
1	-85,43	end of 1	389	195916	-8,481	31,3	0,27	87,67	end of 1	1557	0,845	3,15	0,27	3,97
2	-62,53	end of 1	353	117798	-9,369	31,3	0,30	99,46	end of 1	1136	1,313	3,15	0,42	8,25

Model 8 - Load case 1 - Second artillery floor														
Beam	Max bending moment [kNm]	Span	Height [mm]	Second moment of area [cm^4]	σ_{moment} [MPa]	f_m [MPa]	μ_{moment}	Max shear force [kN]	Span	Area [cm^2]	τ_{shear} [MPa]	f_v [MPa]	μ_{shear}	Max deformation [mm]
A	12,34	3	245	31686	4,771	14,5	0,33	11,32	1	676	0,251	1,69	0,15	9,5
B	8,73	1	285	53422	2,329	20,2	0,12	9,4	start of 1	795	0,178	1,89	0,09	4,94
C	22,74	3	325	104460	3,537	18,6	0,19	32,43	1	1195	0,407	2,15	0,19	7,17
D	16,59	1	280	58428	3,975	22,5	0,18	17,59	3	896	0,294	2,16	0,14	10,22
E	-25,79	1	298	72958	-5,267	20,7	0,26	30,26	1	989	0,459	2,25	0,20	9,81
F	13,73	1	295	56199	3,604	20,4	0,18	15,62	3	753	0,311	1,92	0,16	8,3
G	-13,61	1	280	54438	-3,500	21,7	0,16	14,17	1	837	0,254	2,34	0,11	5,36
H	21,29	1	280	43021	6,928	16,1	0,43	19,31	1	667	0,434	1,85	0,23	11,33
I	14,22	3	275	53699	3,641	19,4	0,19	11,65	3	869	0,201	2,15	0,09	8,25
J	-21,53	1	275	45060	-6,570	17,3	0,38	25,26	1	715	0,530	1,95	0,27	6,33
K	-17,92	1	300	67447	-3,985	21,3	0,19	20,22	1	917	0,331	2,30	0,14	5,78
L	-14,8	1	310	74318	-3,087	18,8	0,16	17,93	1	929	0,290	2,09	0,14	6,5
M	13,85	1	298	67472	3,059	21,7	0,14	14,38	3	913	0,236	2,34	0,10	6,87
N	11,67	1	330	82605	2,331	20,0	0,12	10,84	start of 1	919	0,177	2,26	0,08	4,72
O	7,96	3	290	56355	2,048	16,9	0,12	8,23	1	1071	0,115	1,96	0,06	1,7
1	38,68	1	339	107283	6,111	18,2	0,34	75,95	col 3	1049	1,086	1,81	0,60	4,04
2	-42,3	col 6	320	79159	-8,550	17,6	0,49	43,11	1	915	0,707	1,77	0,40	7,43

Model 8 - Load case 1 - First artillery floor														
Beam	Max bending moment [kNm]	Span	Height [mm]	Second moment of area [cm^4]	σ_{moment} [MPa]	f_m [MPa]	μ_{moment}	Max shear force [kN]	Span	Area [cm^2]	τ_{shear} [MPa]	f_v [MPa]	μ_{shear}	Max deformation [mm]
A	18,97	2	290	65850	4,177	16,2	0,26	14,48	1	994	0,219	1,86	0,12	9,04
B	11,38	2	299	67941	2,504	21,5	0,12	12,37	1	913	0,203	2,24	0,09	5,49
C	11,59	3	325	82965	2,270	18,7	0,12	13,5	1	896	0,226	2,10	0,11	7,2
D	14,44	3	308	83418	2,666	21,8	0,12	14,58	1	957	0,229	2,17	0,11	7,62
E	-9,39	end of 1	300	63900	-2,204	15,6	0,14	11,62	1	942	0,185	1,80	0,10	7,24
F	-11,95	end of 1	299	64625	-2,764	19,4	0,14	12,9	1	872	0,222	2,14	0,10	5,87
G	10,91	3	313	79550	2,146	21,6	0,10	11,38	1	805	0,212	2,10	0,10	3,52
H1	8,18	1	288	51687	2,279	20,1	0,11	8,6	1	756	0,171	2,20	0,08	2,04
H3	9,74	3	247	26509	4,538	18,4	0,25	9,28	3	582	0,239	2,05	0,12	6,7
I1	8,23	1	277	50554	2,255	14,8	0,15	8,56	1	784	0,164	1,73	0,09	2,76
I3	10,25	3	330	100816	1,678	22,8	0,07	9,77	3	1121	0,131	2,44	0,05	1,29
J1	7,31	1	291	58680	1,809	17,4	0,10	7,98	1	842	0,142	1,97	0,07	1,71
J3	9,65	3	285	65287	2,103	22,4	0,09	9,27	3	1001	0,139	2,41	0,06	1,97
K1	6,49	1	256	31217	2,661	14,6	0,18	7,45	1	608	0,184	1,71	0,11	3,33
K3	8,56	3	303	51347	2,526	21,4	0,12	8,69	3	824	0,158	2,32	0,07	2,17
L	18,67	3	348	124275	2,614	19,2	0,14	14,43	1	1079	0,201	1,84	0,11	6,47
M	22,07	3	352	115603	3,360	21,6	0,16	20,5	1	900	0,342	2,12	0,16	7,72
N	6,47	2	340	121419	0,906	16,5	0,05	10,71	2	1279	0,126	1,89	0,07	2,31
O	9,9	2	344	108250	1,573	21,0	0,07	13,99	2	1093	0,192	2,29	0,08	2,31
P	-2,08	3	245	30638	-0,832	17,7	0,05	3,92	3	603	0,098	1,99	0,05	2,08
1	-79,75	end of 1	389	195916	-7,917	18,3	0,43	85,07	end of 1	1557	0,820	2,05	0,40	3,95
2	-62,69	end of 1	353	117798	-9,393	22,2	0,42	98,79	end of 1	1136	1,304	2,39	0,55	7,61

Model 9 - Load case 1 - Second artillery floor														
Beam	Max bending moment [kNm]	Span	Height [mm]	Second moment of area [cm^4]	σ_{moment} [MPa]	f_m [MPa]	μ_{moment}	Max shear force [kN]	Span	Area [cm^2]	τ_{shear} [MPa]	f_v [MPa]	μ_{shear}	Max deformation [mm]
A	12,34	3	245	31686	4,771	14,5	0,33	11,32	start of 1	676	0,251	1,69	0,15	9,5
B	8,57	1	285	53422	2,286	20,2	0,11	9,4	end of 2	734	0,191	1,89	0,10	4,94
C	21,51	3	325	104460	3,346	18,6	0,18	30,52	1	1195	0,383	2,15	0,18	7,17
D	15,9	1	280	58428	3,810	22,5	0,17	17,88	3	896	0,299	2,16	0,14	10,22
E	-24,17	1	298	72958	-4,936	20,7	0,24	30,43	1	989	0,462	2,25	0,21	9,81
F	13,48	1	295	56199	3,538	20,4	0,17	15,72	3	753	0,313	1,92	0,16	8,3
G	-12,95	1	280	54438	-3,330	21,7	0,15	14,02	1	837	0,251	2,34	0,11	5,36
H	21,29	1	280	43021	6,928	16,1	0,43	19,31	1	667	0,434	1,85	0,23	11,33
I	14,22	3	275	53699	3,641	19,4	0,19	11,65	3	869	0,201	2,15	0,09	8,25
J	-21,94	1	275	45060	-6,695	17,3	0,39	25,34	1	715	0,532	1,95	0,27	6,33
K	-16,79	1	300	67447	-3,734	21,3	0,18	18,94	1	917	0,310	2,30	0,13	5,78
L	-15,56	1	310	74318	-3,245	18,8	0,17	19,6	1	929	0,316	2,09	0,15	6,5
M	13,36	1	298	67472	2,950	21,7	0,14	14,61	3	913	0,240	2,34	0,10	6,87
N	11,56	1	330	82605	2,309	20,0	0,12	10,79	end of 2	997	0,162	2,26	0,07	4,72
O	9,02	3	290	56355	2,321	16,9	0,14	10,03	end of 1	1071	0,140	1,96	0,07	1,7
1	-37,31	col 3	339	107283	-5,895	18,2	0,32	74,65	col 5	912	1,228	1,81	0,68	4,04
2	-43,96	col 6	320	79159	-8,885	17,6	0,51	45,3	col 6	915	0,743	1,77	0,42	7,43

Model 9 - Load case 1 - First artillery floor														
Beam	Max bending moment [kNm]	Span	Height [mm]	Second moment of area [cm^4]	σ_{moment} [MPa]	f_m [MPa]	μ_{moment}	Max shear force [kN]	Span	Area [cm^2]	τ_{shear} [MPa]	f_v [MPa]	μ_{shear}	Max deformation [mm]
A	18,97	2	290	65850	4,177	16,2	0,26	14,48	1	994	0,219	1,86	0,12	9,04
B	11,89	2	299	67941	2,616	21,5	0,12	12,21	1	913	0,201	2,24	0,09	5,49
C	14,03	3	325	82965	2,748	18,7	0,15	14,44	1	896	0,242	2,10	0,12	7,2
D	14,97	3	308	83418	2,764	21,8	0,13	14,8	1	957	0,232	2,17	0,11	7,62
E	-10,64	end of 1	300	63900	-2,498	15,6	0,16	12,29	1	942	0,196	1,80	0,11	7,24
F	-13,11	end of 1	299	64625	-3,033	19,4	0,16	13,98	1	872	0,240	2,14	0,11	5,87
G	11,07	3	313	79550	2,178	21,6	0,10	11,48	1	805	0,214	2,10	0,10	3,52
H1	8,18	1	288	51687	2,279	20,1	0,11	8,6	1	756	0,171	2,20	0,08	2,04
H3	9,74	3	247	26509	4,538	18,4	0,25	9,28	3	582	0,239	2,05	0,12	6,7
I1	8,23	1	277	50554	2,255	14,8	0,15	8,56	1	784	0,164	1,73	0,09	2,76
I3	10,25	3	330	100816	1,678	22,8	0,07	9,77	3	1121	0,131	2,44	0,05	1,29
J1	7,31	1	291	58680	1,809	17,4	0,10	7,98	1	842	0,142	1,97	0,07	1,71
J3	9,65	3	285	65287	2,103	22,4	0,09	9,27	3	1001	0,139	2,41	0,06	1,97
K1	6,49	1	256	31217	2,661	14,6	0,18	7,45	1	608	0,184	1,71	0,11	3,33
K3	8,56	3	303	51347	2,526	21,4	0,12	8,69	3	824	0,158	2,32	0,07	2,17
L	18,65	3	348	124275	2,611	19,2	0,14	14,44	1	1079	0,201	1,84	0,11	6,47
M	22,12	3	352	115603	3,368	21,6	0,16	20,48	1	900	0,341	2,12	0,16	7,72
N	7,39	2	340	121419	1,035	16,5	0,06	10,44	2	1279	0,122	1,89	0,06	2,31
O	11,06	2	344	108250	1,757	21,0	0,08	13,43	2	1093	0,184	2,29	0,08	2,31
P	-2,08	3	245	30638	-0,832	17,7	0,05	3,92	3	603	0,098	1,99	0,05	2,08
1	-86,02	end of 1	389	195916	-8,540	18,3	0,47	88,85	end of 1	1557	0,856	2,05	0,42	3,95
2	-58,31	end of 1	353	117798	-8,737	22,2	0,39	96,01	end of 1	1136	1,268	2,39	0,53	7,61

Model 8 - Load case 2 - Second artillery floor														
Beam	Max bending moment [kNm]	Span	Height [mm]	Second moment of area [cm^4]	σ_{moment} [MPa]	f_m [MPa]	μ_{moment}	Max shear force [kN]	Span	Area [cm^2]	τ_{shear} [MPa]	f_v [MPa]	μ_{shear}	Max deformation [mm]
A	5,05	3	245	31686	1,952	14,5	0,14	4,64	start of 1	676	0,103	1,69	0,06	4,81
B	15,19	1	285	53422	4,052	20,2	0,20	18,1	3	734	0,369	1,89	0,20	7,44
C	21,79	3	325	104460	3,390	18,6	0,18	36,25	end of 1	1188	0,458	2,15	0,21	8,49
D	22,5	1	280	58428	5,391	22,5	0,24	35,48	3	896	0,594	2,16	0,27	15,54
E	-22	1	298	72958	-4,485	20,7	0,22	38,83	end of 1	989	0,589	2,25	0,26	10,19
F	12,24	1	295	56199	3,213	20,4	0,16	14,96	3	753	0,298	1,92	0,16	8,91
G	9,3	3	285	53658	2,470	21,7	0,11	10,74	end of 1	837	0,192	2,34	0,08	5,06
H	13,43	3	290	56884	3,423	16,1	0,21	10,87	end of 3	812	0,201	1,85	0,11	8,22
I	12,15	3	275	53699	3,111	19,4	0,16	7,59	end of 3	869	0,131	2,15	0,06	6,57
J	-13,58	1	275	45060	-4,144	17,3	0,24	25,37	end of 1	715	0,532	1,95	0,27	4,72
K	-13,23	1	300	67447	-2,942	21,3	0,14	23,88	end of 1	917	0,391	2,30	0,17	5,49
L	13,17	3	310	73236	2,787	18,8	0,15	19,95	end of 1	929	0,322	2,09	0,15	6,87
M	8,49	1	298	67472	1,872	21,7	0,09	12,14	3	913	0,199	2,34	0,09	5,97
N	7,75	1	330	82605	1,548	20,0	0,08	8,9	start of 1	919	0,145	2,26	0,06	4,12
O	5,25	3	290	56355	1,351	16,9	0,08	9,14	end of 1	1071	0,128	1,96	0,07	1,45
1	30,05	1	339	107283	4,748	18,2	0,26	79,24	end of 1	1049	1,133	1,81	0,63	4,03
2	-29,77	col 6	320	76544	-6,223	17,6	0,35	46,22	1	915	0,758	1,77	0,43	8,22

Model 8 - Load case 2 - First artillery floor														
Beam	Max bending moment [kNm]	Span	Height [mm]	Second moment of area [cm^4]	σ_{moment} [MPa]	f_m [MPa]	μ_{moment}	Max shear force [kN]	Span	Area [cm^2]	τ_{shear} [MPa]	f_v [MPa]	μ_{shear}	Max deformation [mm]
A	10,92	2	290	65850	2,405	16,2	0,15	10,18	start of 1	1024	0,149	1,86	0,08	7,17
B	10,8	3	299	68805	2,347	21,5	0,11	14,27	end of 1	913	0,234	2,24	0,10	5,9
C	9,97	2	313	73115	2,131	18,7	0,11	17,14	end of 1	896	0,287	2,10	0,14	8,14
D	12,54	3	300	88389	2,125	21,8	0,10	20,36	end of 1	957	0,319	2,17	0,15	8,53
E	6,52	3	253	37941	2,174	15,6	0,14	13,51	end of 1	842	0,241	1,80	0,13	6,94
F	11,39	3	309	75155	2,342	19,4	0,12	18,17	end of 1	872	0,313	2,14	0,15	6,63
G	10,15	3	313	80990	1,961	21,6	0,09	13,44	end of 1	805	0,250	2,10	0,12	3,86
H1	3,49	1	288	51687	0,972	20,1	0,05	3,67	1	756	0,073	2,20	0,03	1,16
H3	4,02	3	247	26509	1,873	18,4	0,10	3,83	end of 3	574	0,100	2,05	0,05	4,06
I1	3,54	1	277	49494	0,991	14,8	0,07	3,68	1	784	0,070	1,73	0,04	1,64
I3	4,66	3	330	100816	0,763	22,8	0,03	4,44	3	1121	0,059	2,44	0,02	0,84
J1	7,01	1	291	58680	1,735	17,4	0,10	6,73	start of 1	842	0,120	1,97	0,06	1,99
J3	9,48	3	285	106555	1,266	22,4	0,06	6,75	start of 3	1001	0,101	2,41	0,04	2,25
K1	6,45	1	261	31217	2,696	14,6	0,18	8,37	end of 1	608	0,206	1,71	0,12	4,32
K3	8,77	3	279	51347	2,383	21,4	0,11	10,31	start of 3	824	0,188	2,32	0,08	2,75
L	17,2	3	348	124275	2,408	19,2	0,13	18,89	end of 1	1086	0,261	1,84	0,14	7,41
M	16,43	3	352	115603	2,501	21,6	0,12	24,14	end of 1	900	0,402	2,12	0,19	7,4
N	5,65	2	340	121419	0,791	16,5	0,05	13,79	end of 2	1181	0,175	1,89	0,09	2,17
O	5,04	2	344	108250	0,800	21,0	0,04	13,62	end of 2	1222	0,167	2,29	0,07	1,95
P	0,88	3	245	30638	0,352	17,7	0,02	3,33	3	603	0,083	1,99	0,04	1,9
1	-58,41	end of 1	389	195916	-5,792	18,3	0,32	61,59	end of 1	1557	0,593	2,05	0,29	3,86
2	-45,77	end of 1	353	117798	-6,853	22,2	0,31	102,58	end of 1	1136	1,354	2,39	0,57	8,52

Model 8 - 1.35*selfweight - First artillery floor													
Beam	Max bending moment [kNm]	Span	Height [mm]	Second moment of area [cm^4]	σ_{moment} [MPa]	f_m [MPa]	μ_{moment}	Max shear force [kN]	Span	Area [cm^2]	τ_{shear} [MPa]	f_v [MPa]	μ_{shear}
A	2,63	2	290	65850	0,579	16,2	0,04	2,07	1	994	0,031	1,86	0,02
B	1,98	2	299	67941	0,436	21,5	0,02	1,87	1	913	0,031	2,24	0,01
C	2,02	3	325	82965	0,396	18,7	0,02	2,07	1	896	0,035	2,10	0,02
D	2,5	3	308	83418	0,462	21,8	0,02	2,36	1	957	0,037	2,17	0,02
E	-1,43	end of 1	300	63900	-0,336	15,6	0,02	1,66	1	942	0,026	1,80	0,01
F	-1,92	end of 1	299	64625	-0,444	19,4	0,02	2,04	1	872	0,035	2,14	0,02
G	1,76	3	313	79550	0,346	21,6	0,02	1,67	1	805	0,031	2,10	0,01
H1	1,14	1	288	51687	0,318	20,1	0,02	1,2	1	756	0,024	2,20	0,01
H3	1,16	3	247	26509	0,540	18,4	0,03	1,1	3	582	0,028	2,05	0,01
I1	1,19	1	277	50554	0,326	14,8	0,02	1,24	1	784	0,024	1,73	0,01
I3	1,87	3	330	100816	0,306	22,8	0,01	1,78	3	1121	0,024	2,44	0,01
J1	1,13	1	291	58680	0,280	17,4	0,02	1,24	1	842	0,022	1,97	0,01
J3	1,68	3	285	65287	0,366	22,4	0,02	1,61	3	1001	0,024	2,41	0,01
K1	0,81	1	256	31217	0,332	14,6	0,02	0,93	1	608	0,023	1,71	0,01
K3	1,3	3	303	51347	0,384	21,4	0,02	1,31	3	824	0,024	2,32	0,01
L	3,84	3	348	124275	0,538	19,2	0,03	3,39	1	1079	0,047	1,84	0,03
M	3,61	3	352	115603	0,550	21,6	0,03	3,16	1	900	0,053	2,12	0,02
N	1,25	2	340	121419	0,175	16,5	0,01	1,83	2	1279	0,021	1,89	0,01
O	1,93	2	344	108250	0,307	21,0	0,01	2,63	2	1093	0,036	2,29	0,02
P	-0,29	3	245	30638	-0,116	17,7	0,01	0,54	3	603	0,013	1,99	0,01
1	-14,49	end of 1	389	195916	-1,439	18,3	0,08	15,71	end of 1	1557	0,151	2,05	0,07
2	-11,13	end of 1	353	117798	-1,668	22,2	0,08	17,07	end of 1	1136	0,225	2,39	0,09

Model 8 - 1.5*1 kN/m^2 - First artillery floor													
Beam	Max bending moment [kNm]	Span	Height [mm]	Second moment of area [cm^4]	σ_{moment} [MPa]	f_m [MPa]	μ_{moment}	Max shear force [kN]	Span	Area [cm^2]	τ_{shear} [MPa]	f_v [MPa]	μ_{shear}
A	4,09	2	290	65850	0,901	16,2	0,06	3,1	1	994	0,047	1,86	0,03
B	2,35	2	299	67941	0,517	21,5	0,02	2,62	1	913	0,043	2,24	0,02
C	2,4	3	325	82965	0,470	18,7	0,03	2,86	1	896	0,048	2,10	0,02
D	2,99	3	308	83418	0,552	21,8	0,03	3,06	1	957	0,048	2,17	0,02
E	-1,99	end of 1	300	63900	-0,467	15,6	0,03	2,49	1	942	0,040	1,80	0,02
F	-2,51	end of 1	299	64625	-0,581	19,4	0,03	2,71	1	872	0,047	2,14	0,02
G	2,29	3	313	79550	0,451	21,6	0,02	2,43	1	805	0,045	2,10	0,02
H1	1,76	1	288	51687	0,490	20,1	0,02	1,85	1	756	0,037	2,20	0,02
H3	2,15	3	247	26509	1,002	18,4	0,05	2,04	3	582	0,053	2,05	0,03
I1	1,76	1	277	50554	0,482	14,8	0,03	1,83	1	784	0,035	1,73	0,02
I3	2,09	3	330	100816	0,342	22,8	0,01	2	3	1121	0,027	2,44	0,01
J1	1,54	1	291	58680	0,381	17,4	0,02	1,69	1	842	0,030	1,97	0,02
J3	1,99	3	285	65287	0,434	22,4	0,02	1,92	3	1001	0,029	2,41	0,01
K1	1,42	1	256	31217	0,582	14,6	0,04	1,63	1	608	0,040	1,71	0,02
K3	1,82	3	303	51347	0,537	21,4	0,03	1,84	3	824	0,034	2,32	0,01
L	3,71	3	348	124275	0,519	19,2	0,03	2,76	1	1079	0,038	1,84	0,02
M	4,62	3	352	115603	0,703	21,6	0,03	4,34	1	900	0,072	2,12	0,03
N	1,31	2	340	121419	0,183	16,5	0,01	2,22	2	1279	0,026	1,89	0,01
O	1,99	2	344	108250	0,316	21,0	0,02	2,84	2	1093	0,039	2,29	0,02
P	-0,45	3	245	30638	-0,180	17,7	0,01	0,84	3	603	0,021	1,99	0,01
1	-16,32	end of 1	389	195916	-1,620	18,3	0,09	17,34	end of 1	1557	0,167	2,05	0,08
2	-12,89	end of 1	353	117798	-1,931	22,2	0,09	20,42	end of 1	1136	0,270	2,39	0,11

Model 8 - Load case 2 - Second artillery floor - Removed primary beam 1														
Beam	Max bending moment [kNm]	Span	Height [mm]	Second moment of area [cm^4]	σ_{moment} [MPa]	f_m [MPa]	μ_{moment}	Max shear force [kN]	Span	Area [cm^2]	τ_{shear} [MPa]	f_v [MPa]	μ_{shear}	Max deformation [mm]
A	5,05	3	245	31686	1,952	14,5	0,14	4,64	start of 1	676	0,103	1,69	0,06	4,81
B	20,83	1	285	53422	5,556	20,2	0,27	15,2	start of 1	795	0,287	1,89	0,15	15,49
C	23,15	3	325	104460	3,601	18,6	0,19	26,26	end of 3	1195	0,330	2,15	0,15	20,9
D	28,57	1	280	58428	6,846	22,5	0,30	21,19	3	896	0,355	2,16	0,16	27,61
E	16,87	1	298	72958	3,440	20,7	0,17	12,63	start of 1	989	0,192	2,25	0,09	18,97
F	13,81	1	295	56199	3,625	20,4	0,18	8,43	3	753	0,168	1,92	0,09	14,97
G	20,39	1	280	54438	5,244	21,7	0,24	17,53	end of 2	796	0,330	2,34	0,14	13,99
H	13,4	3	290	56884	3,416	16,1	0,21	10,87	end of 3	812	0,201	1,85	0,11	7,38
I	12,15	3	275	53699	3,111	19,4	0,16	7,59	end of 3	869	0,131	2,15	0,06	6,78
J	21,03	1	275	45060	6,417	17,3	0,37	17,17	end of 2	843	0,306	1,95	0,16	22,61
K	13,57	1	300	67447	3,018	21,3	0,14	9,07	start of 3	928	0,147	2,30	0,06	11,73
L	12,6	1	310	74318	2,628	18,8	0,14	18,3	start of 3	915	0,300	2,09	0,14	13,05
M	11,86	1	298	67472	2,615	21,7	0,12	10,84	start of 1	915	0,178	2,34	0,08	12,25
N	11,98	1	330	82605	2,393	20,0	0,12	10,78	start of 1	919	0,176	2,26	0,08	8,39
O	9,1	3	290	56355	2,341	16,9	0,14	13,87	start of 1	1071	0,194	1,96	0,10	3,33
1														
2	-85,8	col 6	320	76544	-17,935	17,6	1,02	81,83	col 6	915	1,341	1,77	0,76	22,37

Model 8 - Load case 2 - Second artillery floor - Removed primary beam 2														
Beam	Max bending moment [kNm]	Span	Height [mm]	Second moment of area [cm^4]	σ_{moment} [MPa]	f_m [MPa]	μ_{moment}	Max shear force [kN]	Span	Area [cm^2]	τ_{shear} [MPa]	f_v [MPa]	μ_{shear}	Max deformation [mm]
A	5,05	3	245	31686	1,952	14,5	0,14	4,64	start of 1	676	0,103	1,69	0,06	4,81
B	7,44	1	285	53422	1,985	20,2	0,10	13,5	end of 1	795	0,255	1,89	0,13	5,25
C	15,75	3	325	104460	2,450	18,6	0,13	12,83	end of 3	1195	0,161	2,15	0,07	7,56
D	-10,27	1	280	58428	-2,461	22,5	0,11	20,95	start of 2	912	0,345	2,16	0,16	6,97
E	-12,6	1	298	72958	-2,569	20,7	0,12	11,85	end of 1	989	0,180	2,25	0,08	6,49
F	-8,97	1	295	56199	-2,354	20,4	0,12	9,28	end of 1	779	0,179	1,92	0,09	3,34
G	19,56	3	285	53658	5,195	21,7	0,24	17,34	end of 1	837	0,311	2,34	0,13	13,75
H	10,64	1	280	43021	3,462	16,1	0,21	7,63	end of 1	667	0,172	1,85	0,09	6,91
I	0,72	1	275	53699	0,184	19,4	0,01	1,72	end of 1	869	0,030	2,15	0,01	4,86
J	-17,04	1	275	45060	-5,200	17,3	0,30	15,3	end of 3	715	0,321	1,95	0,16	11,57
K	10,97	3	315	74649	2,315	21,3	0,11	10,72	end of 1	917	0,175	2,30	0,08	5,3
L	18,41	3	310	73236	3,896	18,8	0,21	18,37	end of 1	929	0,297	2,09	0,14	11,6
M	8	1	298	67472	1,764	21,7	0,08	10,07	3	913	0,165	2,34	0,07	6,83
N	7,44	3	330	89152	1,377	20,0	0,07	8,4	start of 1	919	0,137	2,26	0,06	5,39
O	7,45	1	290	56355	1,917	16,9	0,11	12,98	start of 1	1071	0,182	1,96	0,09	2,53
1	-38,52	1	339	107283	-6,086	18,2	0,33	70,84	col 3	1049	1,013	1,81	0,56	6,37
2														

Model 8 - Load case 2 - Second artillery floor - Removed primary beam 1 & 2														
Beam	Max bending moment [kNm]	Span	Height [mm]	Second moment of area [cm^4]	σ_{moment} [MPa]	f_m [MPa]	μ_{moment}	Max shear force [kN]	Span	Area [cm^2]	τ_{shear} [MPa]	f_v [MPa]	μ_{shear}	Max deformation [mm]
A														
B														
C														
D														
E														
F														
G	104,72	3	285	53658	27,811	21,7	1,28	40,66	end of 3	796	0,766	2,34	0,33	262,1
H														
I														
J	101,74	3	295	59849	25,074	17,3	1,45	39,79	end of 3	843	0,708	1,95	0,36	347,3
K														
L														
M														
N														
O														
1														
2														

H Calculation of utilization ratios regarding buckling

Model 1 - Load case 1								
Column	Edge of column	Max normal force [kN]	Length [m]	L_e [m]	MOE [GPa]	Second moment of area [cm^4]	N_{cr} [kN]	$\mu_{buckling}$
3	First artillery floor	104,87	3,7	3,7	10,5	120121	9092	0,012
3	Second artillery floor	102,33	3,7	3,7	10,5	120121	9092	0,011
4	First artillery floor	16,12	3,7	3,7	10,5	128825	9751	0,002
4	Second artillery floor	13,35	3,7	3,7	10,5	128825	9751	0,001
5	First artillery floor	120,52	3,7	3,7	10,5	110589	8371	0,014
5	Second artillery floor	117,98	3,7	3,7	10,5	110589	8371	0,014
6	First artillery floor	91,44	3,7	3,7	10,5	150182	11368	0,008
6	Second artillery floor	88,65	3,7	3,7	10,5	150182	11368	0,008

Model 2 - Load case 1								
Column	Edge of column	Max normal force [kN]	Length [m]	L_e [m]	MOE [GPa]	Second moment of area [cm^4]	N_{cr} [kN]	$\mu_{buckling}$
3	First artillery floor	105,68	3,7	3,7	8,4	120121	7274	0,015
3	Second artillery floor	103,13	3,7	3,7	8,4	120121	7274	0,014
4	First artillery floor	17,31	3,7	3,7	9	128825	8358	0,002
4	Second artillery floor	14,54	3,7	3,7	9	128825	8358	0,002
5	First artillery floor	118,24	3,7	3,7	9,7	110589	7733	0,015
5	Second artillery floor	115,7	3,7	3,7	9,7	110589	7733	0,015
6	First artillery floor	91,62	3,7	3,7	8,7	150182	9419	0,010
6	Second artillery floor	88,82	3,7	3,7	8,7	150182	9419	0,009

Model 3 - Load case 1								
Column	Edge of column	Max normal force [kN]	Length [m]	L_e [m]	MOE [GPa]	Second moment of area [cm^4]	N_{cr} [kN]	$\mu_{buckling}$
3	First artillery floor	105,77	3,7	3,7	11,2	120121	9699	0,011
3	Second artillery floor	103,2	3,7	3,7	11,2	120121	9699	0,011
4	First artillery floor	16,4	3,7	3,7	11,2	128825	10401	0,002
4	Second artillery floor	13,61	3,7	3,7	11,2	128825	10401	0,001
5	First artillery floor	121,23	3,7	3,7	11,2	110589	8929	0,014
5	Second artillery floor	118,66	3,7	3,7	11,2	110589	8929	0,013
6	First artillery floor	90,89	3,7	3,7	11,2	150182	12126	0,007
6	Second artillery floor	88,07	3,7	3,7	11,2	150182	12126	0,007

Model 4 - Load case 1								
Column	Edge of column	Max normal force [kN]	Length [m]	L_e [m]	MOE [GPa]	Second moment of area [cm^4]	N_{cr} [kN]	$\mu_{buckling}$
3	First artillery floor	107,19	3,7	3,7	8,5	120121	7361	0,015
3	Second artillery floor	104,62	3,7	3,7	8,5	120121	7361	0,014
4	First artillery floor	17,22	3,7	3,7	9,1	128825	8451	0,002
4	Second artillery floor	14,42	3,7	3,7	9,1	128825	8451	0,002
5	First artillery floor	119,13	3,7	3,7	9,8	110589	7813	0,015
5	Second artillery floor	116,57	3,7	3,7	9,8	110589	7813	0,015
6	First artillery floor	90,88	3,7	3,7	8,8	150182	9527	0,010
6	Second artillery floor	88,06	3,7	3,7	8,8	150182	9527	0,009

Model 5 - Load case 1								
Column	Edge of column	Max normal force [kN]	Length [m]	L_e [m]	MOE [GPa]	Second moment of area [cm^4]	N_{cr} [kN]	$\mu_{buckling}$
3	First artillery floor	103,69	3,7	3,7	10,5	114467	8664	0,012
3	Second artillery floor	101,25	3,7	3,7	10,5	114467	8664	0,012
4	First artillery floor	15,25	3,7	3,7	10,5	106956	8096	0,002
4	Second artillery floor	12,73	3,7	3,7	10,5	106956	8096	0,002
5	First artillery floor	120,03	3,7	3,7	10,5	103215	7813	0,015
5	Second artillery floor	117,56	3,7	3,7	10,5	103215	7813	0,015
6	First artillery floor	91,99	3,7	3,7	10,5	150197	11369	0,008
6	Second artillery floor	89,22	3,7	3,7	10,5	150197	11369	0,008

Model 6 - Load case 1								
Column	Edge of column	Max normal force [kN]	Length [m]	L_e [m]	MOE [GPa]	Second moment of area [cm^4]	N_{cr} [kN]	$\mu_{buckling}$
3	First artillery floor	104,53	3,7	3,7	8,4	114467	6932	0,015
3	Second artillery floor	102,09	3,7	3,7	8,4	114467	6932	0,015
4	First artillery floor	16,44	3,7	3,7	9	106956	6939	0,002
4	Second artillery floor	13,92	3,7	3,7	9	106956	6939	0,002
5	First artillery floor	117,7	3,7	3,7	9,7	103215	7217	0,016
5	Second artillery floor	115,23	3,7	3,7	9,7	103215	7217	0,016
6	First artillery floor	92,19	3,7	3,7	8,7	150197	9420	0,010
6	Second artillery floor	89,42	3,7	3,7	8,7	150197	9420	0,009

Model 7 - Load case 1								
Column	Edge of column	Max normal force [kN]	Length [m]	L_e [m]	MOE [GPa]	Second moment of area [cm^4]	N_{cr} [kN]	$\mu_{buckling}$
3	First artillery floor	104,56	3,7	3,7	11,2	114467	9242	0,011
3	Second artillery floor	102,1	3,7	3,7	11,2	114467	9242	0,011
4	First artillery floor	15,54	3,7	3,7	11,2	106956	8636	0,002
4	Second artillery floor	12,99	3,7	3,7	11,2	106956	8636	0,002
5	First artillery floor	120,69	3,7	3,7	11,2	103215	8334	0,014
5	Second artillery floor	118,2	3,7	3,7	11,2	103215	8334	0,014
6	First artillery floor	91,43	3,7	3,7	11,2	150197	12127	0,008
6	Second artillery floor	88,63	3,7	3,7	11,2	150197	12127	0,007

Model 8 - Load case 1								
Column	Edge of column	Max normal force [kN]	Length [m]	L_e [m]	MOE [GPa]	Second moment of area [cm^4]	N_{cr} [kN]	$\mu_{buckling}$
3	First artillery floor	106,01	3,7	3,7	8,5	114467	7014	0,015
3	Second artillery floor	103,55	3,7	3,7	8,5	114467	7014	0,015
4	First artillery floor	16,34	3,7	3,7	9,1	106956	7016	0,002
4	Second artillery floor	13,8	3,7	3,7	9,1	106956	7016	0,002
5	First artillery floor	118,55	3,7	3,7	9,8	103215	7292	0,016
5	Second artillery floor	116,06	3,7	3,7	9,8	103215	7292	0,016
6	First artillery floor	91,45	3,7	3,7	8,8	150197	9528	0,010
6	Second artillery floor	88,65	3,7	3,7	8,8	150197	9528	0,009

Model 9 - Load case 1								
Column	Edge of column	Max normal force [kN]	Length [m]	L_e [m]	MOE [GPa]	Second moment of area [cm^4]	N_{cr} [kN]	$\mu_{buckling}$
3	First artillery floor	104,38	3,7	3,7	9,2	114467	7592	0,014
3	Second artillery floor	101,92	3,7	3,7	9,2	114467	7592	0,013
4	First artillery floor	14,98	3,7	3,7	9,2	106956	7094	0,002
4	Second artillery floor	12,43	3,7	3,7	9,2	106956	7094	0,002
5	First artillery floor	120,85	3,7	3,7	9,2	103215	6845	0,018
5	Second artillery floor	118,36	3,7	3,7	9,2	103215	6845	0,017
6	First artillery floor	92,33	3,7	3,7	9,2	150197	9961	0,009
6	Second artillery floor	89,53	3,7	3,7	9,2	150197	9961	0,009

Model 8 - Load case 2								
Column	Edge of column	Max normal force [kN]	Length [m]	L_e [m]	MOE [GPa]	Second moment of area [cm^4]	N_{cr} [kN]	$\mu_{buckling}$
3	First artillery floor	82,26	3,7	3,7	8,5	114467	7014	0,012
3	Second artillery floor	79,8	3,7	3,7	8,5	114467	7014	0,011
4	First artillery floor	1,62	3,7	3,7	9,1	106956	7016	0,000
4	Second artillery floor	-0,92	3,7	3,7	9,1	106956	7016	0,000
5	First artillery floor	77,03	3,7	3,7	9,8	103215	7292	0,011
5	Second artillery floor	74,54	3,7	3,7	9,8	103215	7292	0,010
6	First artillery floor	58,81	3,7	3,7	8,8	150197	9528	0,006
6	Second artillery floor	56,01	3,7	3,7	8,8	150197	9528	0,006

I Prediction of maximum load capacity for model 8

Lower floor

1.35 x (selfweight + flooring)

$\mu_{M.self.lower} := 0.078$ prim 1

$\mu_{V.self.lower} := 0.09$ prim 2

1.5 x (1 kN/m^2)

$\mu_{M.ref.lower} := 0.09$ prim 1

$\mu_{V.ref.lower} := 0.11$ prim 2

Upper floor

1.35 x (selfweight + flooring)

$\mu_{M.self.upper} := 0.08$ prim 2

$\mu_{V.self.upper} := 0.10$ prim 1

1.5 x (1 kN/m^2)

$\mu_{M.ref.upper} := 0.10$ prim 2

$\mu_{V.ref.upper} := 0.12$ prim 1

Calculation of how many loads of 1 kN/m^2 that can be applied in the ULS combination

$$n_{M.lower} := \frac{1 - \mu_{M.self.lower}}{\mu_{M.ref.lower}} = 10.238$$

$$n_{V.lower} := \frac{1 - \mu_{V.self.lower}}{\mu_{V.ref.lower}} = 8.273$$

$$n_{lower} := \min\left(n_{M.lower}, n_{V.lower}\right) = 8.273$$

$$n_{M.upper} := \frac{1 - \mu_{M.self.upper}}{\mu_{M.ref.upper}} = 9.2$$

$$n_{V.upper} := \frac{1 - \mu_{V.self.upper}}{\mu_{V.ref.upper}} = 7.5$$

$$n_{upper} := \min\left(n_{M.upper}, n_{V.upper}\right) = 7.5$$

Maximum load

$$Load_{max} := n_{lower} \cdot 1 \cdot \frac{kN}{m^2} = 8.273 \frac{kN}{m^2}$$

Maximum load

$$Load_{max} := n_{upper} \cdot 1 \cdot \frac{kN}{m^2} = 7.5 \frac{kN}{m^2}$$

Verification of 1.35 x (selfweight) + 1.5 x 7.5 kN/m^2

$V_{max.upper} := 143.91kN$

$A_{upper} := 1049cm^2$

$f_{v.upper} := 2.1MPa$

$$\tau_{upper} := \frac{3 \cdot V_{max.upper}}{2 \cdot A_{upper}} = 2.058MPa$$

$$\mu_{max} := \frac{\tau_{upper}}{f_{v.upper}} = 0.98$$ Close to 1